AD NUMBER

AD371676

CLASSIFICATION CHANGES

TO: unclassified

FROM: confidential

LIMITATION CHANGES

TO:

Approved for public release, distribution unlimited

FROM:

Distribution authorized to U.S. Gov't. agencies and their contractors; Administrative/Operational Use; Apr 1966. Other requests shall be referred to Air Force Rocket Propulsion Lab., Edwards AFB, CA.

AUTHORITY

31 Dec 1972 per GDS marking; Air Force Rocket Propulsion Lab ltr dtd 7 May 1973

GENERAL DECLASSIFICATION SCHEDULE

IN ACCORDANCE WITH
DOD 5200.1-R & EXECUTIVE ORDER 11652

THIS DOCUMENT IS:

Subject to General Declassification Schedule of Executive Order 11652-Automatically Downgraded at 2 Years Intervals-DECLASSIFIED ON DECEMBER 31, 1972

BY

Defense Documentation Center
Defense Supply Agency
Cameron Station
Alexandria, Virginia 22314

FINAL PROGRAM REPORT

Development, Design, Fabrication, and Demonstration of Packageable High-Expansion-Ratio Nozzles for Solid Propellant Rocket Motors (U)

Robert E. Morris

April 1966

SPECIAL HANDLING REQUIRED
NOT RELEASABLE TO FOREIGN NATIONALS
The information contained in this document will not be released to foreign nationals or their representatives.

ROCKET PROPULSION LABORATORY
Air Force Systems Command
Edwards Air Force Base, California

Report AFRPL-TR-66-45

FINAL PROGRAM REPORT

Development, Design, Fabrication, and Demonstration of Packageable High-Expansion-Ratio Nozzles for Solid Propellant Rocket Motors (u)

Robert E. Morris

April 1966

SPECIAL HANDLING REQUIRED
NOT RELEASABLE TO FOREIGN NATIONALS
The information contained in this document will not be released to foreign nationals or their representatives.

ROCKET PROPULSION LABORATORY
Air Force Systems Command
Edwards Air Force Base, California

1627T

REPRODUCTION QUALITY NOTICE

This document is the best quality available. The copy furnished to DTIC contained pages that may have the following quality problems:

- Pages smaller or larger than normal.
- Pages with background color or light colored printing.
- Pages with small type or poor printing; and or
- Pages with continuous tone material or color photographs.

Due to various output media available these conditions may or may not cause poor legibility in the microfiche or hardcopy output you receive.

☐ If this block is checked, the copy furnished to DTIC contained pages with color printing, that when reproduced in Black and White, may change detail of the original copy.

PAGES _____

ARE

MISSING

IN

ORIGINAL

DOCUMENT

FOREWORD

(u) This is the final report for a development program sponsored by the Air Force Systems Command, Rocket Propulsion Laboratory, Edwards Air Force Base, California, from 1 June 1964 to 15 April 1966 on the development, design, fabrication, and demonstration of packageable high-expansion-ratio nozzles for solid propellant rocket motors. The research and development efforts on the program were performed by Aerojet-General Corporation, Sacramento, California, under Contract AF 04(611)-9896, and this report, dated April 1966, is submitted in fulfillment of that contract.

(u) This report contains classified information extracted from Report AEDC-TR-65-254, "Demonstration Tests of Two Types of Packageable High-Expansion-Ratio Nozzles for Solid-Propellant Rocket Motors," ARO, Inc., Bryan, Ohio, January 1966. The security classification of this report is Group 4, Confidential.

(u) This technical report has been reviewed and is approved.

UNCLASSIFIED ABSTRACT

(u) The objectives of this program were the development, design, fabrication, and demonstration of packageable high-expansion-ratio nozzles for solid propellant rocket motors. A subscale testing program conducted at Aerojet-General's Von Karman Center altitude facility was successful in providing information for evaluating three elastomeric materials (nitrile butadiene (V-44®), styrene butadiene, and butyl) and two refractory metals (90Ta-10W and columbium) for use in exit cones. Erosion data was also gathered on these elastomeric materials. A demonstration test program was conducted at Arnold Engineering Development Center, using three 30KS-5000 solid propellant motors, two with an elastomeric V-44® exit cone and one with a columbium expandable exit cone. Objectives were to test deployment, determine the materials' integrity under operating conditions, obtain data pertaining to specific impulse at altitude conditions, and obtain postfire heat-soak data for 30 sec. Successful motor ignition, operation, and postfire heat-soak for all three tests were conducted at simulated altitudes in excess of 100,000 feet. Attempts to deploy the elastomeric V-44® exit cone from a folded position at altitude conditions were only partially successful. However, the principle of deployment was demonstrated during sea-level tests. All three exit cones were stable during motor operation and were in excellent postfire condition. The columbium exit cone did not expand fully (area ratio of 38.0, instead of 50). High-quality optical data were obtained of the nozzle deployment, nozzle performance during motor operation, and postfire condition.

TABLE OF CONTENTS

APPENDIXES

TABLE LIST

FIGURE LIST

FIGURE LIST (cont.)

FIGURE LIST (cont.)

SECTION I

INTRODUCTION

(u) The concept of expandable exit cones for high-expansion-ratio rocket nozzles offers improved performance (as well as lighter weight, in many applications) in volume- or diameter-limited systems. In recognition of the potential of this concept, active development of the expandable exit cone was initiated at Aerojet in January 1960.

(u) Specific preliminary engineering tasks included: design applications, materials investigation, theoretical analysis of heat transfer and shock, structural analysis, gas dynamics, packaging, and nozzle deployment as applied to liquid rocket engines.

(u) Selected for the initial testing was a modified 200-lb-thrust, bipropellant, water-cooled Lark thrust chamber. This chamber operated at a chamber pressure of 120 psia, burning WIFNA/UDMH at a mixture ratio of 2.8:1 oxidizer to fuel, with a total propellant flow rate of 0.75 lb/sec. The expandable nozzle was attached at an area ratio of 8:1, expanding to 27:1 at the exit with a 15° cone half-angle.

(u) This test engine was operated at approximately 100,000 ft in a small-scale altitude simulator at Aerojet-General's Von Karman Center. The objectives of the first tests were to verify the radiation-cooled exit cone wall temperatures and internal supersonic shock analyses on expandable metallic exit cones. These tests were successful and served to verify the theoretical predictions.

(u) The next phase of the program was to develop a flexible nonmetallic exit cone that could be folded along both length and diameter. A great many elastomeric materials were tested on the same Lark engine. Materials were successfully demonstrated, thus substantiating the validity of the design concept.

(u) Following this small-scale development and demonstration, Aerojet-General received an Air Force contract (AF 04(647)-652/SAA) to continue development. Direction was under the Rocket Propulsion Laboratories at Edwards Air Force Base. Work was initiated in April 1962 and has been continued under two follow-on contracts. This work included advanced theoretical investigations in the various areas of heat transfer, internal and external gas dynamics, materials, fabrication techniques, and various experimental programs.

(u) To date there have been two test series conducted at Arnold Engineering Development Center (AEDC), Tullahoma, Tennessee. The test engine used was made from surplus Titan hardware; the basic thrust chamber was a 17.5° half-angle conical chamber that had been used previously to develop the XLR91-AJ-3.

(u) The expandable nozzles were attached to the combustion chamber at an area ratio of 7.07:1 expanding out to area ratios up to 40:1. The exit cones were designed to have a half-angle of 17.5° when fully expanded. The expandable exit cone wall length was 55.12 in. with an inside diameter at the attachment point of 24.6 in. and an exit plane inside diameter of 57.75 in. for the fully expanded nozzle.

I, Introduction (cont.)

(u) In general, the metallic exit cones were successful in both test series, whereas the elastomeric exit cones were unsuccessful in all tests but one in each test series. One test in 1963 and one test in 1964 of the elastomeric exit cone were partial successes and they served to verify the practicability of the concept. A complete discussion of this work is presented in Ref 1 and 2.

(u) In March 1964, in answer to Purchase Request 3059430 from the Air Force Flight Test Center, Edwards Air Force Base, Aerojet-General subuitted a proposal (Ref 3) for the development, design, fabrication, and demonstration of packageable high-expansion-ratio nozzles for solid propellant rocket motors. As a result of this proposal, a contract was subsequently awarded to Aerojet-General to conduct a program to accomplish the above objectives.

(u) The program was accomplished by conducting: (1) a design and analysis program adapting liquid technology to solid propellant motors, (2) a subscale test program to verify the selected materials, and (3) a demonstration test program that demonstrated the feasibility of elastomeric and metallic packageable exit cones for solid motors.

SECTION II

SUMMARY

(u) This report presents the results of a program for the development, design, fabrication, and demonstration of packageable high-expansion-ratio nozzles for solid propellant rocket motors. The program was conducted by AGC under Contract AF 04(611)-9896.

(u) The program encompassed three main parts:

(u) (1) A basic design and analysis phase to design both an elastomeric foldable and a metallic expandable nozzle exit cone for solid rocket application using liquid rocket experience and technology and a minimum of original design effort.

(u) (2) A subscale testing phase to confirm the material selection, design techniques, and analytical methods based on current technology, as well as to delineate the problems involved in adapting liquid rocket experience to solid rocket motors. Eleven subscale tests were conducted during this phase, nine of the tests with elastomeric exit cones, and two of the tests with metallic exit cones. The subscale exit cones were tested in the expanded position with no attempt at deployment.

(u) (3) The results of the subscale tests were incorporated into the design and fabrication of demonstration exit cones, and three demonstration tests were conducted in the AEDC altitude facilities. Two of the tests were with nitrile butadiene rubber (Gen Gard V-44®, the best elastomeric material from the subscale testing), and one test was with columbium (the better metallic material from the subscale tests). The first elastomeric exit cone was fired in a deployed position, the second elastomeric exit cone was folded and deployed prior to the test, and the metallic exit cone was corrugated into a cylinder that expanded into a conical shape during the firing.

(u) Four motor firings were planned for the third phase, but X-ray examination revealed propellant-liner separation in one of the test motors, and the test series had to be reduced to three firings, thus eliminating a second test of the columbium exit cone.

SECTION III

TECHNICAL DISCUSSION

(u) A great deal of development work on packageable high-expansion-ratio exit cones for liquid rocket motors has been conducted by Aerojet-General. The results of the work on liquid rockets has proved that elastomeric and metallic packageable exit cones can be applied to liquid-rocket-powered missiles to extend range and payload.

(u) As mentioned in the Introduction, two specific types of packageable exit cones have been investigated by Aerojet-General: One type consists of a simple, longitudinally convoluted, sheet-metal exit cone. Before firing, its shape is that of a corrugated cylinder with the convolutions tapering from one end to the other. During motor firing, internal pressure radially expands the exit cone into a truncated conical shape. Longitudinal stiffness is provided by the slight residual corrugations.

(u) The metallic skin of this cone is radiation-cooled, and it is operated at a temperature where the thermal radiation emitted by the external surface is equal to the heat input from the exhaust gas. This is essentially a steady-state condition, and long-duration operation is possible with a very lightweight component.

(u) The second exit cone that has been investigated is one of flexible elastomeric. In this design, the exit cone is folded back over the exterior of the fixed portion of the nozzle. This is deployed before the motor is fired. With this type of exit cone the wall chars and ablates during the firing, and sufficient wall thickness must be provided to supply the necessary structural integrity through the entire firing. The elastomeric exit cone is considerably heavier than the radiation-cooled metallic exit cone, but it offers more promise for obtaining a minimum length and diameter package.

(u) The work performed in Liquid Rocket Operations (LRO) under Contracts AF 05(647)-612/SA4 and AF(694)-212/SA3 and reported in Aerojet-General Reports 652/SA4-22-F-1 and BSD-TDL-64-136 (Ref 1 and 2) indicated that both the metallic and the elastomeric type of exit cones appeared promising for solid rocket motor applications.

(u) The purpose of this program was to take liquid rocket experience and apply it to solid rocket motors, thereby verifying the feasibility of this concept for use on solid rockets. Because of the difference in chemical composition between liquid and solid rocket exhaust gases (as well as the presence of metallic oxide particles in the solid propellant gases), it was necessary to demonstrate that the design concepts developed by the liquid programs could be successfully applied to solid rockets.

(u) As indicated previously, the packageable nozzle program was divided into two test programs. The subscale test program was designed to assess material and verify design for the demonstration test program.

(u) The selection of prospective materials to be evaluated in the subscale test program was based on the testing previously performed in the liquid program.

III, Technical Discussion (cont.)

A. MATERIAL SELECTION

(u) The first major task of the program was to review the various materials, both elastomeric and metallic, that had been tested by Liquid Rocket Operations and to determine their suitability for the solid rocket program. A discussion of materials and determining factors are presented here.

1. Elastomeric Exit Cone Materials

(u) Approximately 30 elastomeric materials were fabricated into exit cones and tested on a small liquid rocket engine under Contracts AF 04(647)-612/SA4 and AF 04(694)-212/SA3 to determine their applicability as a material for packageable exit cones.

(u) In an attempt to adequately evaluate the various elastomeric materials that were tested on the liquid rocket testing program, Liquid Rocket Operations personnel devised a "material effectiveness parameter." This parameter is a function of the following parameters:

1. Test duration
2. Material weight loss
3. Gas recovery temperature
4. Wall temperature
5. Expansion ratio of test exit-cone entrance and exit sections
6. Mass flow rate
7. Throat area

(u) A discussion of the LRO material effectiveness parameter is presented in Appendix I. This "material effectiveness parameter" rates the various materials tested by using weight loss on tested exit cones and normalizes these results by taking into account the variations in total heat flux due to variations in test conditions.

(u) One assumption made in this derivation is that the inner wall temperature for all the materials tested was the same, namely 500°F. Aerojet knows this is not the case; however, it is believed that these material effectiveness parameters do serve as a rough guide to ranking the materials tested.

III, A, Material Selection (cont.)

(u) Analysis of the material effectiveness parameters, an examination of the fired exit cones, and consultations with the personnel responsible for the liquid program revealed that a number of materials showed promise as prospective materials for the development of solid motor foldable exit cones. The three materials that showed the most promise for subscale testing were:

(u) (1) Gen-Gard V-44® nitrile butadiene rubber, silica material, and asbestos reinforced with nylon cord.

(u) (2) General Tire and Rubber 9790-IV-29C styrene butadiene rubber, silica material, and asbestos reinforced with nylon cord.

(u) (3) General Tire and Rubber 7242-I-114X butyl rubber, silica, and asbestos reinforced with nylon cord.

(u) As shown on the table of elastomeric materials tested on the liquid Lark engine (see Appendix I), the above three materials had the highest average material effectiveness parameters. Two other materials, namely ethylene propylene rubber (7409-II-390) and a proprietary material of Raybestos-Manhattan C1-8576-7D, had a high material effectiveness parameter, but these materials had been tested only once, whereas the selected materials received two tests each. The best test of each of the selected materials was equal to the single test of the two rejected materials.

(u) The V-44® material tested on the Lark engine had an acceptably high average. In addition, this material is widely used, with excellent success in many solid rocket motors where subsonic gas flow is experienced. As a result, a great deal is known concerning processing, physical properties, and acceptance criteria for this material. It was thus chosen as a prime candidate for the proposed application.

(u) Large foldable exit cones (approximately 2- to 5-ft-dia) for the second-stage Titan engine made from Gen-Gard V-44® were fabricated and tested by LRO in both the 1963 and 1964 test series, and more tests were planned for 1965. In each of the tests, the main problem experienced was a violent flutter and oscillation during the tests. The V-44® exit cones tested during 1964 had various designs of longitudinal stiffening tubes that provided improved rigidity, and one of these tests was partially successful. The erosion of V-44® was not a problem on these liquid engine tests.

(u) In addition, there were many material evaluation tests conducted with V-44® that provided much pertinent data, so that its performance can be discussed analytically. These tests include plasma tests, RITE motor tests, and tests with the 100-in., 120-in., 260-in., and Minuteman motors. For these reasons, V-44® was a particularly attractive candidate for this program.

III, A, Material Selection (cont.)

2. Metallic Exit Cone Materials

(u) The expandable metallic exit cone program conducted by LRO under Contracts AF 04(647)-652/SA4 and AF 04(694)-212/SA3 was extensive and highly successful. This program included approximately 40 small-scale tests to verify the radiation-cooled exit cone skin temperature and internal supersonic shock analysis.

(u) In 1963, 12 large metallic exit cones were tested at AEDC, and in July 1964, more tests were conducted with large metallic expandable exit cones. All these exit cones were fabricated from 310 stainless steel. In all these tests there were no failures attributed to the thermal environment of pressure loads imposed by the propellant gas stream.

(u) During the 1963 test series of metallic exit cones at AEDC, four failures occurred. Two of these failures were directly attributable to the AEDC altitude facility equipment. The other two failures were due to the exit cone wall striking the top of the diffuser duct during the opening transient.

(u) During opening, the exit cone did not have a true circular cross-section but tended to be elliptical with the major axis rotating. As the expanding wall of the exit cone struck against the diffuser, the thin exit cone ripped in several locations. Those tears did not propagate even though the exit cone folded outward in the ripped area.

(u) All the remaining tests were successful, and durations of up to 113 sec were achieved. In general, flutter occurred during the opening transient with some residual convolutions remaining during the firing. Each of the tests showed that the exit cone was fully open by the time full chamber pressure was reached. At full chamber pressure (and therefore full exit cone internal pressure), the resultant force of the combustion gas pressure was adequate to cause the exit cone to stabilize following the oscillations that occurred as the exit cone opened.

(u) Heat transfer analysis of metal structures is better understood and is more accurate than the thermal analysis of elastomeric material where char and ablation are involved. During the liquid evaluation program, a comprehensive investigation of heat transfer to the metallic exit cone was undertaken, and calculated results were found to agree favorably with the experimental data.

(u) Postfire analysis of both the small exit cone and the considerably larger exit cones fired in the AEDC altitude chamber indicated that the temperatures calculated in the computer program were slightly higher than measured temperatures. Therefore, design based on the computer temperatures were slightly conservative.

III, A, Material Selection (cont.)

(u) Computation of the equilibrium temperature of metallic exit cones that are exposed to solid propellant exhaust gases does not pose any problems. The presence of metallic or metallic-oxide particles in the exhaust gas contributes to the radiant heat-flux into the exit cone, but, at the higher operating pressure of a solid rocket, the total radiative heat flux is small in comparison to the convective heat flux.

(u) The solid particles in the exhaust gases do present another more significant effect in that they obstruct the view of the interior exit cone walls to the outside through the nozzle exit. Thus, the view factor is reduced to zero, and the overall heat-dumping capabilities of the exit cone is therefore lowered.

(u) The fact that the exit cone is cooled by radiation alone tends to make the wall temperature insensitive to small changes in the flux into the wall. The reason for this is fourth-power temperature dependence of radiation heat transfer. A 20% change in the heat flux into the wall results in only about a 4-1/2% change in the wall temperature. Therefore, if the expandable metal exit cone is attached at a point where it can adequately handle the convective heat flux, the radiant heat flux can be neglected.

(u) From this analysis, therefore, it is obvious that the metal exit cone in a solid rocket application will operate at a much higher temperature than the equivalent application in a liquid engine and that some material other than stainless steel must be used to fabricate the expandable exit cones. An analysis of the expected equilibrium temperature for a metallic exit cone on a solid motor has shown that with flame temperatures as high as 6500°F and a chamber pressure of 500 psia, the wall at a 16 to 1 expansion ratio would operate at about 3200°F with an emissivity of one.

(u) At temperatures in this range, the two materials that are attractive from a strength and fabrication consideration are 90% tantalum - 10% tungsten sheet and columbium sheet. For this program, a subscale exit cone was fabricated from each of these materials, and columbium was used for the demonstration-size exit cone.

B. SUBSCALE TEST PROGRAM

(u) A series of 11 subscale tests were conducted in the steam ejector altitude facility at Aerojet-General's Von Karman Center in Azusa during November 1964. These tests served to confirm the material selection, design techniques, and analytical methods used to fabricate the subscale exit cones.

(u) There were nine tests of the elastomeric exit cones, and all nine exit cones were identical except for material composition. Exit cones of each of the three selected materials were tested for 20, 40, and 60 sec. Two tests were made with metallic exit cones, one with columbium, and one with 90% tantalum - 10% tungsten (90Ta - 10W). Each of these was a 40-sec test.

III, B, Subscale Test Program (cont.)

(U) A complete discussion of the designs tested, as well as the supporting activities involved in the subscale test program, is presented in the following sections.

1. Subscale Design

(C) The motor, nozzle, and exit cones tested in this phase of the program are shown in Figure 1. The significant operating parameters of the subscale tests are:

Propellant	ANP-2862 JM Mod II
Chamber pressure, psia	500
Flame temperature, °F	5500
Aluminum content, %	17
Nominal thrust, lbf	134
Mass flow rate, lb/sec	0.45
Expansion ratio of fixed nozzle	20:1
Expansion ratio of test exit cones	20:1 to 50:1
Altitude, ft	70,000
Firing durations:	
Material - Gen Gard V-44®	20, 40, and 60 sec
GTR 9790-IV-29C	20, 40, and 60 sec
GTR 7242-I-114X	20, 40, and 60 sec
90Ta - 10W	40 sec
Columbium	40 sec

(U) Other pertinent design information is discussed in the following paragraphs.

a. Subscale Motor

(U) The motor used for the subscale tests was the Evaluation Test Motor (ETM) shown in Figure 1. This motor is a test vehicle used at Aerojet-General's Von Karman Center. The ETM is a small, end-burning rocket motor used for ablative material screening. It is of heavyweight design and was well suited for the required conditions of this program.

(U) Cartridge grains were used with this motor to facilitate testing. The propellant was cast into an insulating sleeve so the motor could be quickly loaded and unloaded by insertion and removal of this free-standing sleeve.

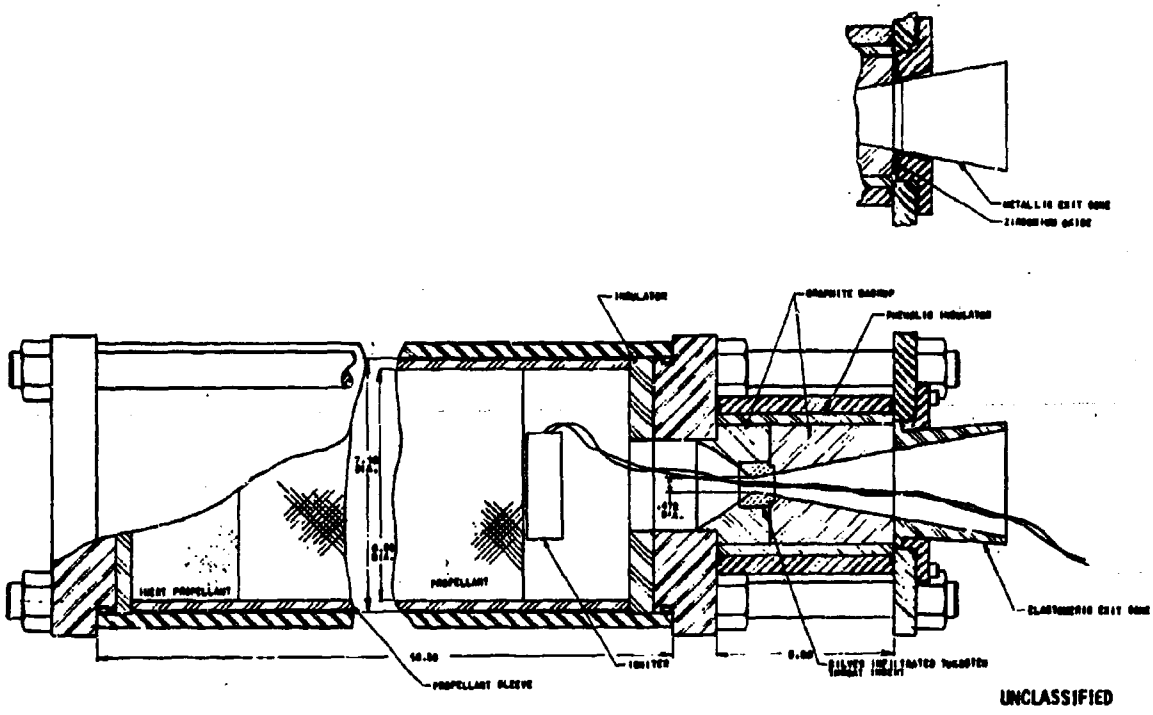

Figure 1. Subscale Motor, Nozzle, and Exit Cone

III, B, Subscale Test Program (cont.)

b. Propellant

(u) The propellant used for both the subscale and demonstration tests was ANP 2862 JM Mod II, an aluminized polyurethane Minuteman propellant. There has been much experience with this propellant, and its properties are well documented. A complete description of the ANP 2862 JM Mod II propellant is given in Table 1.

c. Subscale Nozzle

(u) The nozzle used on the subscale test program is shown in Figure 1. The throat insert is made of silver-infiltrated tungsten. The entrance section and fixed exit-cone section is ATJ graphite. These ATJ graphite pieces also back up the throat insert and provide a heat sink. The graphite pieces are in turn insulated from the steel case by a phenolic sleeve.

d. Elastomeric Subscale Exit Cones

(u) The elastomeric exit cones tested on the subscale motor had the configuration shown in Figure 2. The materials that were used for fabrication as mentioned previously were:

(1) Gen-Gard V-44® - Nitrile butadiene rubber

(2) General Tire and Rubber 9790-IV-29C - Styrene butadiene rubber

(3) General Tire and Rubber 7242-I-114X - Butyl rubber

(u) These exit cones were fabricated by "laying up" the rubber material on a mandrel conforming to the required internal contour. After the rubber was "laid up" to the required thickness (0.44 in. at the entrance, tapering to 0.20 in. at the exit), it was circumferentially wrapped with a single layer of nylon cord. The part was then placed in an autoclave for curing. No longitudinal stiffeners were provided, because the walls of the exit cones were comparatively thick in relation to their diameters and therefore were not expected to be subjected to vibrations that were exhibited in larger exit cones tested by LRO.

(u) The heat-transfer analysis of the subscale exit cone fabricated from Gen-Gard V-44® is presented in III,B,2,a,(2).

e. Metallic Subscale Exit Cones

(u) The two metallic exit cones (one of columbium and one of 90% tantalum - 10% tungsten) that were tested were fabricated in the extended or nonconvoluted (unpackaged) position, as shown in Figure 3, so that only the capability of the material to withstand the thermal and pressure loads in the

TABLE 1

PROPERTIES OF ANP 2682 JM MOD II PROPELLANT (u)

Formulation	Wt%
Ammonium Perchlorate	65.00
Aluminum	17.00
Binder	18.00

Ballistic Properties*

$r = 0.035e^{0.00820\,(T-80)}\,p^{0.39}$

At 80°F

$K = 3.06e^{-0.00082\,(T-80)}\,p^{0.71}$

Mechanical Properties

	-40	0	77
ε_m, %	5	22	49
S_m, psi	767	400	129
E_o, psi	23,090	4,230	575

Thermodynamic Properties

Specific impulse, lbf-sec/lbm	
Theoretical	261.6
Experimental	243.2**
Chamber flame temperature, °F	5650 at 1000 5500 at 500
Exhaust flame temperature, °F	3235 at 1000 3590 at 500
Average molecular weight of gases, g/mol	28.56 exhaust at 1000
Effective isentropic flow coefficient	1.20
Heat of formulation, kcal/100g	-51.789
Density, lb/cu in.	0.0635
Autoignition temperature, °F	520
Impact stability, cm/3kg	15
ICC Shipping classification	B

Constant strain withstood: 15% >168 hr at 40°F C_w = 0.00623 lbm/lbf-sec

* Data from ninety-six 3KS-500-size motors
** Data from eight 10KS-2500-size motors

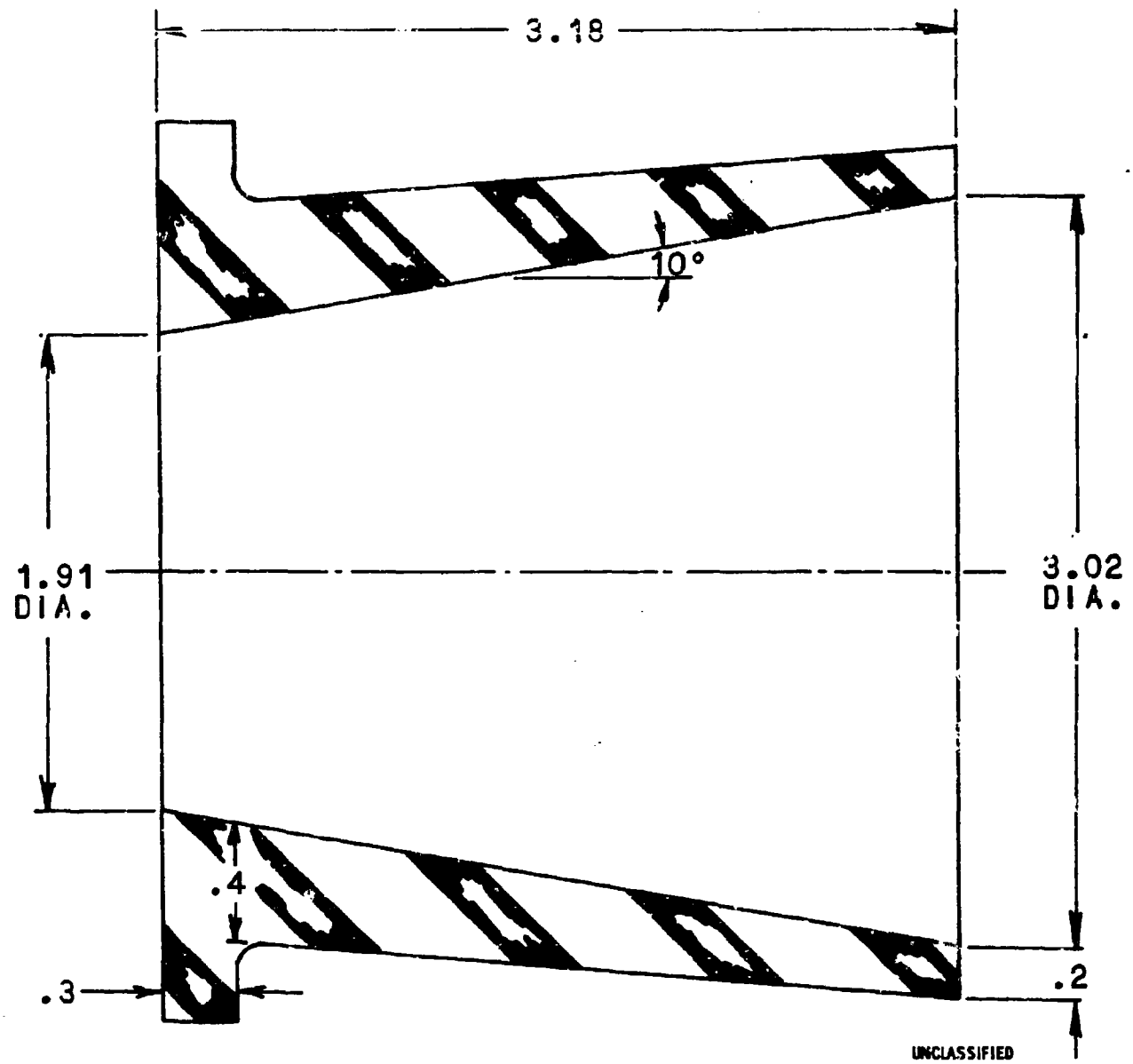

Figure 2. Subscale Elastomeric Exit Cone

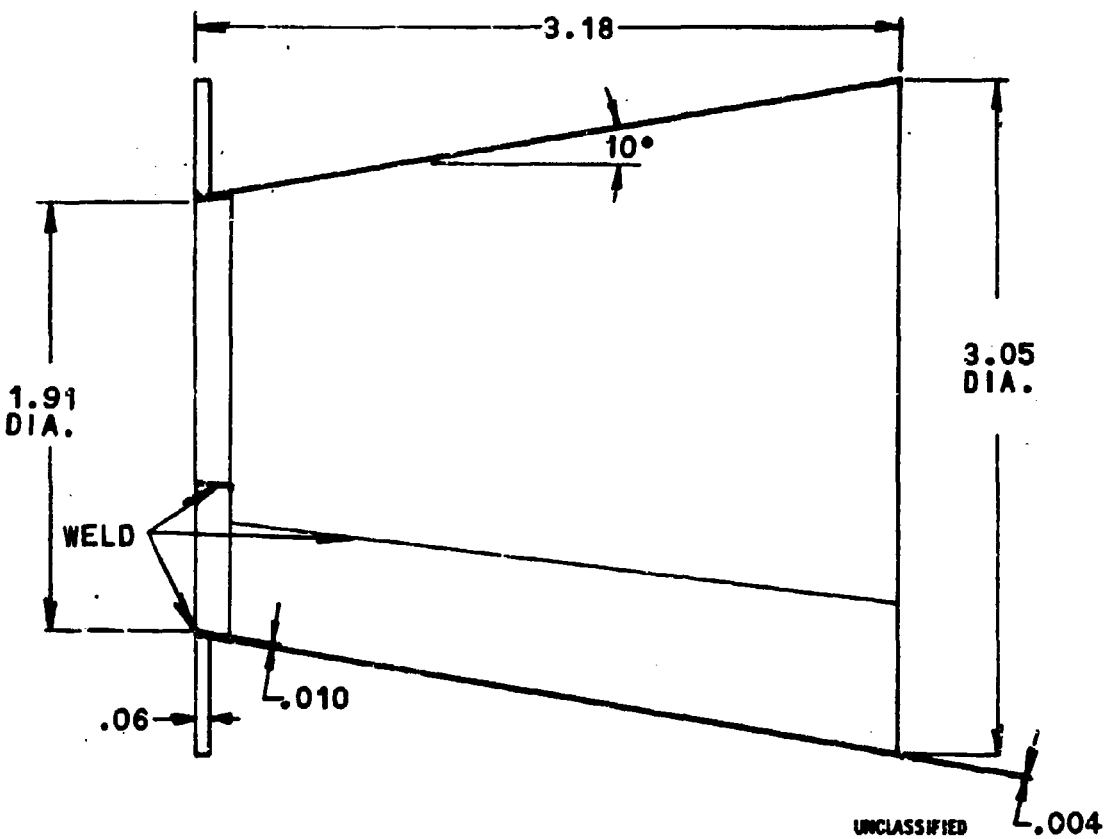

Figure 3. Subscale Metallic Exit Cone

III, B, Subscale Test Program (cont.)

deployed position was determined. These cones were fabricated from 0.005-in.-thick sheet metal. The test exit cones were instrumented with thermocouples to check the predicted radiation levels.

(u) To ease the fabrication problem of welding a flange to the 0.005-in.-thick exit cone, it was deemed advisable to incorporate a local inner ring of 0.010-in.-thick material. This introduced a local discontinuity in the gas flow just downstream from the resulting 0.010-in. step. An analysis of the expected effects on the heat flux in this region indicated they would be slight (Ref 4) and would, therefore, not jeopardize the design. This assumption proved to be true.

f. Subscale Igniter

(u) The igniter to be used for the subscale tests consisted of 7 gm of BPN pellets loaded into a plastic capsule. Igniters of this type were used successfully to ignite end-burning grains in 5KS-500 motors under altitude conditions and proved adequate for this program.

2. Subscale Design Supporting Studies

a. Heat Transfer

(C) This section presents the final results of the heat-transfer analyses that were completed in support of the subscale test program. Included are predicted temperature profiles, erosion depths, and equilibrium temperatures of the subscale nozzle and exit cones. A brief discussion of the physical parameters and procedures utilized in these studies is also presented. All transient thermal analyses were made for a 60-sec firing with a constant chamber pressure of 500 psia. The ANP-2862 JM Mod II propellant to be used on this program had the following thermal and transport properties:

ANP-2862 at 500 psia

$T_c = 5500°F$
$C_W = 0.0063$ lb/sec
$\mu = 6.11 \times 10^{-5}$ lb/ft sec
$C_p = 0.505$ Btu/lb °F
Prandtl No. = 0.450

(u) Based on these data and the appropriate equations given in Appendix II, the throat heat-transfer coefficient is 2700 Btu/hr ft^2 °F. At stations away from the throat, the above heat-transfer coefficients were modified as a function of area ratio by the procedure outlined in Appendix II.

III, B, Subscale Test Program (cont.)

(u) With the above heating rates as boundary conditions, all temperature predictions were calculated using one of the two separate numerical solutions to the general transient heat flow equation that are programed on the IBM 7094 computer. A description of each computer program, including an outline of the applicability of each solution for various nozzle configurations, is given in Appendix III.

(u) Thermal property data for all materials used herein are noted in Table 2.

(1) Nozzle

(u) The initial thermal evaluation considered the throat region of the subscale nozzle. This configuration (Figure 4), because of its small throat diameter, was analyzed considering both radial and axial heat flow. Resulting temperatures are noted in Figures 5 and 6 for the various point locations given in Figure 4. Figure 5 represents the throat region wherein the predicted surface temperature level for the tungsten will be approximately 4150°F after a 60-sec firing. Internal temperatures at this time will be 3575 and 2240°F at the tungsten-graphite and graphite-silica interfaces, respectively.

(u) The thermal environment of the silica tape backup will vary between 2240 to 290°F on the exterior surface. Local charring of the silica can be expected to a depth of approximately half the original thickness. This condition, however, will not adversely influence the design, because the charred material still provides adequate thermal protection.

(u) Data given in Figure 6 represents an area ratio of 6.9. Here the temperature rise is a nominal 3200°F on the graphite surface. Interior temperatures are 2025 and 260°F, respectively, on each side of the silica tape. Again, local charring can be expected and will be the same as found in the throat region.

(u) In general, no undue temperature condition was found to exist in the subscale nozzle throat region.

(2) Elastomeric Exit Cones

(u) Analysis of the rubber expandable exit cones included consideration of several possible material loss mechanisms. First, a one-dimensional temperature prediction at two area ratios (23.8 and 46.6), wherein the local heat transfer coefficients are 155 and 84.5 Btu/hr ft^2 °F, respectively, assumed zero material loss. The rubber used was V-44[illegible], and the resulting temperature histories for a 0.30-in. layer at each location are given in Figure 7.

TABLE 2

THERMAL PROPERTY DATA FOR
EXPANDABLE NOZZLE PROGRAM MATERIALS

Material	Temp. °F	Conductivity, Btu/hr ft°F	Density, lb/ft^3	Specific Heat, Btu/lb°F
ATJ	75	64.5	108	0.205
	1500	35.0		0.442
	3000	24.7		0.530
	5000	21.4		0.550
Tungsten	Avg.	67.0	1187	0.039
90Ta - 10W	Avg.	44.5	1050	0.030
Columbium	Avg.	31.0	535	0.065
V-44®	750	0.133	80.8	0.41
Steel	Avg.	23.0	489	0.123
Phenolic-impregnated insulation	Avg.	0.171	71.8	0.40

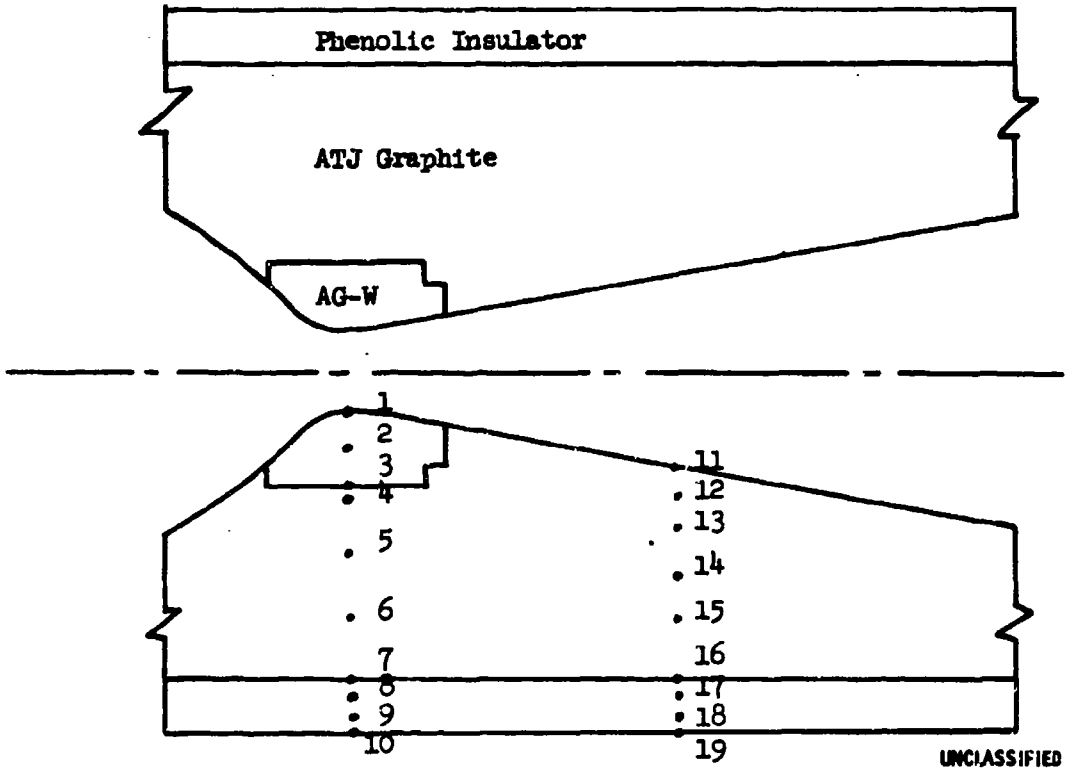

Figure 4. Map of Subscale Nozzle for Thermal Analysis

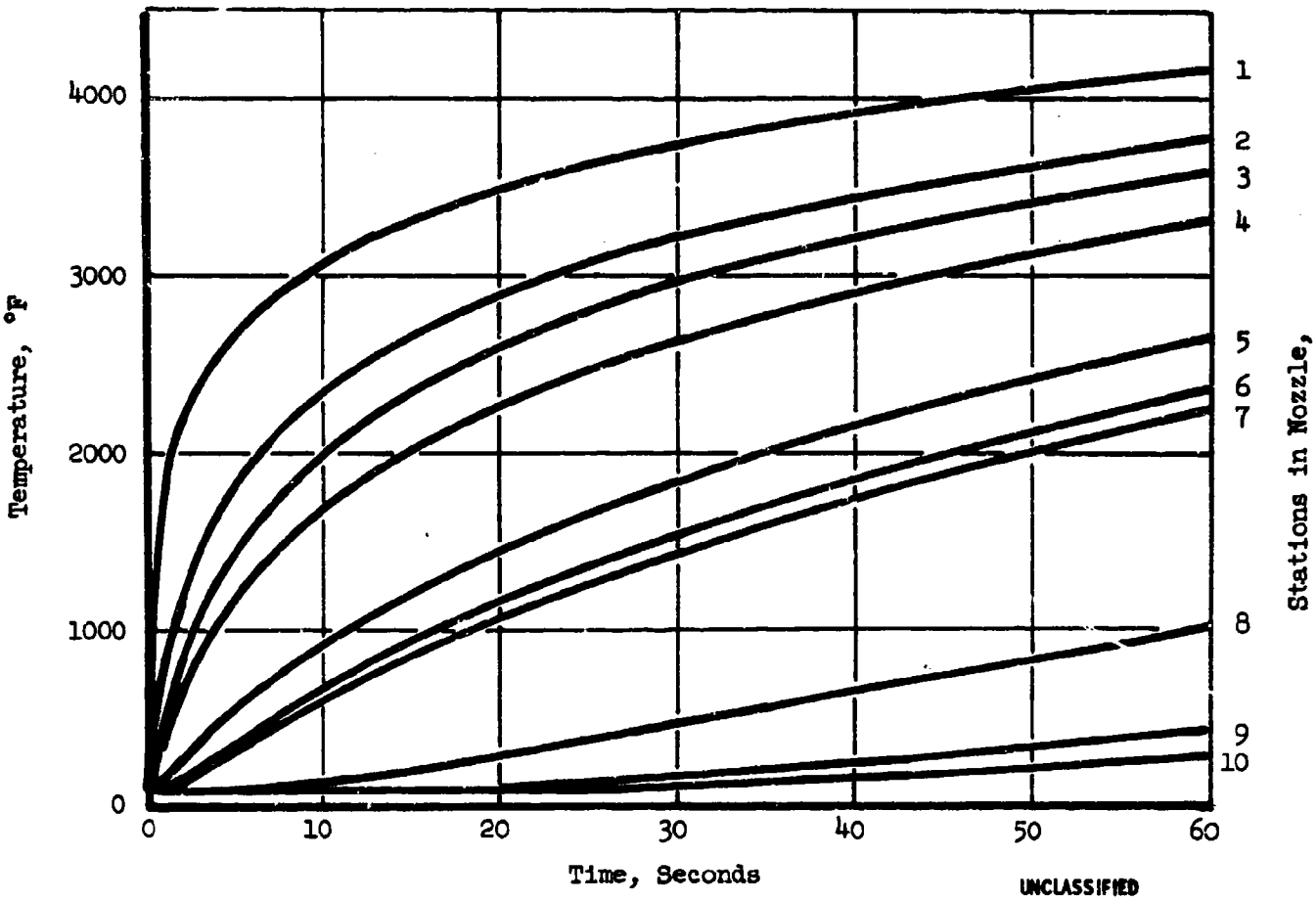

Figure 5. Temperature Profiles at the Throat of Subscale Nozzle

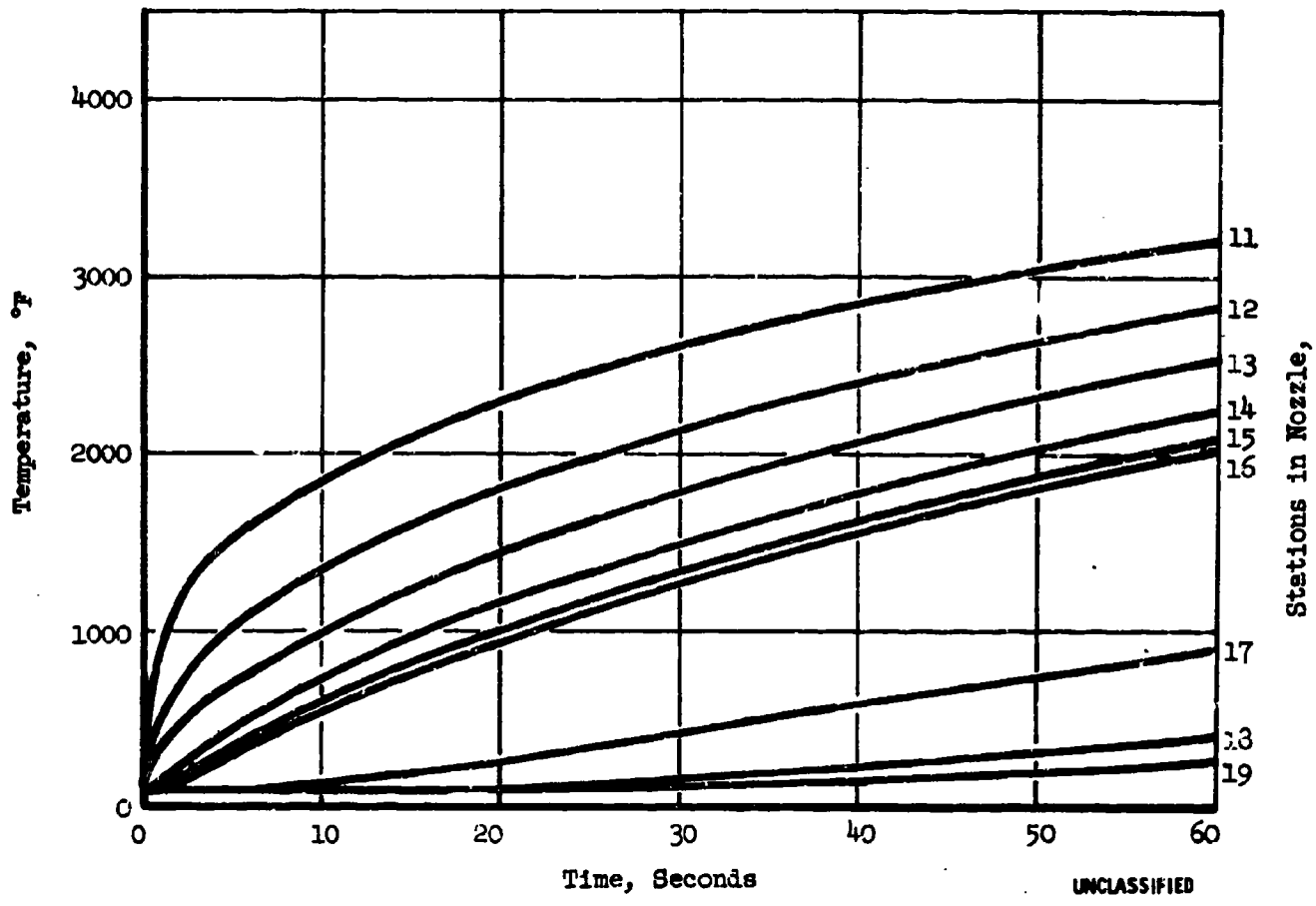

Figure 6. Temperature Profiles in the Exit Cone of Subscale Nozzle, $\epsilon = 6.9$

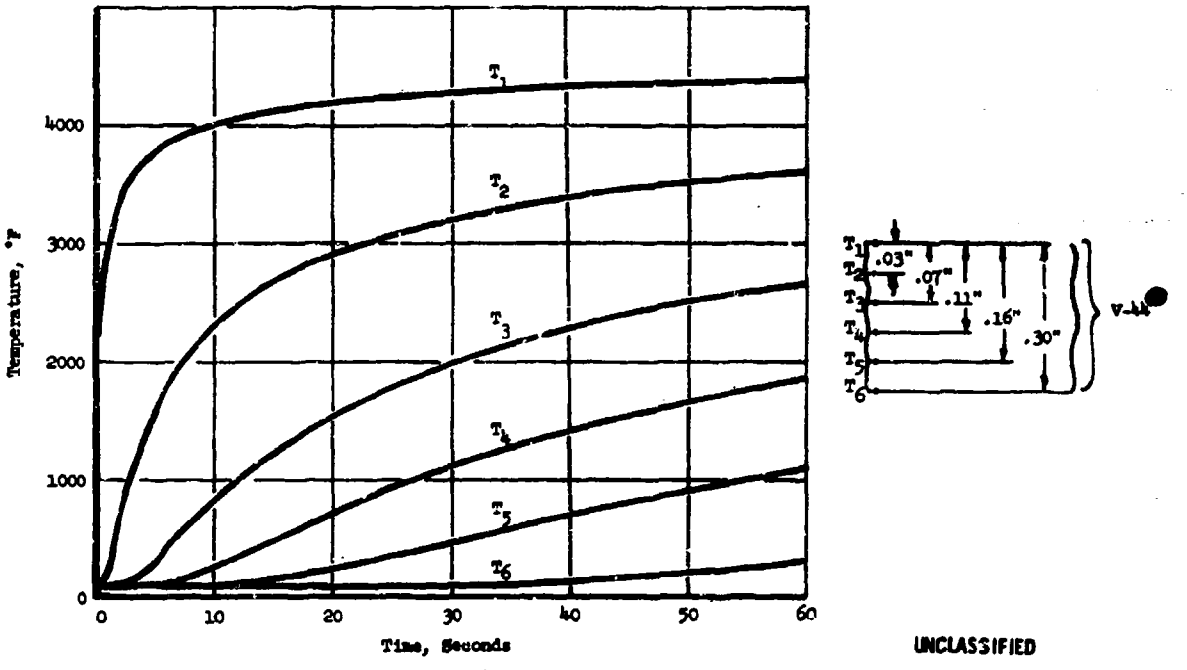

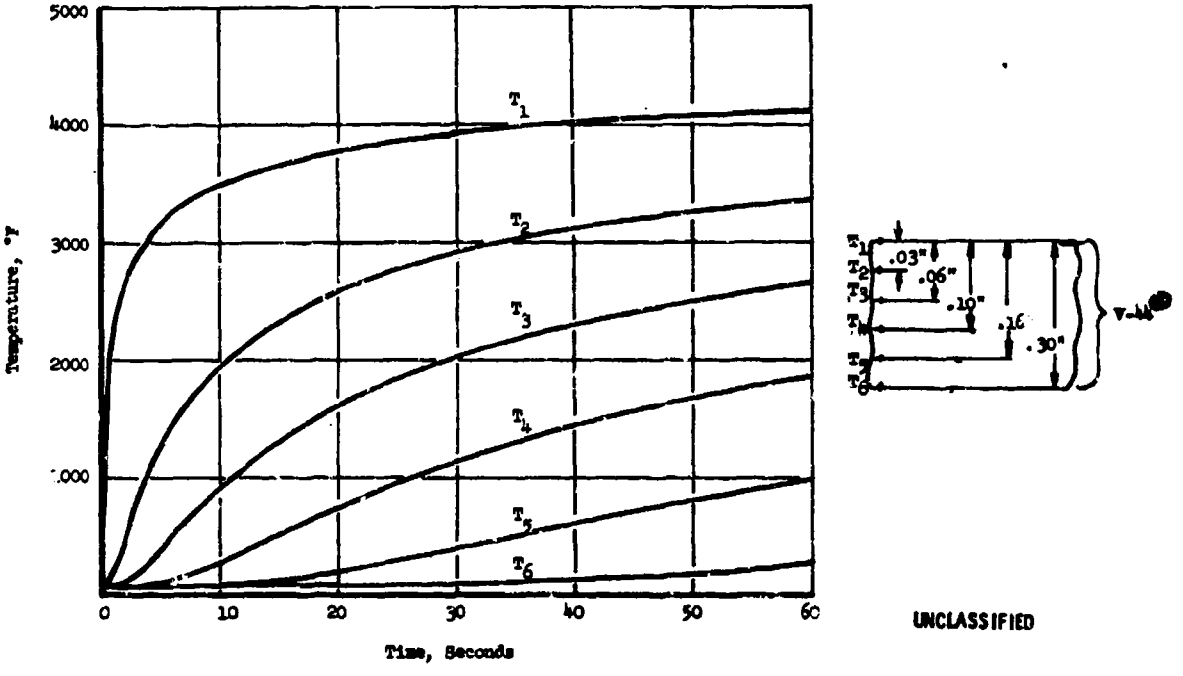

b. at ε = 46.6

Figure 7. Temperature Profiles in Subscale V-44® Exit Cone (Assuming No Material Loss), ε = 23.8, ε = 46.6

III, B, Subscale Test Program (cont.)

(u) For this case, the calculated temperatures range from approximately 4000°F on the interior surface to 300°F on the exterior. These conditions are hypothetical in that the V-44® rubber is not capable of withstanding such a severe thermal environment.

(u) It has been found from plasma-jet tests performed at Aerojet-General that the temperature of initial pyrolysis is approximately 500 to 750°F, while the effective surface temperature of the char is as high as 2800°F (Ref 5). The magnitude of char surface temperature has been verified by thermocouples buried within V-44® rubber insulation in the entrance region of a solid propellant motor nozzle.

(u) It was also found that the measured local erosion rate could be correlated with analytical estimates for a fairly large variation in flow velocity and pressure (heat flux) if the "effective heat of ablation" were taken as 2500 Btu/lb.

(u) Consideration of local flow similarity between the expadable nozzle exit cone flow conditions and the experimental data obtained in the entrance region indicates a lower thermal environment but slightly higher wall shear stress will exist in the exit cone. As a result, it is anticipated that, due primarily to the higher shear stress acting on the char layer, a slightly increased erosion will exist in the exit cone.

(u) The expected temperature histories at the same locations given above (considering the best estimate of local V-44® rubber erosion) are presented in Figure 8. For a 60-sec firing, approximately 0.25 in. of erosion is expected at the lower area ratio.

(u) Near the exit plane, local erosion was estimated to be approximately 0.13 in.; the estimated backside temperature for a 0.3-in. thickness was 600°F at 60 sec. Based on this analysis, a wall thickness of 0.4 in. was selected for the elastomeric exit cones tested in the subscale program.

(u) All estimates of V-44® erosion assume that degradation and subsequent material loss are the result of only the local thermal environment. The influence of mechanical forces, with the exception of the shear stress transmitted from the gas to the wall, which is indirectly incorporated in the above erosion estimates (Reynolds analogy), was not included because of the lack of pertinent data.

(u) It is obvious that rubber exit cones will not exhibit the rigidity which exists within the entrance region of a nozzle. Thus, the influences of vibration and amplitude of motion for the exit cone extensions will be to increase material loss. It is possible that these mechanical forces could strip the char layer as fast as it is formed. As an example, a prediction of the loss rate for the upstream area ratio indicates a 0.3-in. layer could be lost in 3.5 sec, assuming immediate removal at a char formation temperature of 750°F.

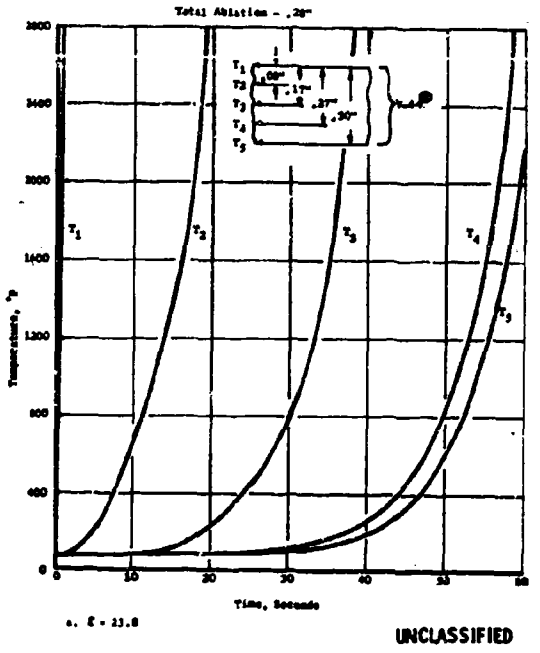

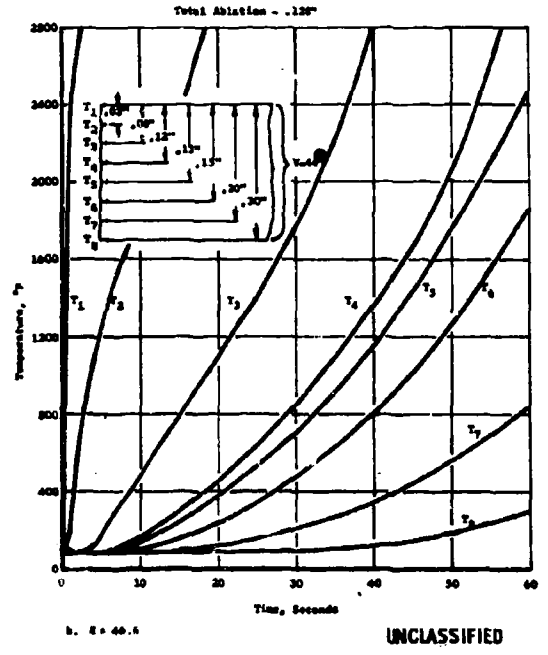

Figure 8. Temperature Profiles in Subscale V-44® Exit Cone (Estimating Erosion), ε = 23.8, ε = 46.6

III, B, Subscale Test Program (cont.)

(u) Inclusion of the mechanical effects for erosion predictions will depend directly on the surface temperature of the exit cone material. First, the surface temperature determines the rate of heat transfer between the gas and the wall; the higher the value, the lower will be the attendant heat input and char formation rate.

(u) Second, the strength temperature relation of the material will be important. The char strength must be as high as possible so as not to fail under the mechanical loads. An estimate of the time for failure of a 0.3-in. V-44® layer at an area ratio of 23.8 for various maximum char surface temperatures is summarized as follows:

Surface Temperatures, °F	Estimated Time to Erode 0.3 in. of V-44®, sec
750	3.5
1640	30
2040	39
2800	53

(u) From this summary, it is apparent that surface temperature and char strength are very important considerations in the design of rubber exit cones. Thus, the use of V-44® as a prospective material is justified because the many applications and tests given it in a subsonic environment have shown it to have a tenacious char layer. Sufficient data was not obtained to thermally analyze the other two candidate elastomeric materials, but it was postulated that the predictions for the V-44® would apply generally to these materials.

(3) Metallic Exit Cones

(u) Analysis of prospective metallic, radiation-cooled, expandable exit cones for the subscale motor considered both 90Ta - 10W and C-103 columbium alloy. The physical properties used in the design are given in Appendix IV. Equilibrium temperatures (radiation from the external surface being equal to the net internal heat input) at exit cone area ratios of 23.8 and 46.6 indicate the following values:

Columbium	$\varepsilon = 23.8$	$T = 3798°F$
	$\varepsilon = 46.6$	$T = 3373°F$
90Ta - 10W	$\varepsilon = 23.8$	$T = 3560°F$
	$\varepsilon = 46.6$	$T = 3034°F$

III, B, Subscale Test Program (cont.)

(u) The above results were obtained by using the total emissivity of the pure untreated material. The values of emissivity used were:

Columbium	ϵ	= 0.179 at 3400°F
	ϵ	= 0.202 at 3600°F
90Ta - 10W	ϵ	= 0.328

(u) If there were suitable exterior coatings available that could increase the effective emissivity, the equilibrium temperature could be decreased as indicated in the following summary:

Assumed Emissivity	Area Ratio	Material	Temperature, °F
0.65	23.8	Columbium	3233
0.65	23.8	90 Ta - 10W	3221
0.65	46.6	Columbium	2833
0.65	46.6	90 Ta - 10W	2758
0.85	23.8	Columbium	3089
0.85	23.8	90 Ta - 10W	3080
0.85	46.6	Columbium	2697
0.85	46.6	90 Ta - 10W	2638

(u) Because the metallic exit cones can withstand the buckling loads (Appendix IV) when operating at the temperatures predicted from the low emissivity values, no attempt was made to coat the surface of the metallic exit cones to improve the emissivity of the surface, as this effort was beyond the scope of this program.

b. Thermal Stress

(u) The thermal stress analysis of the subscale motor, nozzle, and metallic exit cone indicated that all stress levels were well within satisfactory levels to withstand the required firing conditions. This complete and comprehensive study is included as Appendix IV, along with the description of the digital computer program utilized.

(u) The analysis indicated that the critical stress for the subscale metallic exit cones was the hoop stress in the columbium cone. The margin of safety for this critical condition was 1.63.

III, B, Subscale Test Program (cont.)

3. Subscale Test Results

(u) A series of 11 subscale tests were conducted in the steam ejector altitude facility at Aeojet-General's Von Karman Center during the first and second week of November 1964. A complete discussion of the test results, as well as the test objectives, is presented in the following sections.

a. Subscale Motor

(u) The motor, nozzle, and exit cones that were tested on the subscale program are shown in Figure 1. (Figure 1 indicates a throat insert of silver-infiltrated tungsten, whereas on the test series some of the inserts were silver-infiltrated tungsten and others were forged tungsten.)

(u) The motors and fixed nozzles survived the complete test series in excellent condition. The graphite entrance pieces and the graphite exit cones had very little erosion. The throat inserts had no erosion, but they were coated with aluminum oxide deposits at the end of the firing.

(u) Pressure-time and thrust-time histories for each test are presented in Figures 9 thru 13. As is evident on these curves, the thrust traces are all neutral, whereas the pressure traces are all regressive to varying degrees.

(u) One reason for the overpressurization evident at the start of each test is the aluminum oxide deposits that occur in the throat. At the beginning of each test the aluminum deposits on the small (0.427-in.-dia) cold throat insert, thereby reducing the throat area and raising the chamber pressure. The thrust tends to remain relatively constant as long as the nozzle throat area is reduced in proportion to the pressure rise.

(u) The thrust curves are in question because a zero shift occurred during each test, and a complete force calibration of the test fixture was not made for each test. The oscillograph records do indicate that the thrust was neutral as shown, but the absolute value of the thrust cannot be determined with sufficient accuracy to establish exit cone thrust performance in the subscale test.

(u) Excellent performance data were obtained on demonstration tests conducted at Arnold Engineering Development Center that served to verify the near-theoretical performance capability of packageable exit cones. These results are discussed in the Demonstration Tests, III,C,2.

(u) The subscale tests did provide (1) erosion data on the tested elastomeric materials, (2) a screening vehicle for the two tested metallic materials, columbium and 90Ta - 10W, and (3) heat transfer data on all of these materials.

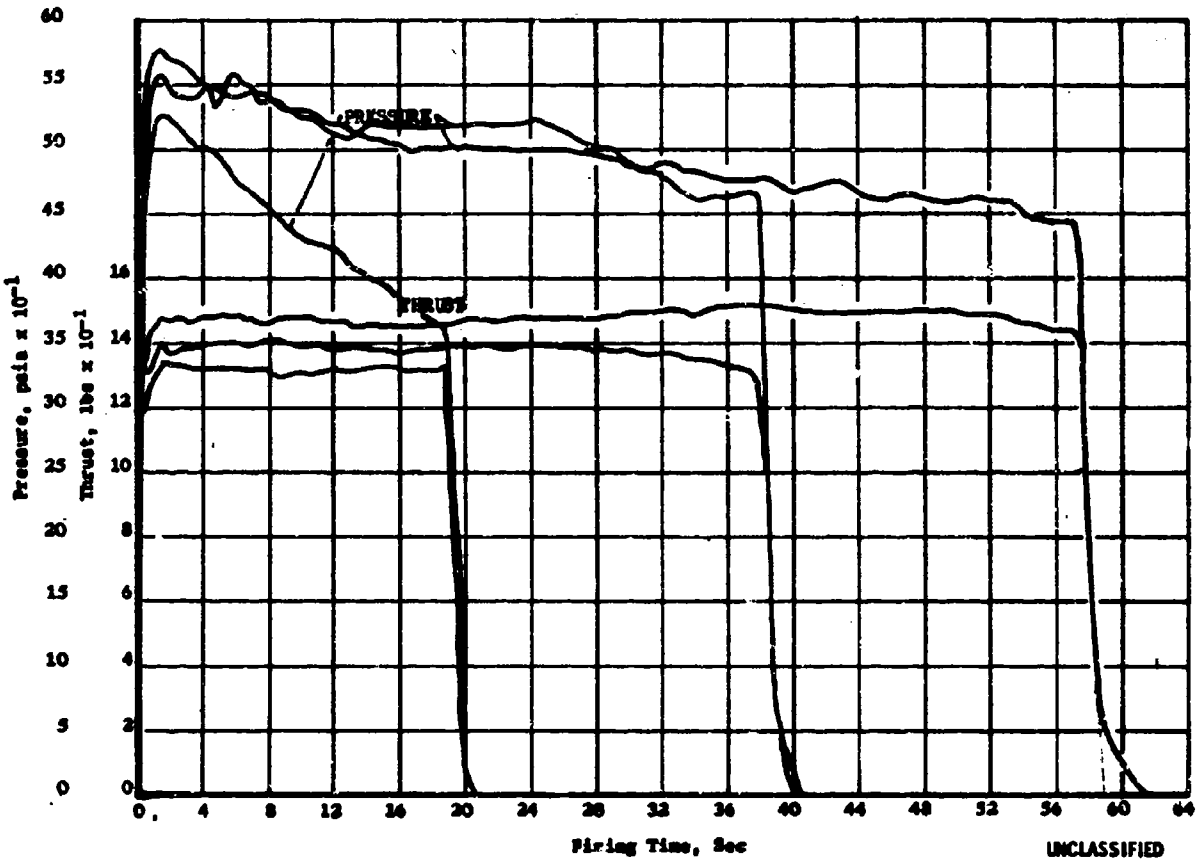

Figure 9. Pressure and Thrust for V-44® Subscale Tests

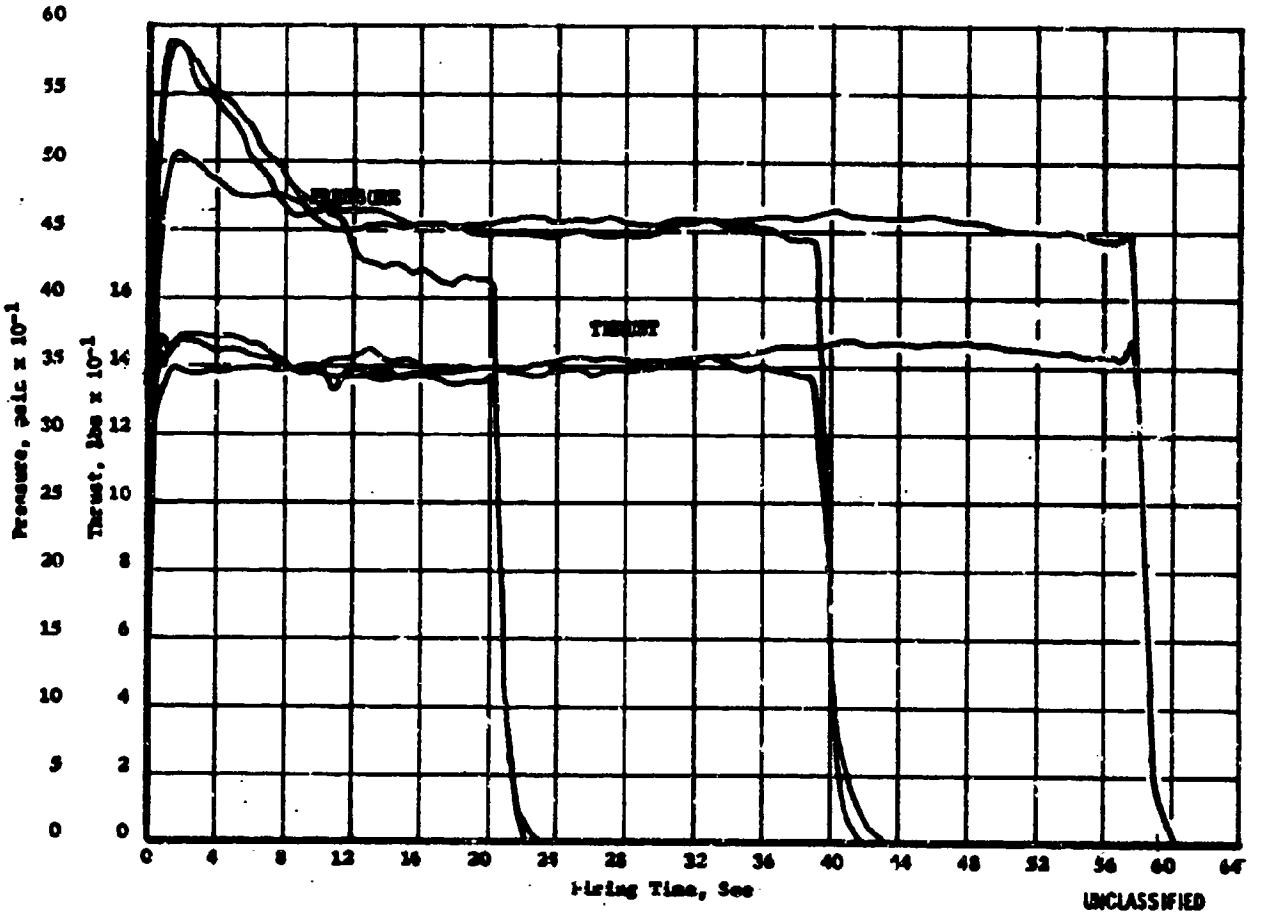

Figure 10. Pressure and Thrust for Styrene Butadiene Subscale Tests

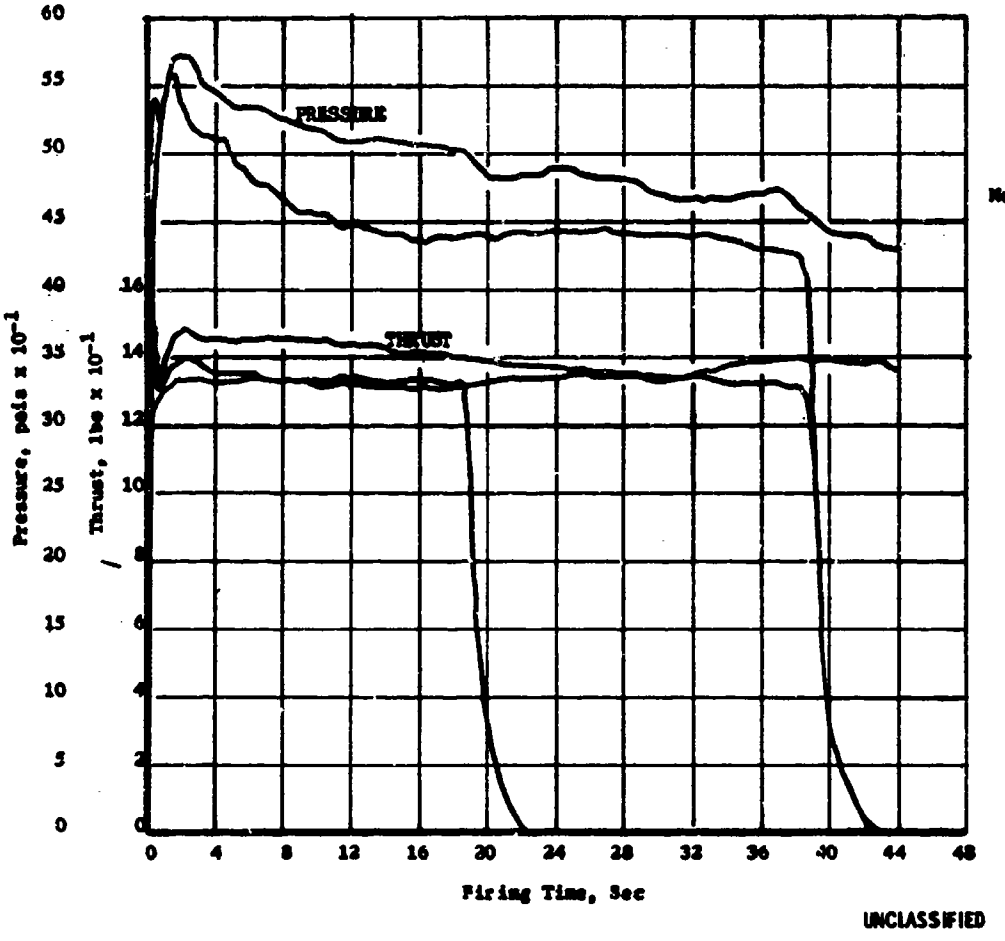

Note: Oscillograph paper ran out during 60 sec test.

Pressure tap was plugged on 20 sec test.

Figure 11. Pressure and Thrust for Butyl Subscale Tests

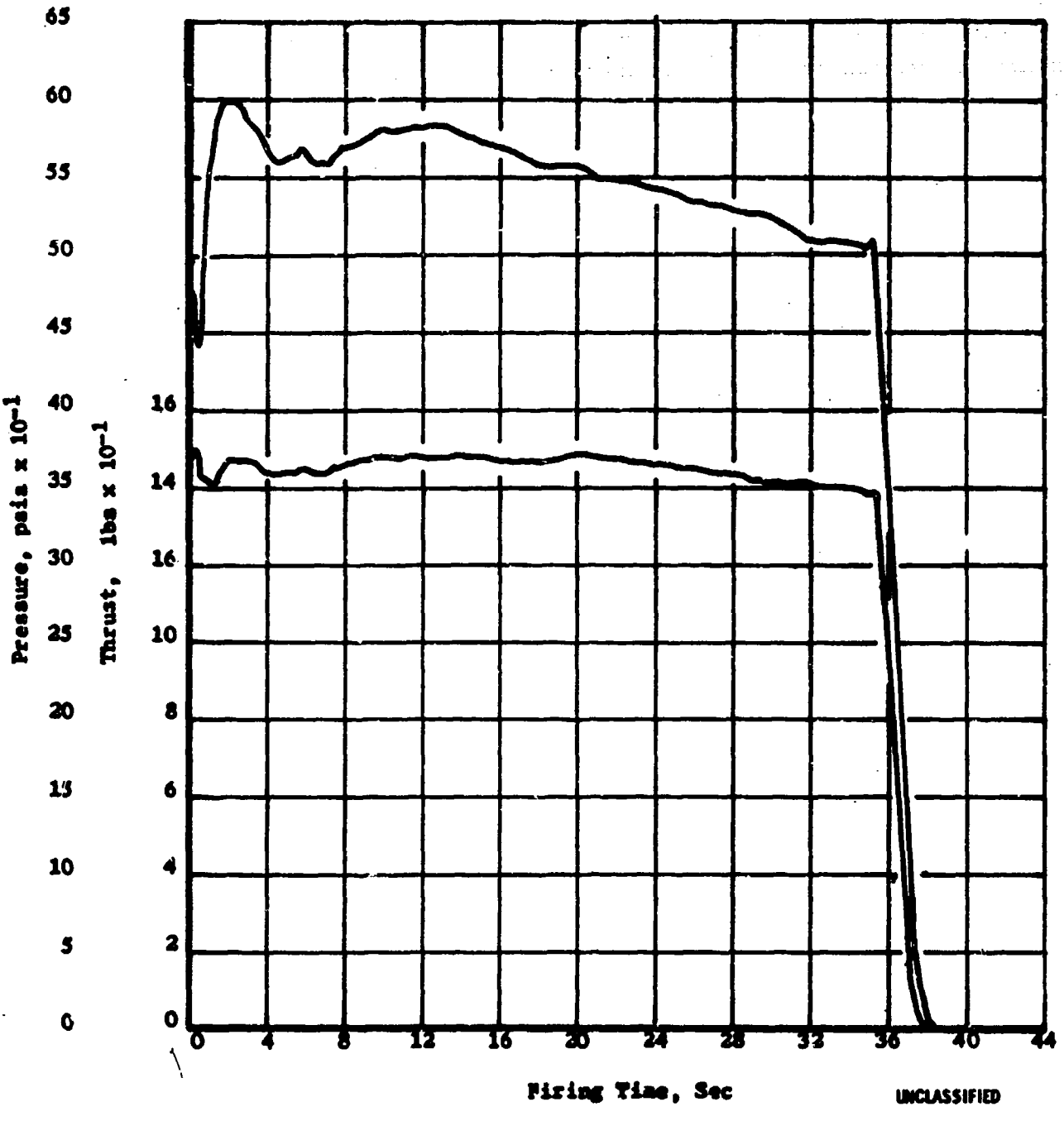

Figure 12. Pressure and Thrust for Columbium Subscale Test

Figure 13. Pressure and Thrust for 90Ta - 10W Subscale Test

III, B, Subscale Test Program (cont.)

b. Elastomeric Exit Cones

(u) The elastomeric exit cone that was tested on the subscale motor is shown in Figure 14. The materials tested were:

(1) Gen-Gard V-44® - Nitrile butadiene rubber, silica- and asbestos-filled, reinforced with a nylon cord wrap.

(2) General Tire and Rubber 9790-IV-29C - Styrene butadiene rubber, silica- and asbestos-filled, reinforced with a nylon cord wrap.

(3) General Tire and Rubber 7242-I-114X - Butyl rubber, silica- and asbestos-filled, reinforced with a nylon cord wrap.

(u) Each of the above materials showed promise for use in foldable exit cones. Each material that was tested for a 20-sec duration survived in excellent condition.

(u) An anomaly that was exhibited on all the elastomeric exit cones tested was the presence of longitudinal grooves that ran the length of the cone and were spaced around the perimeter, giving the part a scalloped effect. This grooving can probably be attributed to the aluminum oxide deposits in the throat, which would result in an asymmetrical flow pattern and/or the "sluffing off" of these hot aluminum deposits and could sear the elastomeric material.

(u) Motion picture coverage was provided on each of the 60-sec tests. From the film it was determined that the amount of exit cone flutter during the tests was negligible. There did appear to be some vibration near the end of these tests after the elastomeric wall had been eroded in the exit area.

(u) An examination of the fired parts showed that there was high erosion in the exit area on the longer tests. As the part eroded and the wall thickness was reduced, the ability to withstand the pressure loads was impaired. Once the part became weak enough to allow vibration, the char layer was broken off, and the erosion process accelerated.

(1) Nitrile Butadiene (V-44®)

(u) The pressure, thrust, and temperature traces for the three tests are shown in Figures 9 and 15. The postfire condition of the three exit cones fabricated from this material is shown on Figure 16. The V-44® material proved to be the best of the three candidates on the 60-sec tests.

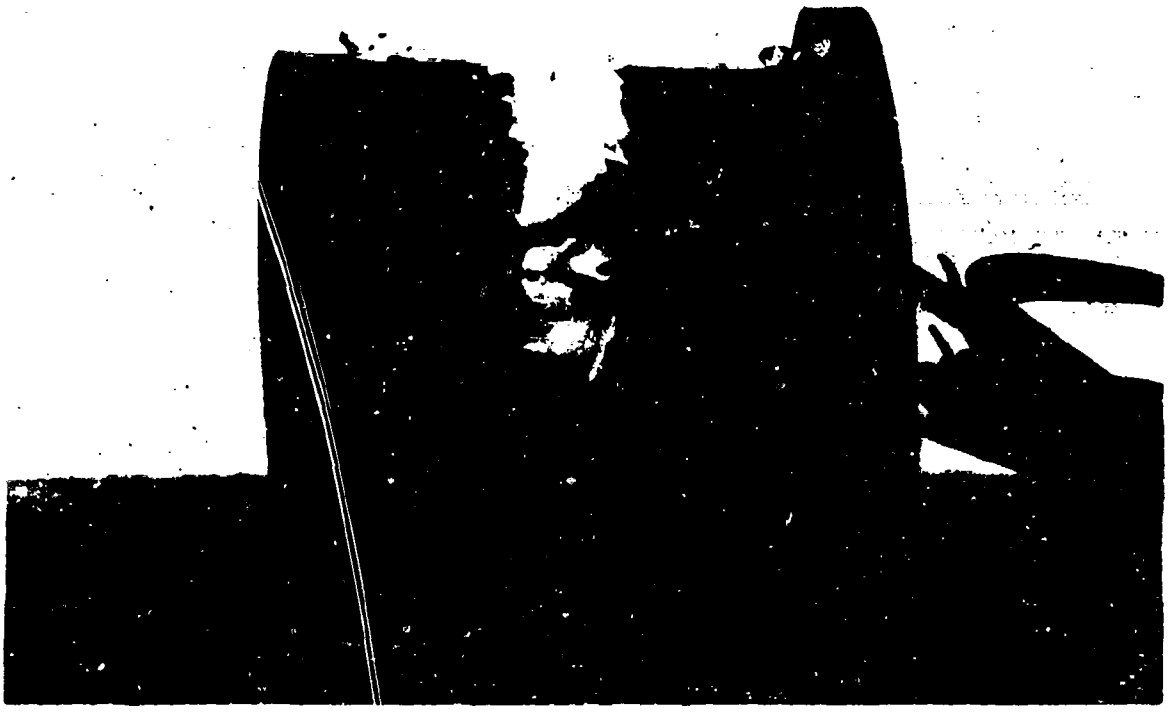

UNCLASSIFIED

UNCLASSIFIED

Figure 14. Prefired Elastomeric Exit Cone with Thermocouples

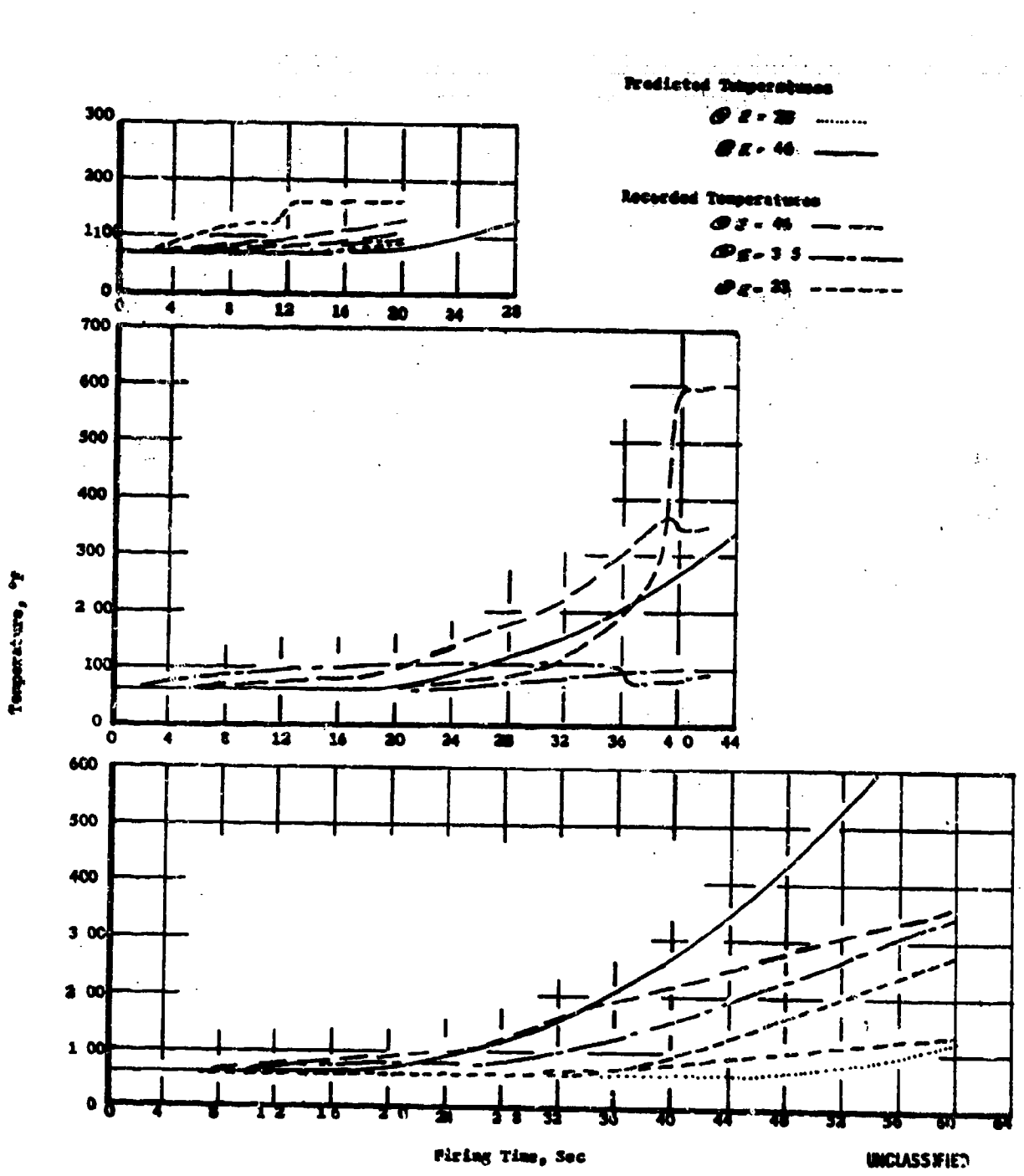

Figure 15. Backside Temperatures for V-44® Subscale Exit Cone Tests

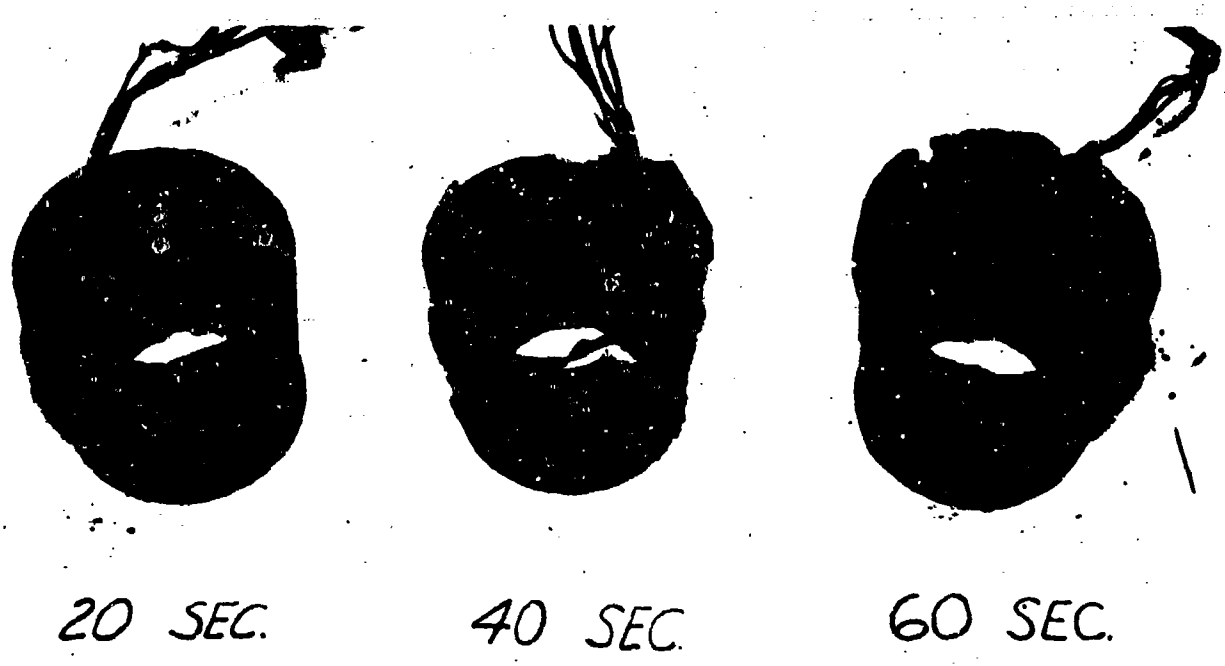

UNCLASSIFIED

Figure 16. Postfired V-44® Subscale Exit Cones

III, B, Subscale Test Program (cont.)

(a) 20-Sec Test

(u) The total erosion was approximately 35 gm or 16.5% of total weight. Prorated over the entire surface area exposed to the flame, this would amount to an erosion of 0.0683 in. or 3.4 mils/sec. The indicated temperature rise on the back side was minimal, as was predicted for this short duration.

(b) 40-Sec Test

(u) The total erosion was approximately 105.5 gm or 49.5% of total weight, and, prorated over the entire surface area, 0.205 in. of erosion. Actually, the erosion was more pronounced downstream at the exit section. As can be seen in Figure 16, the exit is scalloped, the material is completely eroded in some places, and is paperthin at other points. The thermocouples located where the area ratio was 46 to 1 measured a temperature rise late in the test because of the high erosion in this area.

(c) 60-Sec Test

(u) The total erosion in this test was approximately 66 gm or 31% of total weight. Over the entire surface this would amount to 0.129 in. of erosion. As can be seen from the weight loss shown in Table 3 and the photograph shown in Figure 16, this part was in better condition than the one from the 40-sec test. There is no known explanation for this anomaly because there were no known variations in test conditions or material properties. The exit section on this exit cone did become bell-shaped during the firing, and this is clearly evident in the motion pictures late in the test.

(2) Styrene Butadiene

(u) The pressure, thrust, and [illegible]s for the three tests are shown in Figures 10 and 17. The postfire p[illegible] these exit cones is shown in Figure 18. This material was the be[illegible]terials tested for 40 sec, but it was destroyed during the 60-sec test.

(a) 20-Sec Test

(u) The total erosion was approximately 36 gm or 16.9% of total weight. Over the entire surface this would amount to 0.0702 in. of erosion. The recorded temperature rises were minimal.

(b) 40-Sec Test

(u) This exit cone was the best of the three tested for 40 sec. Two of the thermocouple readings indicated a 100°F temperature rise. The other thermocouple indicated a temperature rise to 315°F at 28 sec, at which point the

TABLE 3

EROSION DATA FROM SUBSCALE TESTS OF ELASTOMERIC HEAT GUNS (M)

Material Duration, sec	Weight Loss, gm	Weight Loss, %	Erosion Rate Based On Weight Loss, mils/sec	Measured Erosion Rates* at ε = 23, mils/sec Max.	Avg.	Measured Erosion Rates* at ε = 35, mils/sec Max.	Avg.	Predicted Erosion Rates (V-44)[8] (See Fig. 8) ε = 23	ε = 46
Nitrile Butadiene (V-44)[8]									
1. 20	35	16.5	3.4	6.0	3.9	7.0	4.0	4.0	1.5
2. 40	105.5	49.5	5.2	4.5	3.9	7.0	4.8	4.5	2.0
3. 60	66	31.0	2.2	3.0	2.3	3.0	2.1	4.7	2.2
Styrene Butadiene									
1. 20	36	16.9	3.5	6.0	3.8	6.0	4.6		
2. 40	75.5	35.4	3.7	4.5	3.0	5.0	3.1		
3. 60	Destroyed during test								
Butyl Rubber									
1. 20	30	14	2.9	7.0	3.8	10.0	4.3		
2. 40	97.5	46.7	4.8	4.3	3.1	6.5	4.0		
3. 60	106.5	50.5	3.5	3.7	2.7	5.3	3.3		

* Figures 21 thru 23 show the erosion for the listed area ratios.

** Erosion data is present at ε = 35 because the sectioned parts could be sectioned at this point and not at ε = 46 as was originally calculated.

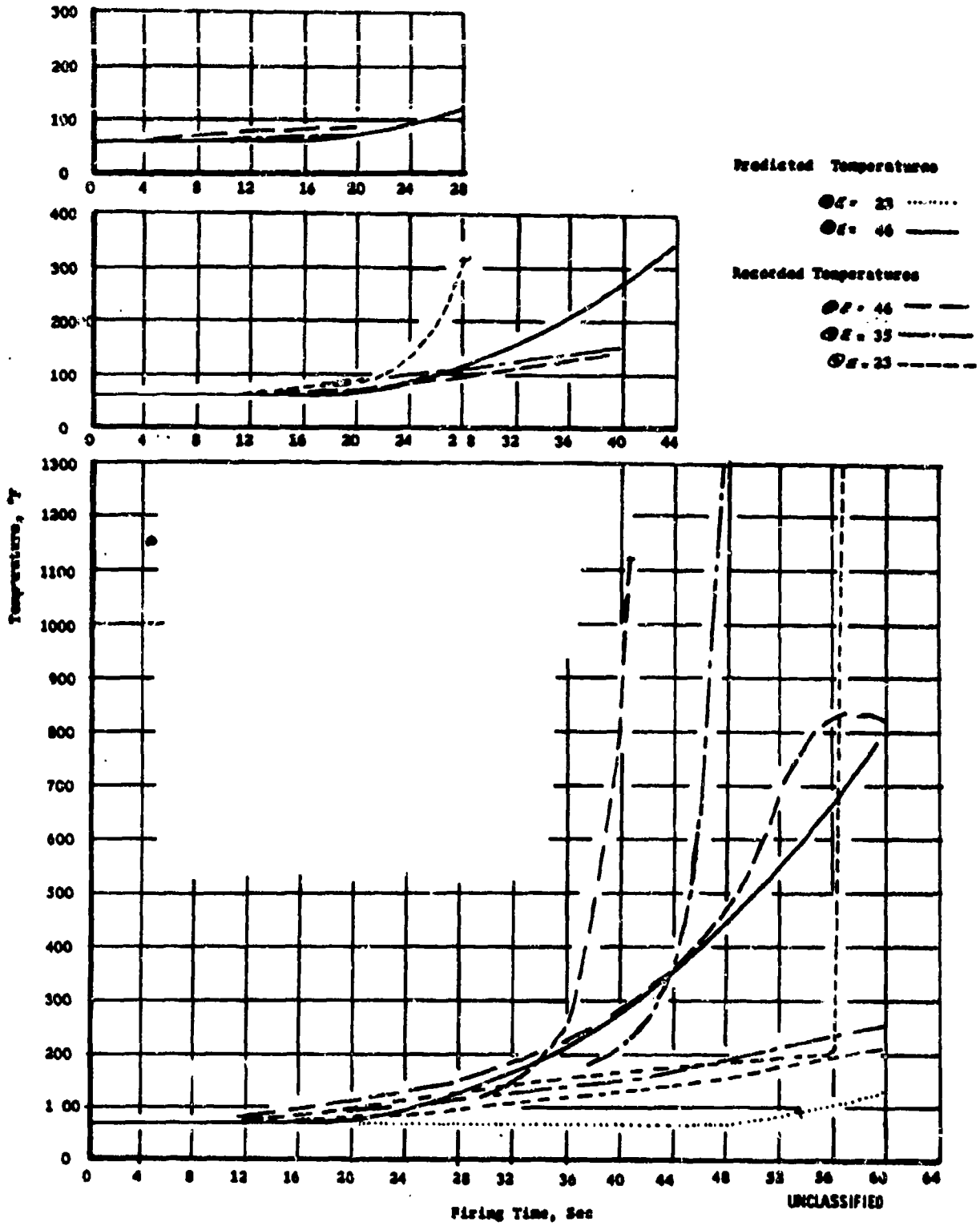

Figure 17. Backside Temperatures for Styrene Butadiene Subscale Exit Cone Tests

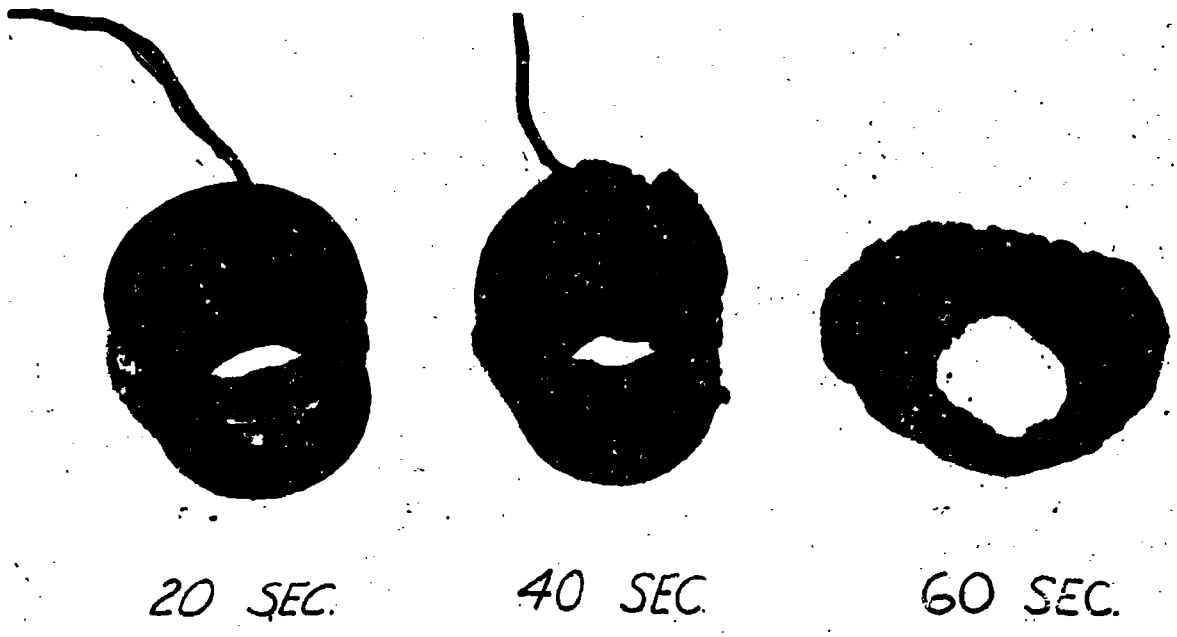

UNCLASSIFIED

Figure 18. Postfired Styrene Butadiene Subscale Exit Cones

III, B, Subscale Test Program (cont.)

trace went off the oscillograph paper. Considering the excellent condition of the part after testing, especially at the point of thermocouple attachment, this particular temperature is questionable.

(c) 60-Sec Test

(u) The part was almost completely destroyed during this test, as is evident in the photograph shown in Figure 18. The films of this test indicate that the failure occurred toward the end of the test. The temperature recordings show the first burnthrough at the exit section at 40 sec, and the other two thermocouples on that side go off-scale at 48 and 56 sec respectively. The thermocouple at the exit area on the other side recorded a temperature peak of 840°F at the end of the test.

(u) The motor insulation was burning after motor shutdown, and part of the damage to the exit cone occurred after tailoff, as indicated by the thermocouple readings and the visual evidence when the altitude chamber was opened after the test.

(3) Butyl

(u) The pressure, thrust, and temperature traces for the tests are shown in Figures 11 and 19. The postfire condition of each of these exit cones is shown in Figure 20. This material did not prove to be the best for any of the test durations, but it was not significantly inferior on any of these tests.

(a) 20-Sec Test

(u) The pressure port was plugged for this test, and no pressure record is available. The thermal histories show minimal temperatures as was expected.

(b) 40-Sec Test

(u) The trace of the thermocouple located where the expansion ratio was $\varepsilon = 46.6$ went off the graph at 34 seconds. Postfire visual inspection revealed a burnthrough at that point.

(c) 60-Sec Test

(u) The recorder ran out of oscillograph paper at 44 sec, so most of the data of the end of the firing were lost. The thermocouple readings, from a strip chart recorder, show peaks at the end of the test at an area ratio of 46.6. An examination of the part shows that the material had eroded back to the thermocouple leads.

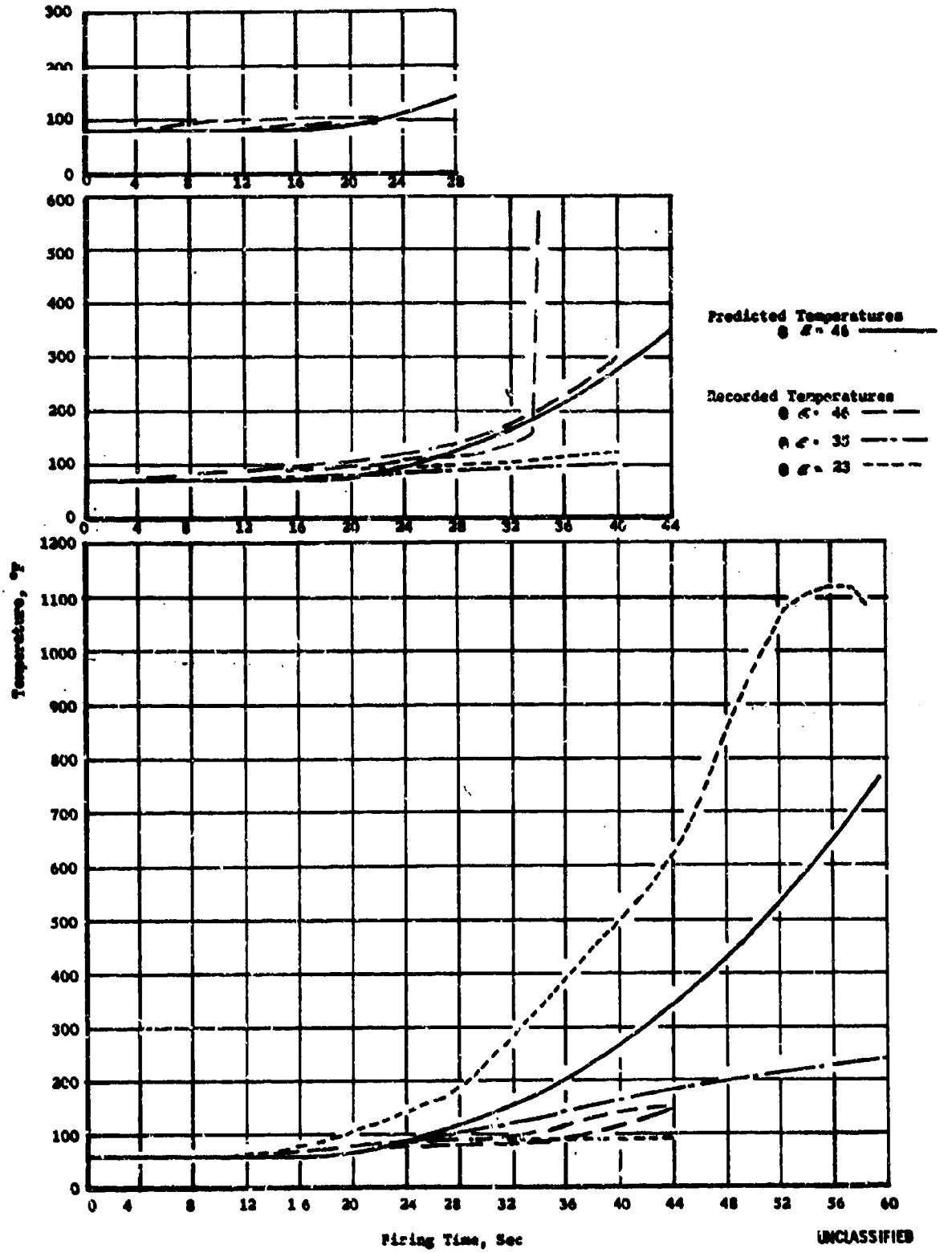

Figure 19. Backside Temperatures for Butyl Subscale Exit Cone Tests

UNCLASSIFIED

Figure 20. Postfired Butyl Subscale Exit Cones

III, B, Subscale Test Program (cont.)

(u) A summary of the erosion data for all the subscale tests is presented in Table 3. Figures 21 through 23 show the erosion at cross-sections corresponding to ϵ = 23 and ϵ = 35. Erosion data was taken at ϵ = 35 rather than at ϵ = 46.6, as was used in the analysis, because of the severe erosion on many of the parts at the higher expansion ratio.

(4) Conclusions

(u) On the basis of the subscale tests, each of the three materials can be considered prospects for foldable exit cones. Each survived satisfactorily for a duration of 20 sec. At test durations greater than 20 sec, these particular materials (in the thicknesses tested) were marginal.

(u) Because successful tests at durations of 40 and 60 sec were achieved during this test series, it is also evident that workable designs can be made for these longer durations. The temperature data from all the elastomeric tests show that in only one case did the temperature rise above 200°F by 30 sec. A maximum reading of 315°F at 28 sec was recorded on this case before the trace went off the oscillograph paper.

(u) Furthermore, the movies of the 60-sec tests also verify the integrity of the tested exit cones through more than half of the firing.

(u) Most of the material loss occurred in the high-expansion portion of the elastomeric exit cones. Because all of the tested subscale parts had a tapered wall section (from 0.4 to 0.2) and are cantilever supported, the exit portions of these parts are not so structurally stable as the entrance section. Thus, the greater material loss in this portion of the exit cones can be attributed in part to the difference in the rigidity of wall section, even though the heat flux is approximately half that of the entrance section.

(u) On this basis, an elastomeric demonstration exit cone with a firing duration of 30 sec can be designed with a high degree of confidence using any of the above materials. V-44® material was selected for the demonstration tests for the following reasons:

(1) The minimum erosion on the subscale 60-sec test;

(2) The great amount of test data from subsonic applications for use in design and test comparisons;

(3) The availability of this standard material with complete specification control; and

(4) The fabrication experience with V-44® based on the many subsonic applications in which it is presently used.

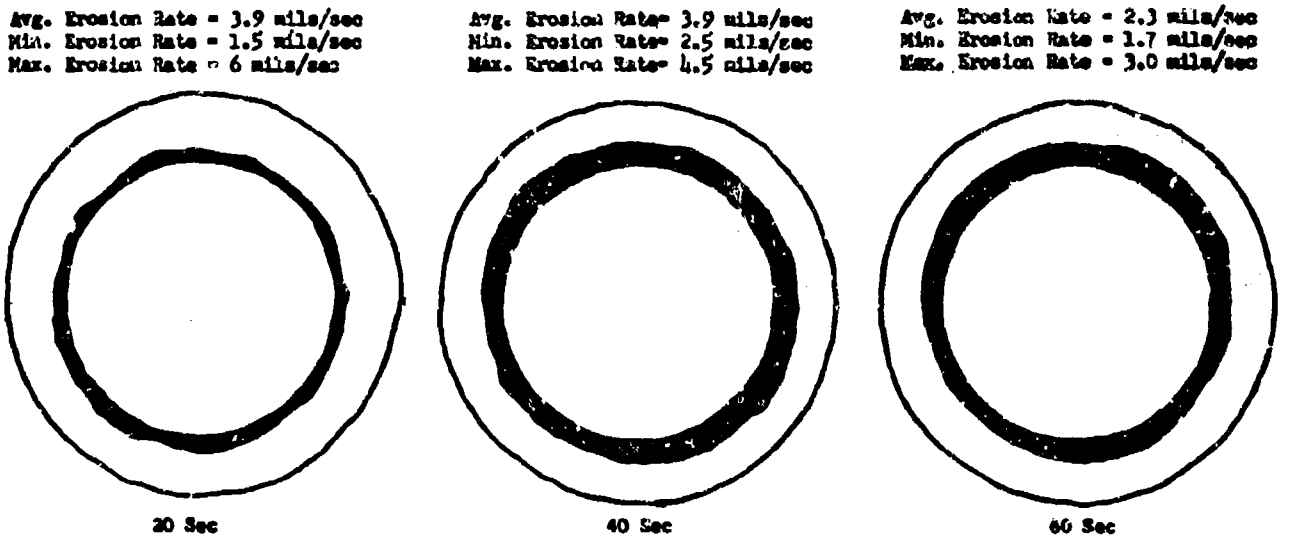

a. at $\varepsilon = 23$

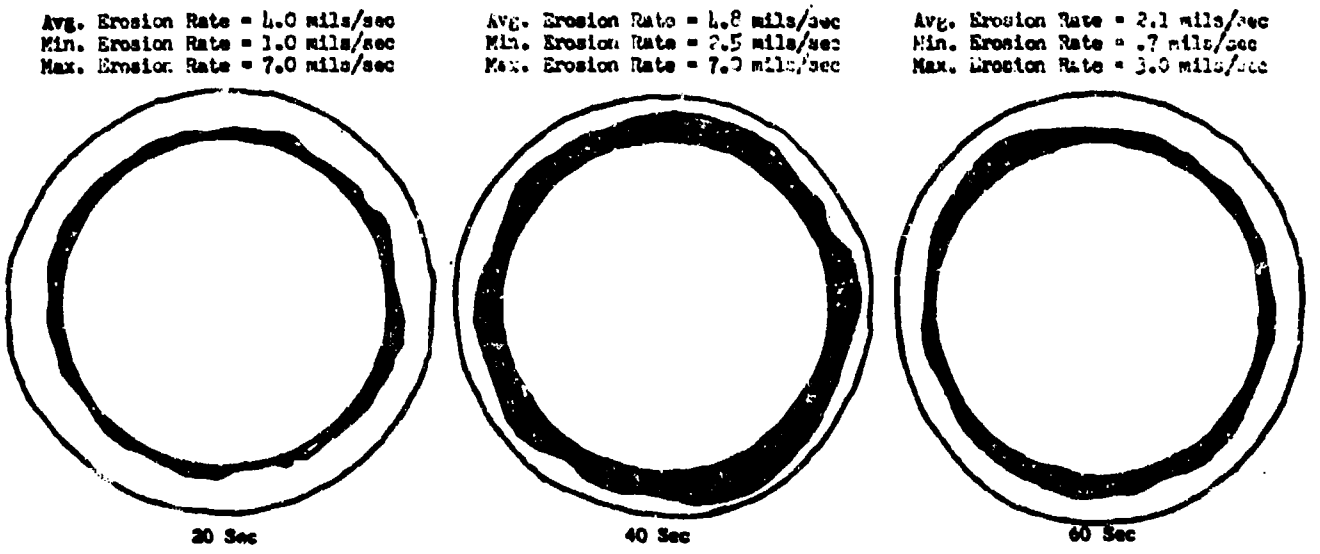

b. at $\varepsilon = 35$

Figure 21. Section View Showing Erosion of V-44[D] Subscale Exit Cone, $\varepsilon = 23$, $\varepsilon = 35$

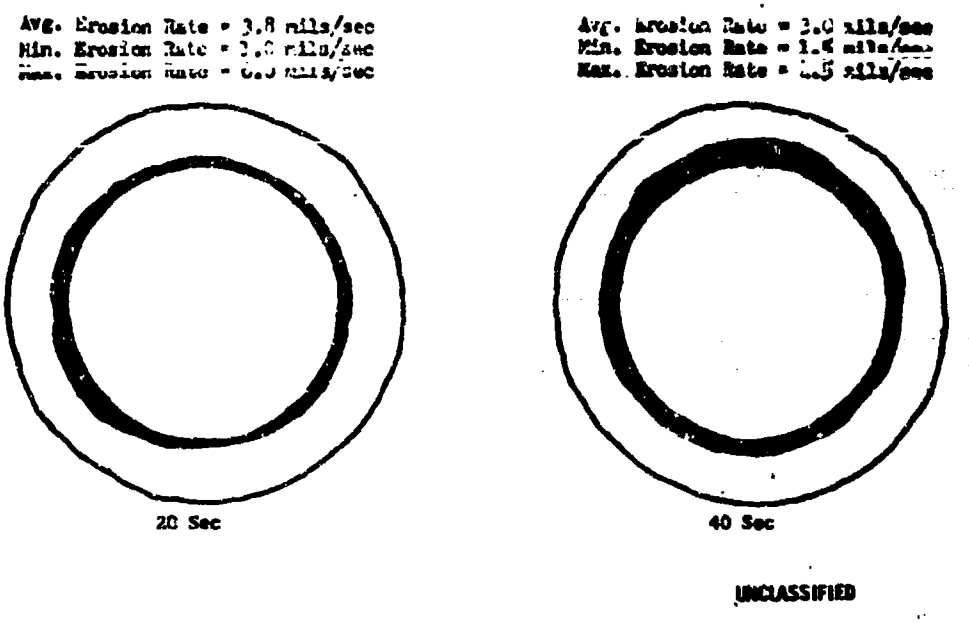

a. at ε = 23

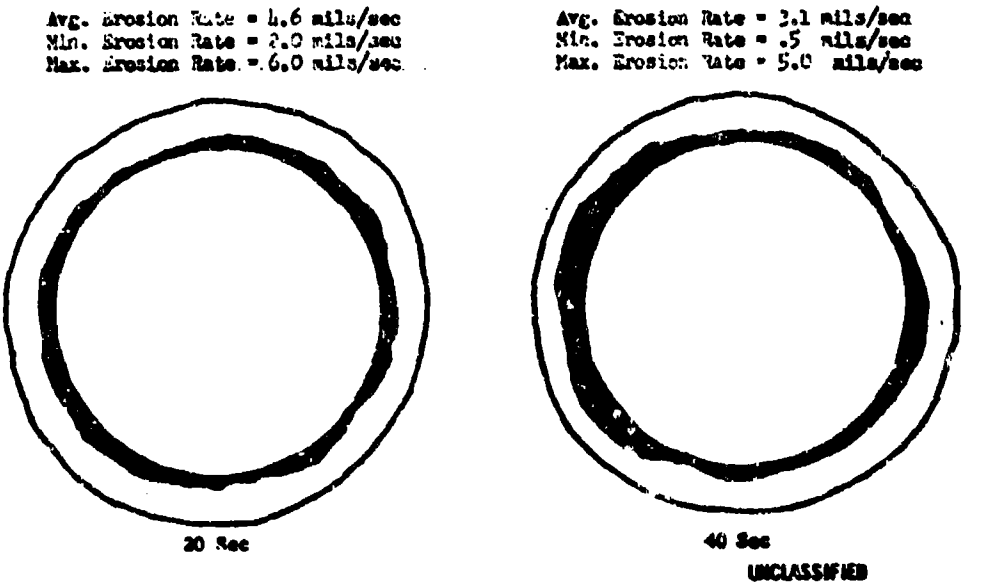

b. at ε = 35

Figure 22. Section View Showing Erosion of Styrene Butadiene Subscale Exit Cone, ε = 23, ε = 35

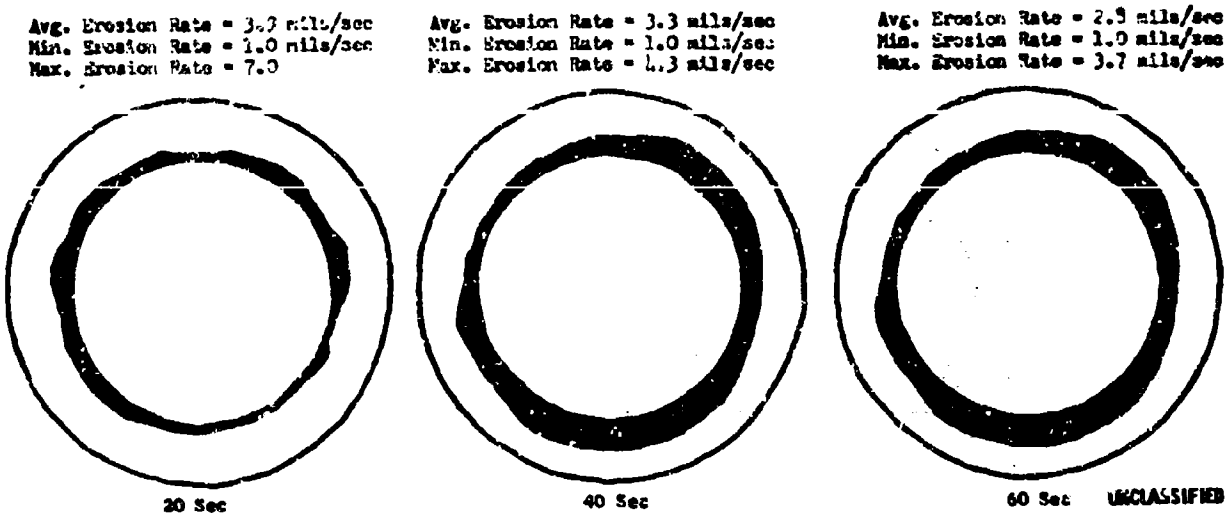

a. at ε = 23

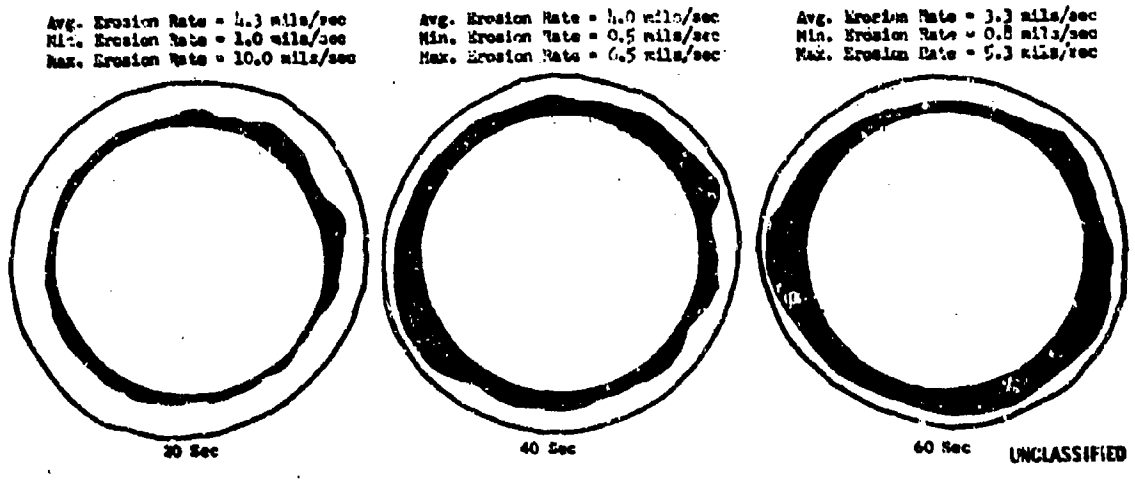

b. at ε = 35

Figure 23. Section View Showing Erosion of Butyl Subscale Exit Cone, ε = 23, ε = 35

III, B, Subscale Test Program (cont.)

c. Metallic Exit Cones

(u) One columbium and one 90Ta - 10W metallic exit cone, each made from 0.005-in.-thick sheet stock, were tested for 40 sec. The columbium exit cone survived the test in excellent condition, whereas the 90Ta - 10W broke circumferentially.

(1) Columbium

(u) The postfire condition of the columbium exit cone is shown in Figure 24, and the pressure and thrust history in Figure 12. The recorded operating temperature of 2200°F (Figure 25) for the columbium was approximately 1400°F below the calculated value of 3560°F. This is attributed primarily to aluminum oxide deposits during the test. The measured wall temperatures are below the solidification-temperature for aluminum oxide and would cause the aluminum particles to deposit on the cold wall.

(u) Calculations show that a 0.037-in. layer of Al_2O_3 at an ϵ = 23 and a 0.010-in. layer of Al_2O_3 at an ϵ = 46 would reduce the wall temperature to 2200°F. The aluminum oxide deposit is a good insulator; the flame surface remains hot, and thus reduces the total heat flux to the wall. The aluminum oxide layer deposited on the exit cone varied from 0.010 to 0.028 in.

(u) The films of this test are of good quality and show the exit cones heating to a glowing orange. Actually, the exit cone had bright and dark areas that changed throughout the firing. This, again, is attributed to a deposition layer that changes in thickness through the test.

(2) 90Ta - 10W

(u) A postfire photograph of the 90Ta - 10W exit cone is shown in Figure 26. The pressure and thrust histories are shown in Figure 13 and the temperature record in Figure 27. This exit cone broke circumferentially, but the time of the break is not known with any degree of certainty. The thrust trace is essentially neutral throughout the firing, which would indicate that the break did not occur before tailoff.

(u) A possible cause of the fracture was a gaseous nitrogen purge that was directed at the part after the motor was shut down. The part appeared intact at the end of the test, but the end came off when the motor was removed from the test chamber. The movies of this test are of poor quality because the camera window became clouded during the test; therefore, the movies do not help in determining the time of part failure. An examination of the fracture indicates a clean break and not a burn through; furthermore, there are no oxide deposits as would be expected if the break occurred during the test.

UNCLASSIFIED

Figure 24. Postfired Columbium Subscale Exit Cone

Figure 25. Backside Temperatures for Columbium Subscale Exit Cone

UNCLASSIFIED

Figure 26. Postfire 90Ta - 10W Subscale Exit Cone

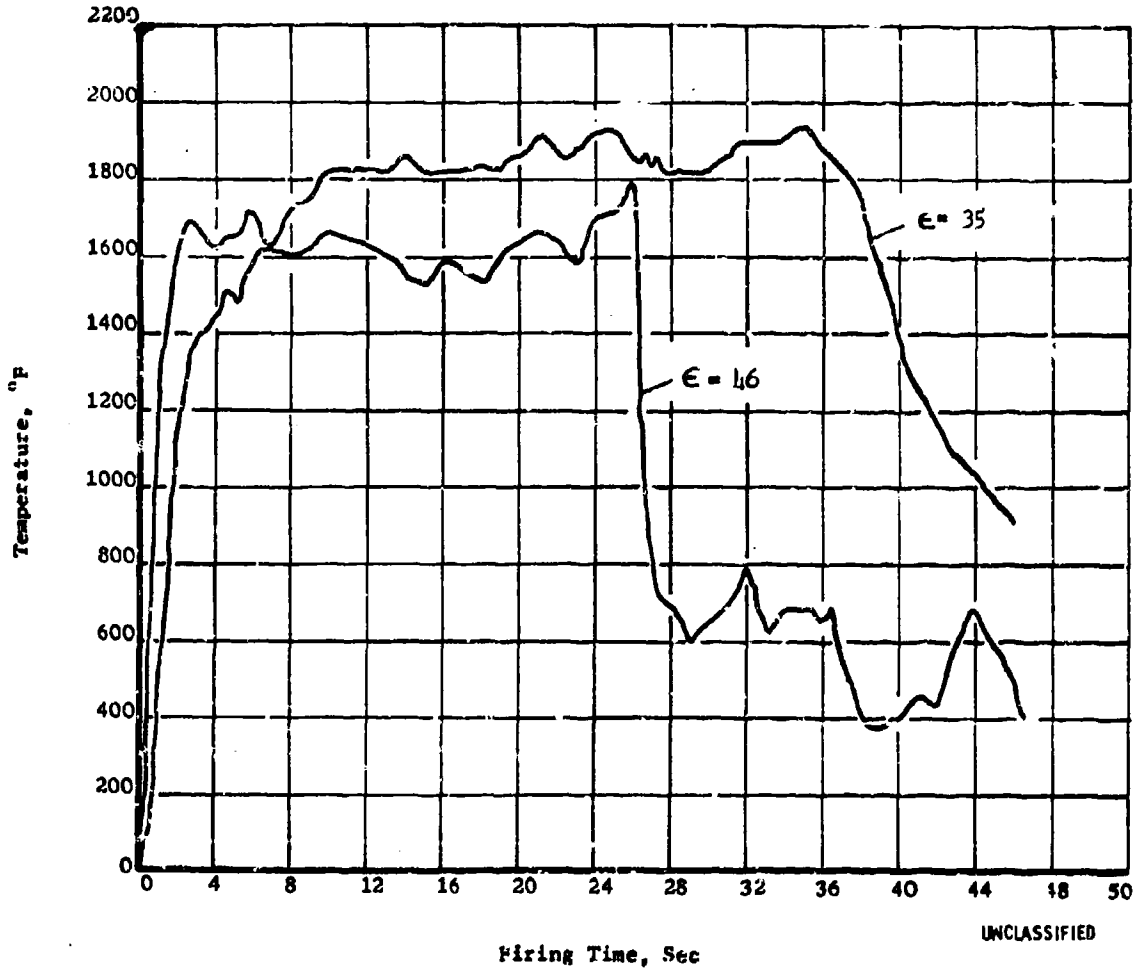

Figure 27. Backside Temperatures for 90Ta - 10W Subscale Exit Cone

(u) As was the case with the columbium exit cone, the 90Ta - 10W exit cone had a layer of aluminum oxide deposits. The hot surface of the aluminum oxide that is exposed to the flame reduces the heat flux into the wall; this accounts for the thermocouple readings that were 1300°F below the predicted value.

(u) Welding of the 90Ta - 10W exit cone was much more difficult than was the welding of columbium. Although part of the 90Ta - 10W fracture occurred in part at the weld seam, the failure did not seem to be due to the weldment.

(3) Conclusions

(u) On the basis of these two tests, columbium appeared to be the better prospect for use on the demonstration exit cones. The results of the tests with 90Ta - 10W suggest that this material can be used for a radiation-cooled exit cone and probably would be required for more severe temperature conditions. Other advantages of columbium for radiation-cooled exit cones is lower cost, lower weight, and ease of fabrication as compared to 90Ta - 10W.

III, Technical Discussion (cont.)

C. DEMONSTRATION TEST PROGRAM

(u) This program culminated with the firing of three demonstration exit cones at Arnold Engineering Development Center. Two of these exit cones were V-[illegible], and the other one was fabricated from columbium. These tests were conducted at a simulated altitude of 110,000 ft.

(u) Prior to the demonstration tests at AEDC, a demonstration motor was fired at Aerojet-General, Sacramento. This test was at sea level and served to qualify the motor for the AEDC tests. For this test, prospective elastomeric materials were assembled to the exit cone in an attempt to provide additional data on the erosion resistance and char retention capabilities of these materials.

(u) All the material samples were eroded and/or blown out by the gas stream so that no useful erosion data was obtained on this test. This test served to verify the grain design, acceptability of the propellant batch, and nozzle design.

(u) A discussion of the design that was tested, as well as the supporting activities involved in the demonstration program is presented in the following sections.

1. Demonstration Design

(C) The significant parameters of the demonstration motor (Figure 28) using the ANP 2862 JM Mod II propellant, are as follows:

Chamber pressure, psia	500
Nominal thrust, lbf	5000
Flame temperatures, °F	5500
Aluminum content, Wt %	17
Throat area, sq. in.	5.80
Mass flow rate, lb/sec	18.5
Firing duration, sec	27
Propellant grain diameter, in.	14.6
[illegible]llant burning surface, in.^{2}	1145
Propellant weight, lb	525
For the qualification test at sea level:	
Expansion ratio	8:1
For the four demonstration tests at AEDC:	
Expansion ratio of fixed nozzle	20:1
Expansion ratio of test fixture	20:1 to 50:1

a. Motor Chamber

(u) The chamber was a modified BM-14 chamber originally designed for the Genie motor (see Figure 28). In addition to an extensive [illegible] history with different propellant formulations, the hardware had been used successfully for other

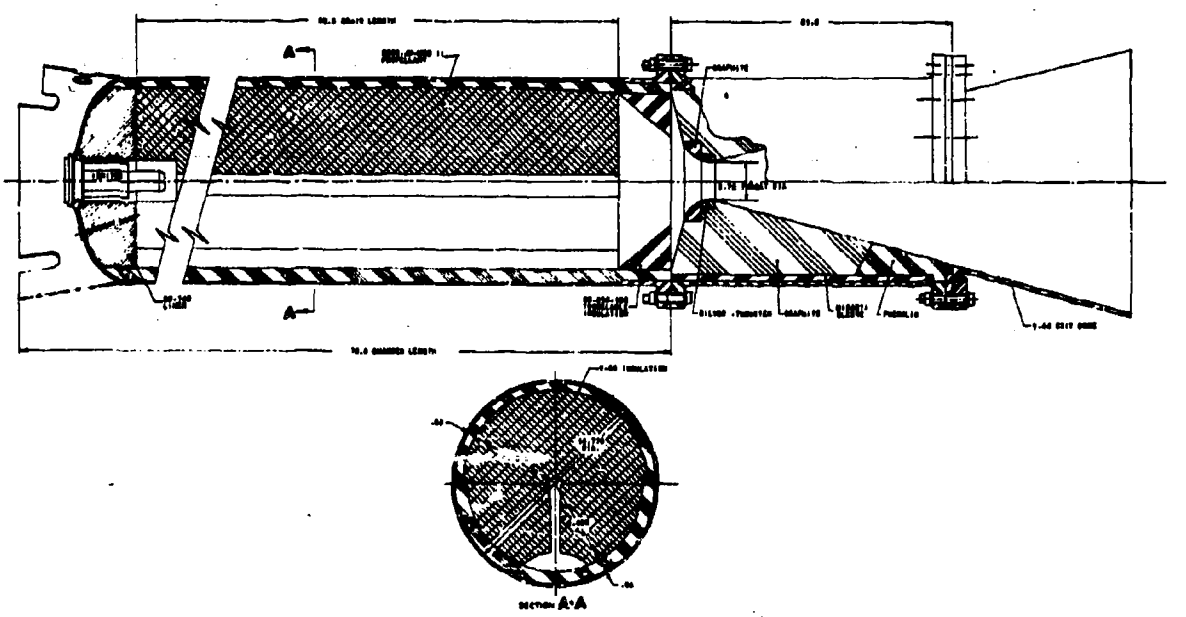

UNCLASSIFIED

Figure 28. Demonstration Motor, Nozzle, and Exit Cone

(U) II, C, Demonstration Test Program (cont.)

development tests during which the following operating conditions were achieved: altitude ignition, 19-lb/sec mass flow, 14,000-lbf thrust, and a 600-psia operating pressure. The hydrotest pressure for this chamber is 1200 psi.

(u) Because these conditions exceed the requirements of the present program, this chamber was selected with a high degree of confidence. A discussion of the stress analysis for this chamber is presented in Appendix IV.

b. Grain Design

(u) To obtain the required thrust level and firing duration, it was necessary to use a keyslot grain. The keyslot grain used in the development motors is shown in Figure 28. This particular grain had previously been fired twice successfully by Aerojet-General in the DM-14 chamber.

(u) This grain design was analyzed with a computer program that takes into account the effects of erosive burning. The predicted pressure and thrust histories are presented in Figure 29.

(u) The use of a keyslot grain raises the possibility of asymmetric gas flow in the nozzle. It was expected that the entrance section of the nozzle would experience asymmetric erosion, but that any asymmetric flow condition would not exit downstream to the point at which the test exit cones were to be attached.

(u) The sea level qualification test did reveal an excessive amount of erosion at two points in the aft chamber insulation. At these two points the chamber inner wall was exposed for an area approximately one in. in diameter. The exposed steel wall was coated with aluminum oxide. This localized erosion was next to the chamber side wall and existed at two points on the opposite side of the chamber from this passage. An Aerojet-General-proprietary trowelable rubber insulation (SD-850-15B) was installed in the four demonstration motors to be tested at AEDC to provide additional protection in this area.

c. Nozzle Design

(u) The nozzle to be used on the demonstration motor (Figure 28) was similar to the one used on the subscale motor, namely, a tungsten throat backed up by graphite and insulated from the steel housing by silica cloth. This nozzle was thermally analyzed, and the expected temperatures in the throat region and exit cone are presented in Figure 30. Surface temperature of the insert attain 4300°F maximum at 30 sec, and a gradient of 900°F was predicted to vary from 3400°F on the flame surface to a nominal 100°F on the exterior surface. No extreme thermal environment was found for the throat design.

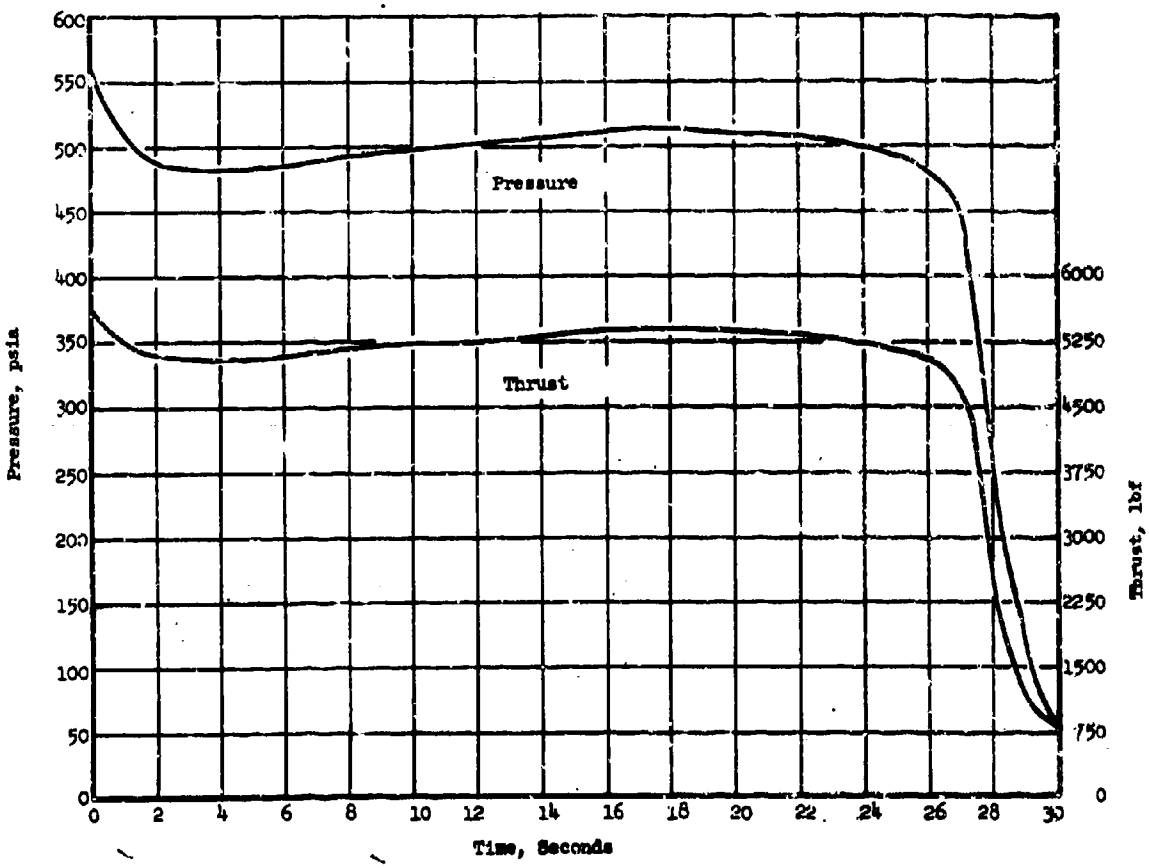

CONFIDENTIAL

Figure 29. Demonstration Motor Predicted Pressure and Thrust History (U)

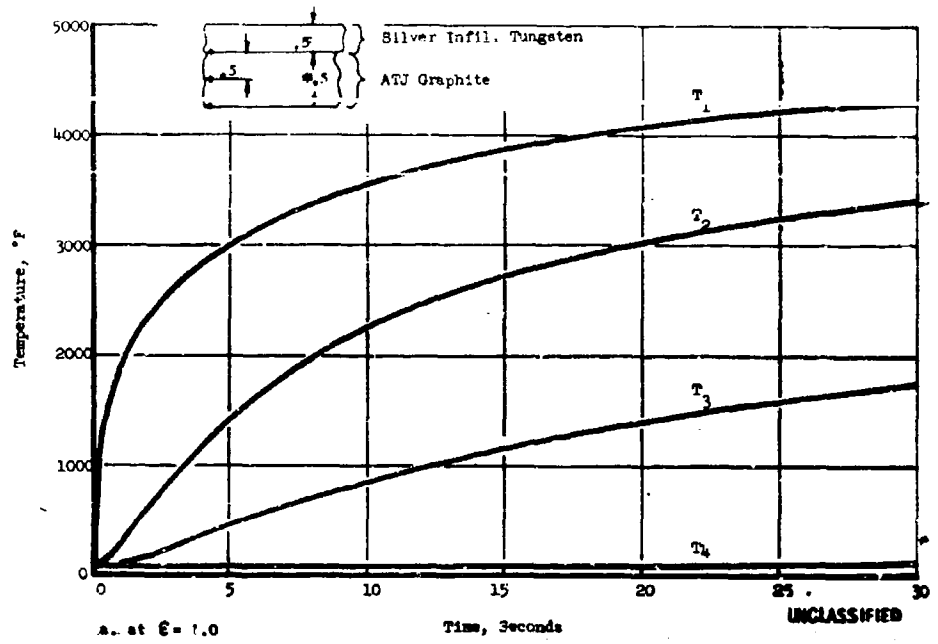

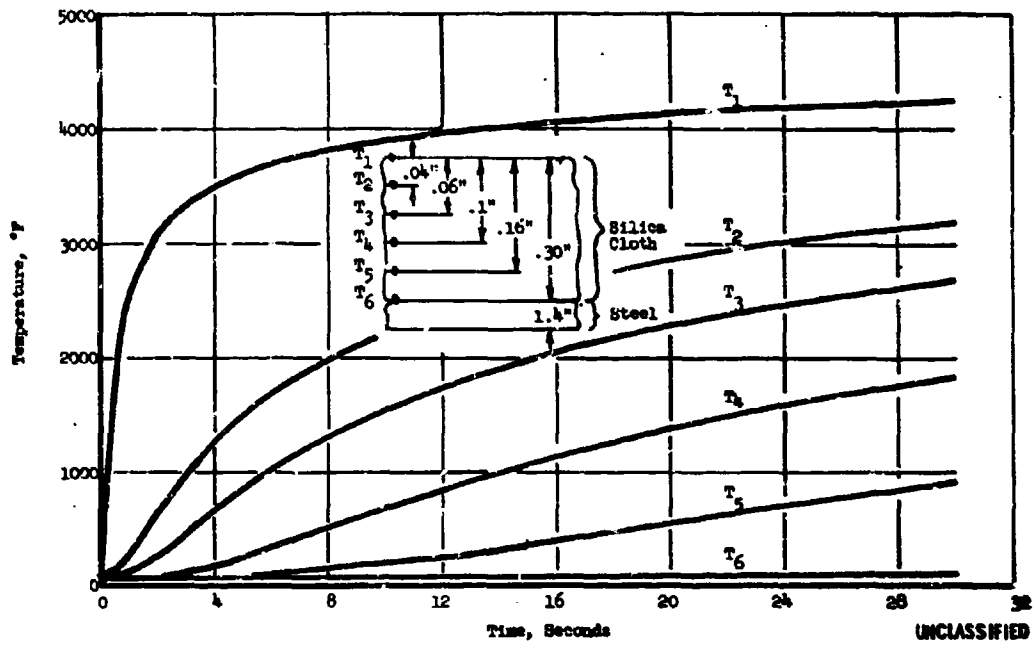

Figure 30. Temperature Profiles of Demonstration Motor Nozzle, ε = 1.0, ε= 20.0

III, C, Demonstration Test Program (cont.)

d. Demonstration Motor Igniter

(u) The igniter used with the demonstration motor was an altered production igniter, Model 34F (Figure 31), with Alco pellets replaced by BPN pellets. In addition, an auxiliary torus chamber and initiating squibs were incorporated to provide a larger ignition charge. The necessity for this revision became evident on the sea level qualification test. The auxiliary igniter charge was not used on this firing, and the motor had an abnormally long ignition delay, indicating a marginal igniter design. The revised igniters provided successful motor ignition in the AEDC tests.

e. Elastomeric Exit Cones

(u) The demonstration elastomeric exit cones (Figure 32) were scaled up versions of the V-44[2] subscale exit cones with the following changes:

(u) The wall thickness was made a constant 0.3 in., rather than a tapered section, as was used on the subscale parts. The exit sections of the subscale cones had as much or more erosion than the entrance sections. This was due in part to the greater deflections that were present at the exit area. For the area ratios tested, the erosion does not appear to be a strong function of area ratio. The use of a constant wall section aids the fabrication of these parts. The use of a constant wall thickness does add weight, but it was decided that the increase in rigidity at the exit plane more than compensated for this small weight increase.

(u) Originally, the elastomeric exit cones were to be packaged by folding the exit section over the outside of the entrance section into an S-shape as shown in Figure 33 (the typical packaging method used in the liquid test program).

(u) This means of folding was difficult to achieve on the two exit cones tested on this program for two reasons: (1) these cones have a relatively thick wall (0.3-in.) for their size (12.2- to 19.2-in.-dia), and (2) these cones were reinforced by a nylon cloth tape on their exterior surface to provide the required hoop strength which added considerably to the stiffness.

(u) For these reasons, it was decided to fold the exit portion into the cone and to demonstrate deployment by inflating a circumferential rubber tube attached to the exterior surface of the cone near the exit area (see Figure 34) and "popping" the cone out into shape. This method of deployment proved successful on a bench test.

(u) Because these cones were rather rigid due to the wall thickness-to-diameter ratio, it was believed that there existed sufficient wall strength to prevent excessive flutter during the planned 30-sec tests. A more elaborate means of providing additional cone support was deemed beyond the scope of this program.

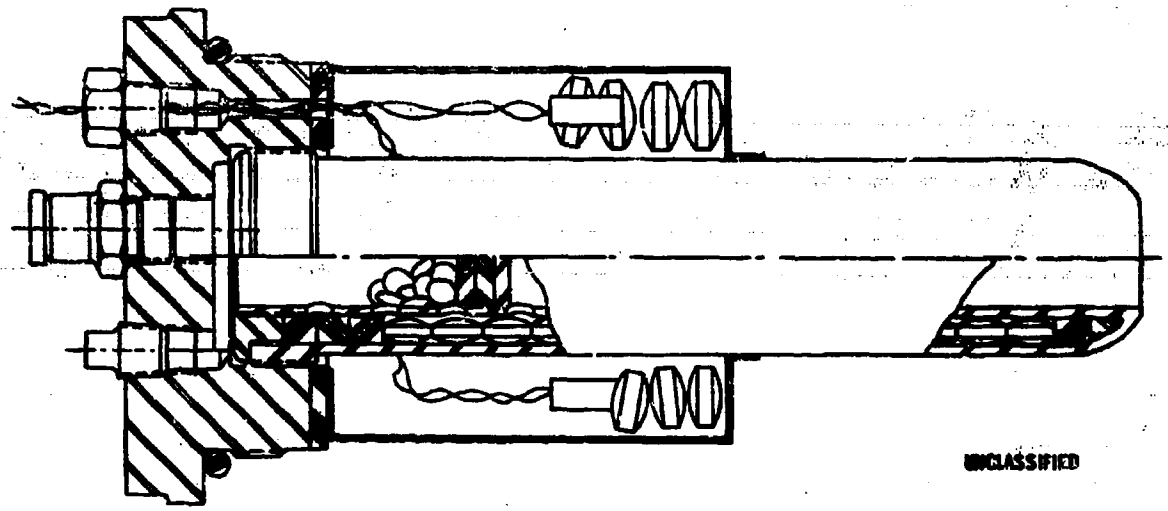

Figure 31. Demonstration Motor Igniter

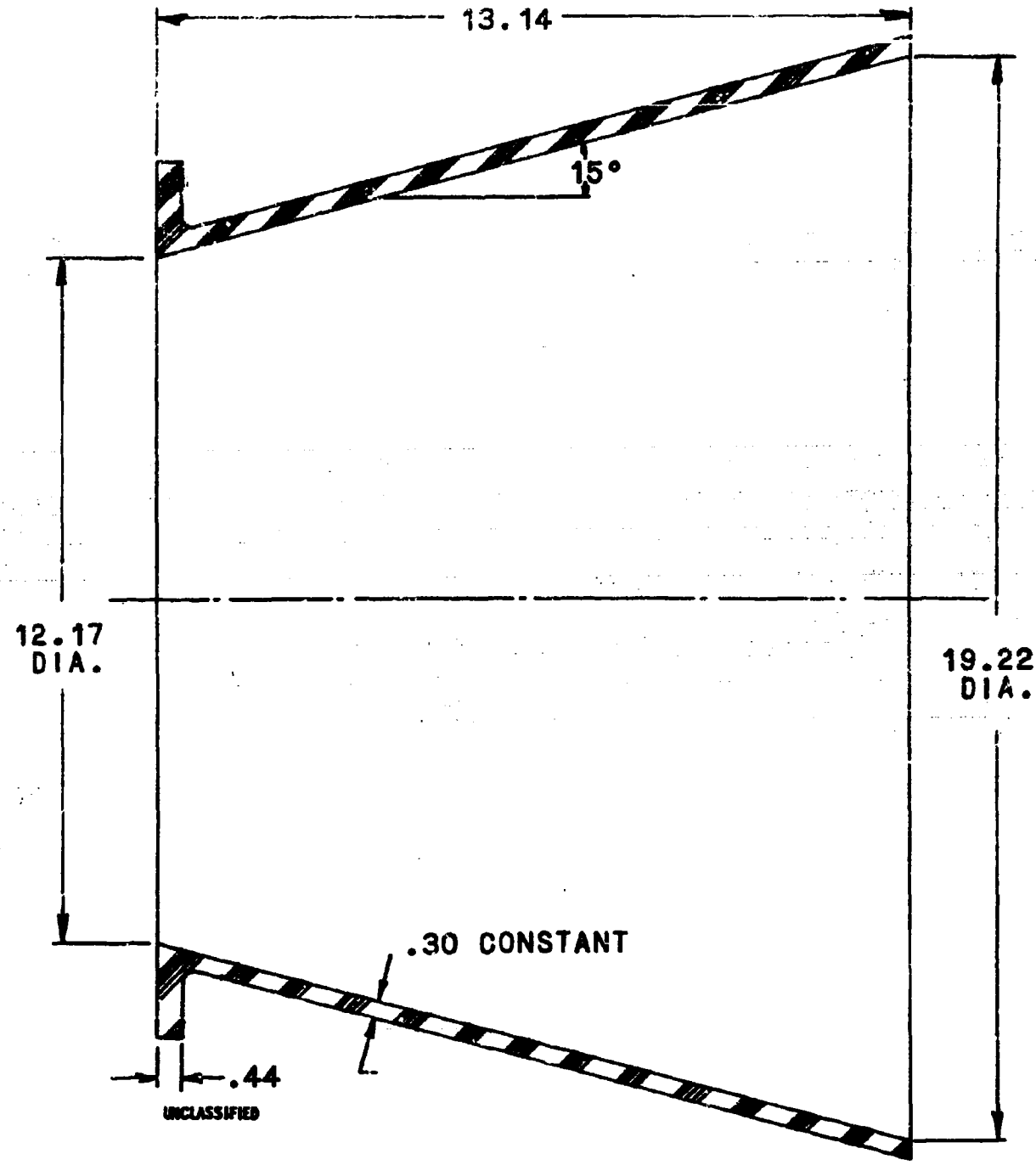

Figure 32. Demonstration V-44® Exit Cone

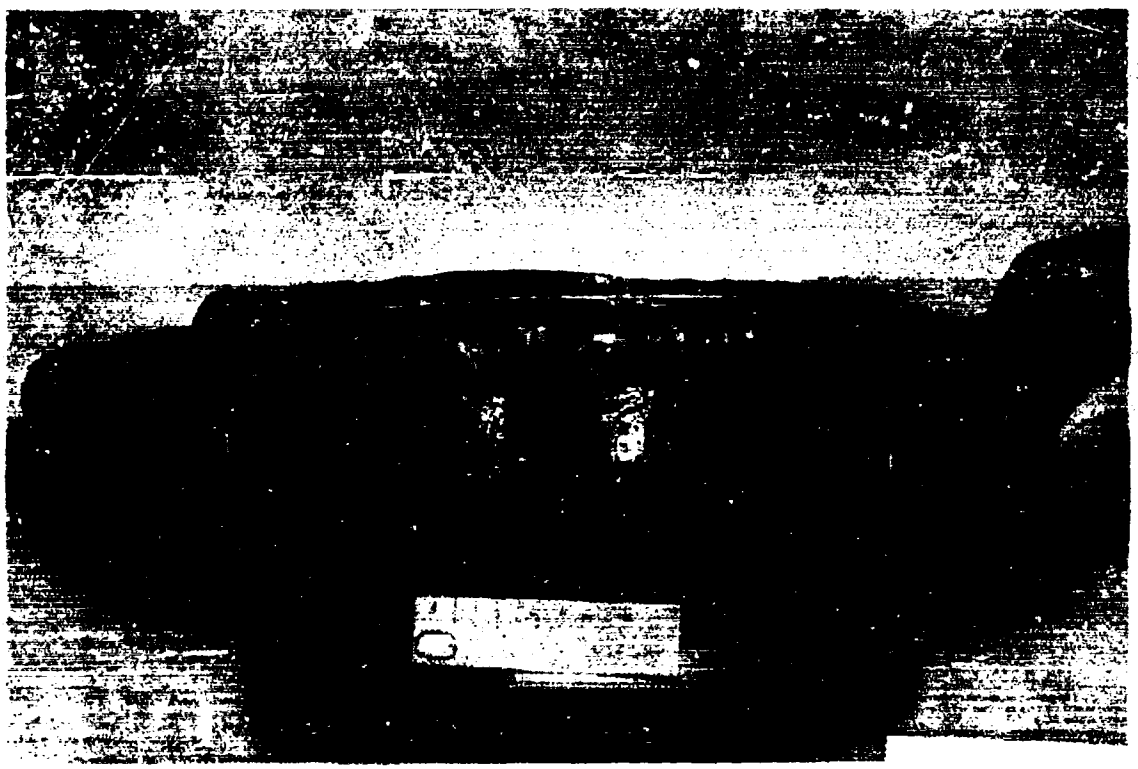

UNCLASSIFIED

Figure 33. Typical Folded Position of Liquid Rocket Operations Elastomeric Exit Cones

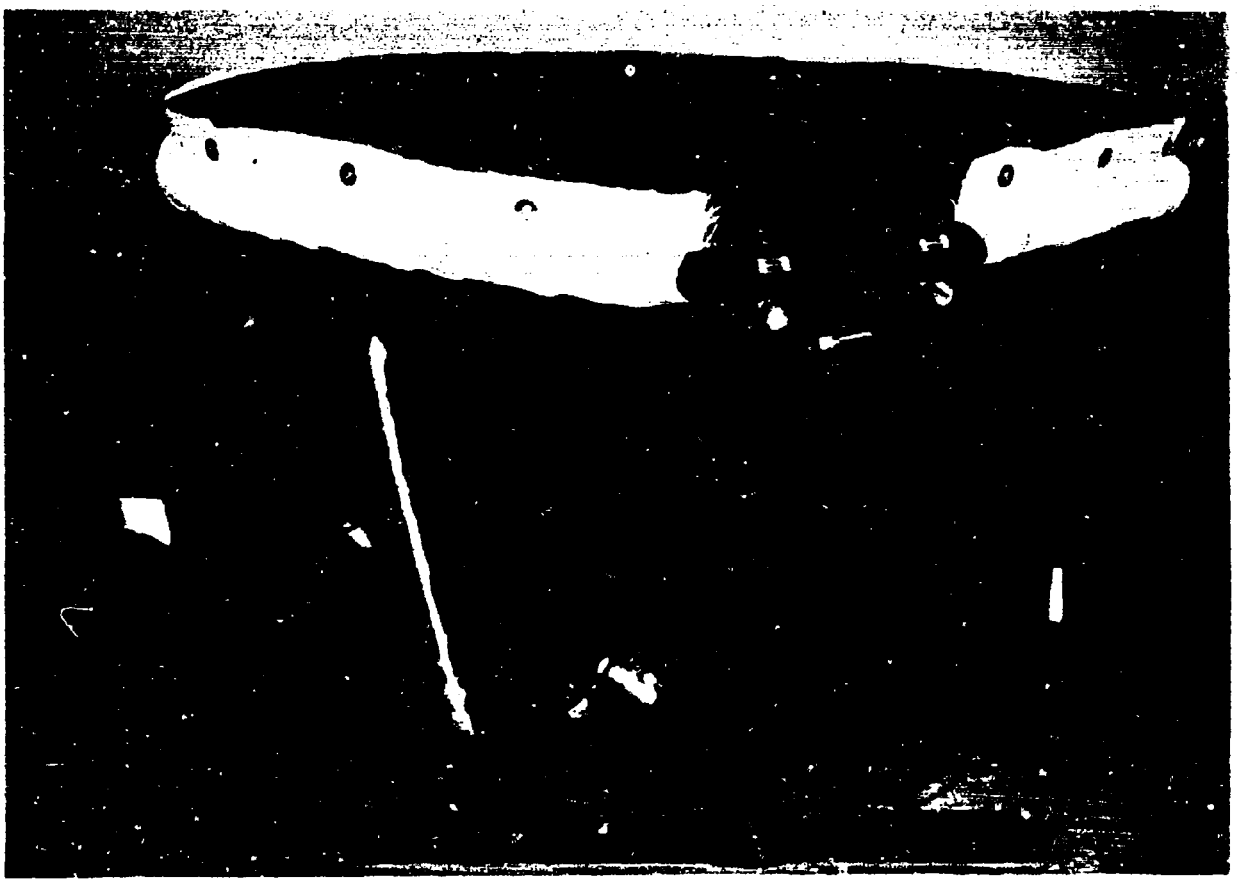

UNCLASSIFIED

Figure 34. Demonstration V-44D Exit Cone with Deployment Tubes

III, C, Demonstration Test Program (cont.)

f. Metallic Exit Cones

(u) The metallic exit cones were made from 0.015-in.-thick sheet columbium and were fabricated into a corrugated cylinder with convolutions tapering from one end to the other (Figure 35). During ignition the convolutes open up, and the part assumes a conical shape with some residual convolution remaining to provide additional strength. A stress analysis that considers the opening of the corrugations and buckling loads was performed on this part and is presented in Appendix IV.

2. Demonstration Tests

a. Sea Level Qualification Test

(u) The motor qualification test was conducted at Aerojet-General, Sacramento, on 26 January 1965, with the motor achieving the predicted pressure and thrust levels. These data are presented in Figure 36. Two problems were evident on this test and have been discussed previously, namely, insulation erosion in the aft end of the chamber and ignition delay. The remaining motors and igniters were reworked to eliminate these problems. The nozzle assembly exhibited no problem areas.

b. Test Program at Arnold Engineering Development Center

(u) The three test firings for this program were conducted at AEDC during the first two weeks in October 1965 in Test Cell J-5 (see Figure 37). This is a horizontal test cell capable of testing solid rocket motors with thrust up to 100,000 lbf at altitudes in excess of 100,000 ft. A complete description of these tests is presented in Ref 6. No major problems were encountered, and all the program objectives were achieved.

(u) The motor performed as predicted with no abnormalties. The measured thrust-time curve for each firing is presented in Figure 38 along with chamber pressure and test cell pressure. The trowelable insulation (SD-850-15B) solved the aft-end erosion problem that existed on the sea level test conducted at Aerojet-General, Sacramento.

(u) The revised igniter assembly (Figure 31) provided a soft, reproducible ignition. Ignition delay, defined as the time from application of ignition current until the first indicated rise in chamber pressure, varied from 36 to 44 msec. An analog trace of thrust, chamber pressure, and igniter pressure for the ignition transient of the third firing is typical and is shown in Figure 39.

(u) On the second and third tests, the case of the fixed nozzle sustained a hot spot (Figure 40). Heating was not sufficient to cause failure. It is evident that chamber gas leaked between the micarta sleeve insulator and the nozzle case, with some localized gas circulation. Future test firings with this nozzle design would require that this area be better sealed.

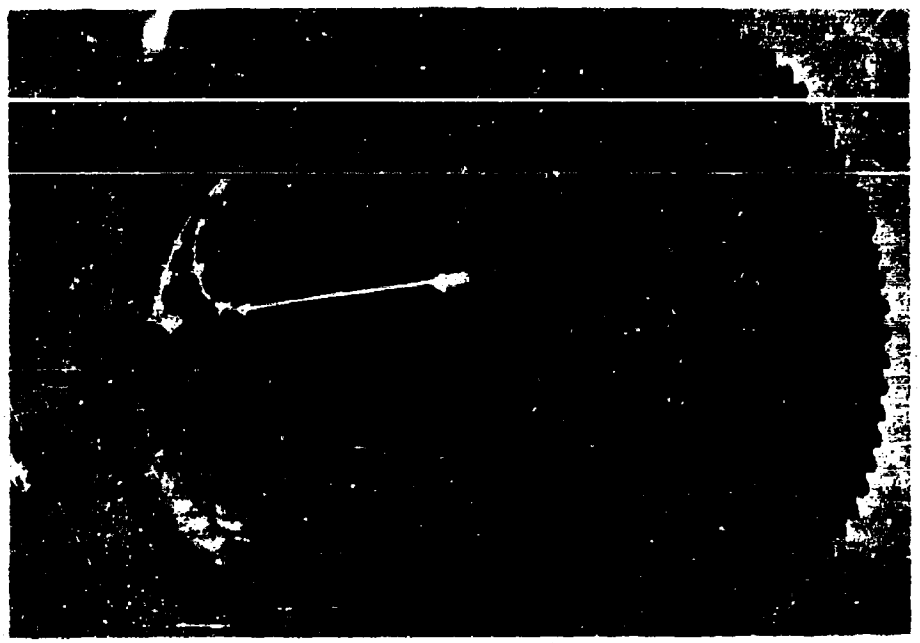

UNCLASSIFIED

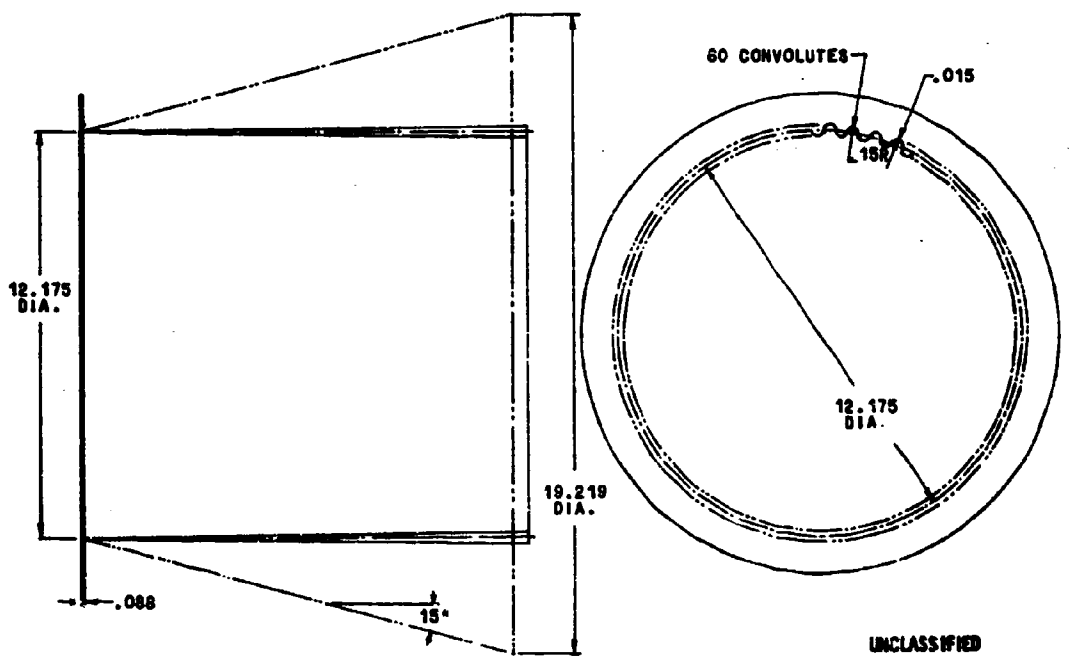

UNCLASSIFIED

Figure 35. Demonstration V-44® Exit Cone

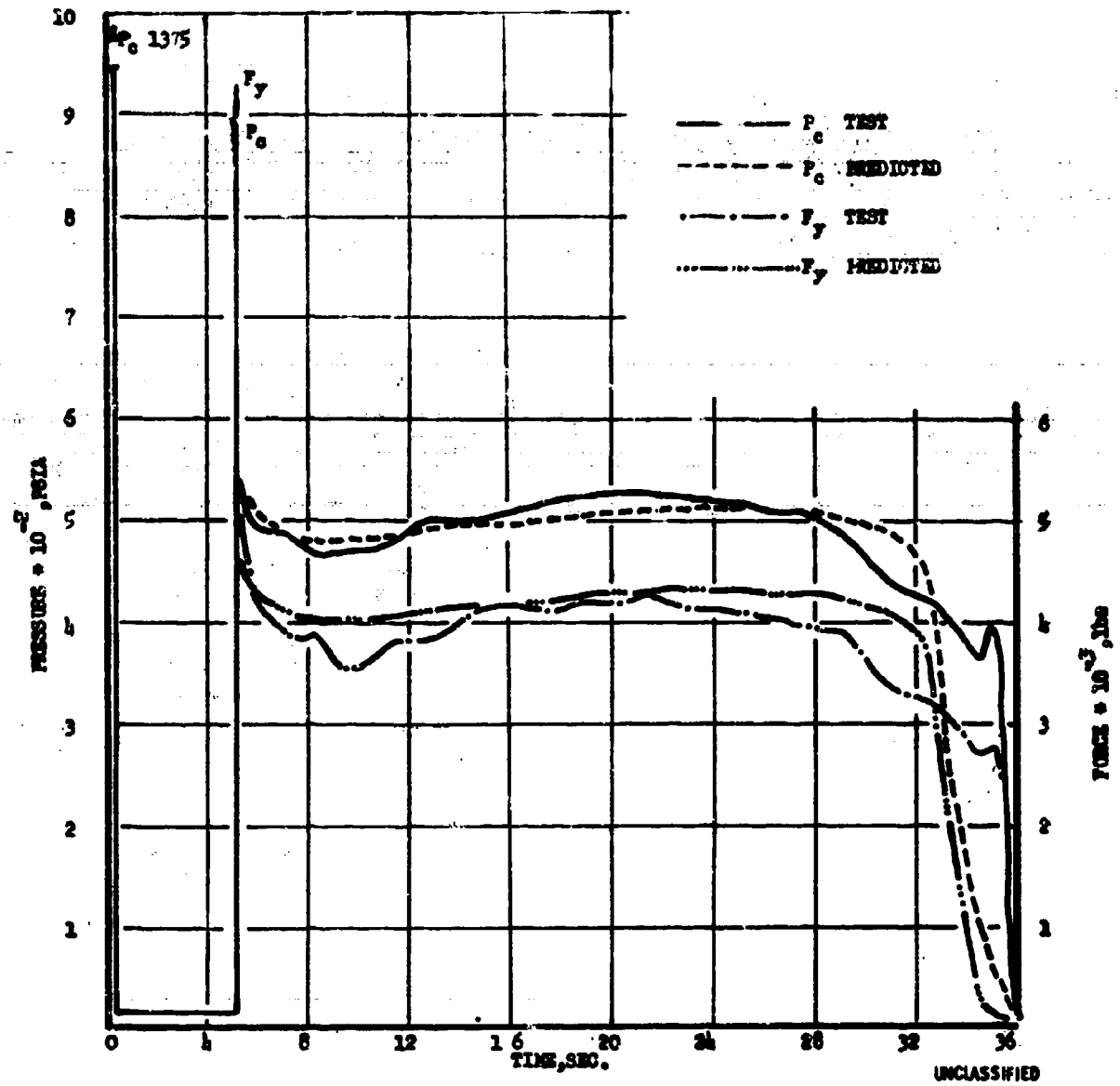

Figure 36. Pressure and Thrust for Demonstration Motor Sea Level Test

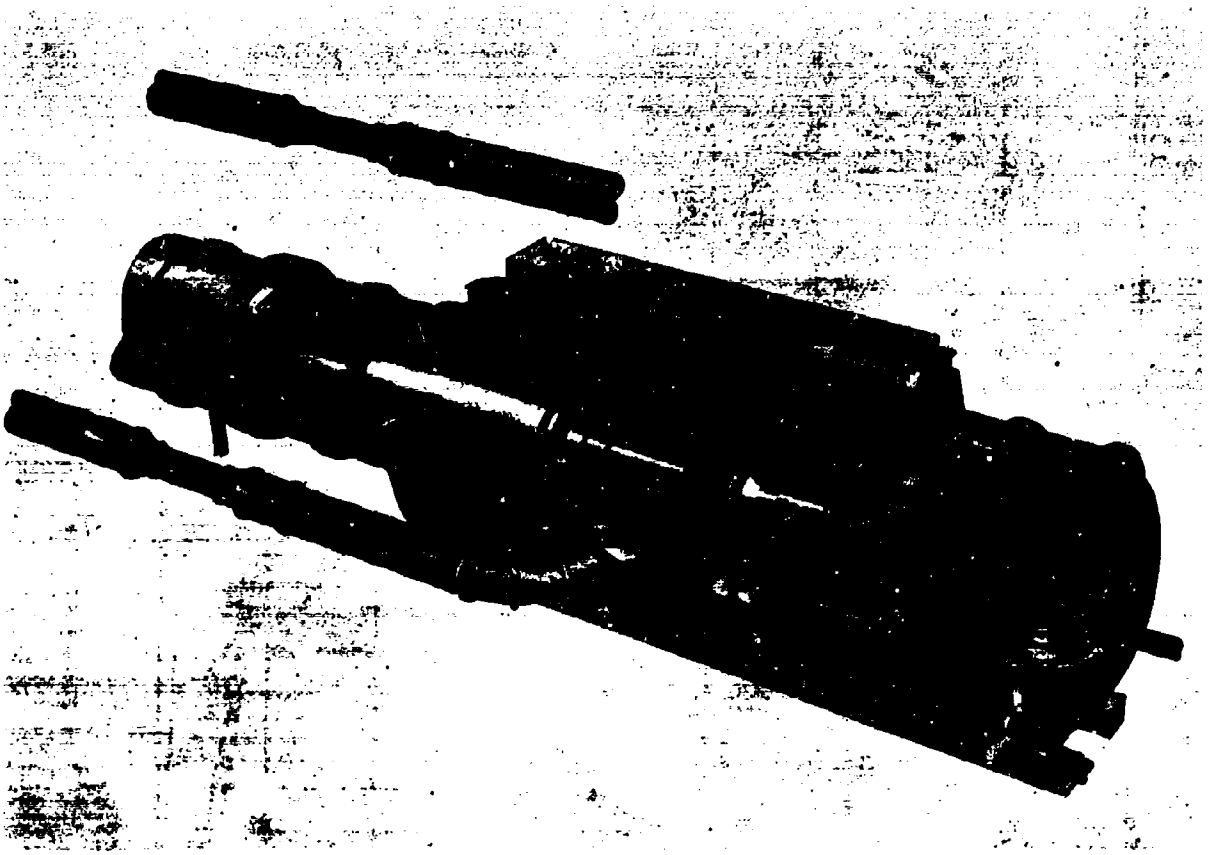

Figure 37. Demonstration Motor in Arnold Engineering Development Center Test Cell J-5

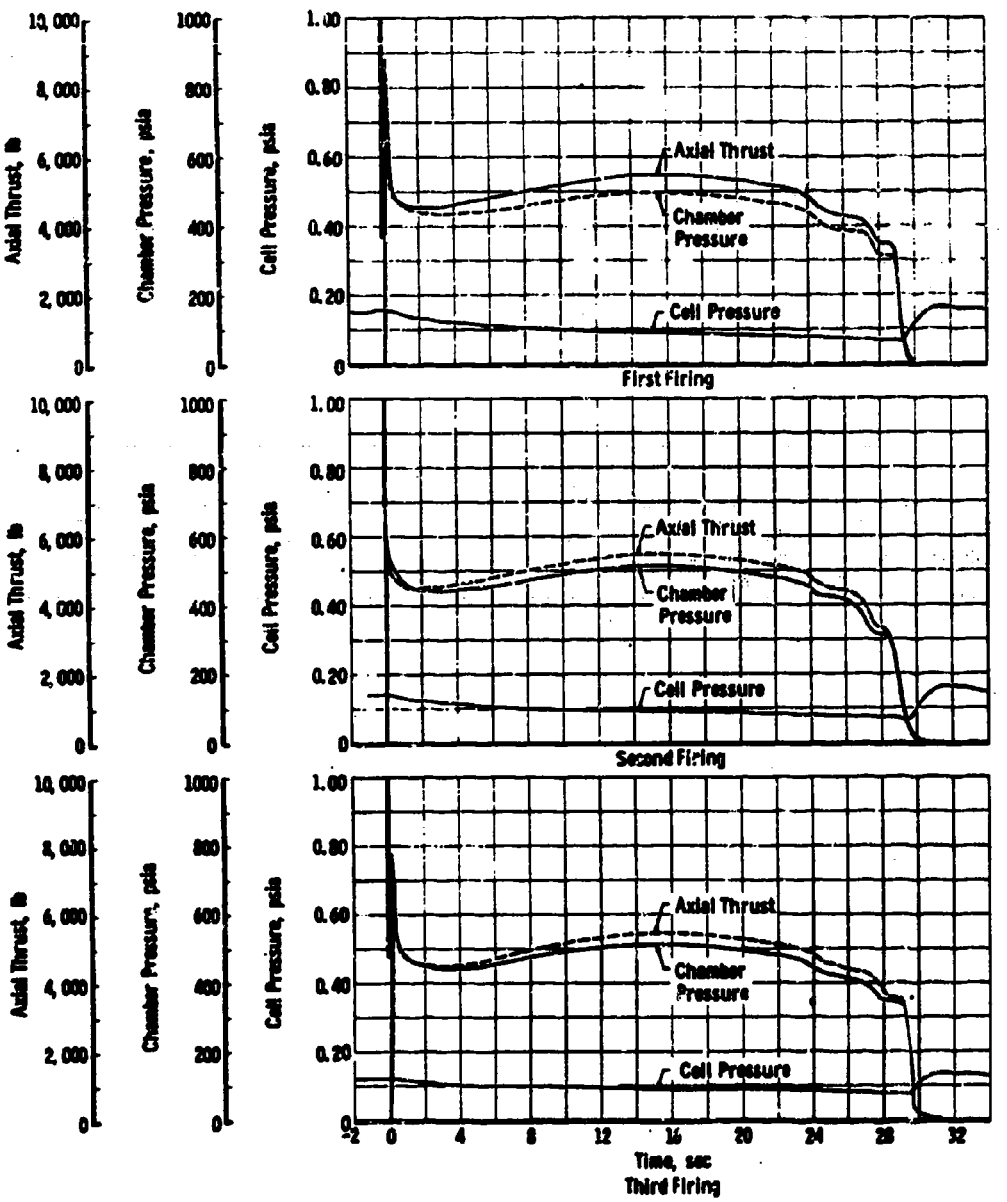

CONFIDENTIAL

Figure 38. Measured Ballistic Performance of Demonstration Motors (u)

CONFIDENTIAL

Figure 39. Demonstration Motor Ignition Detail (u)

UNCLASSIFIED

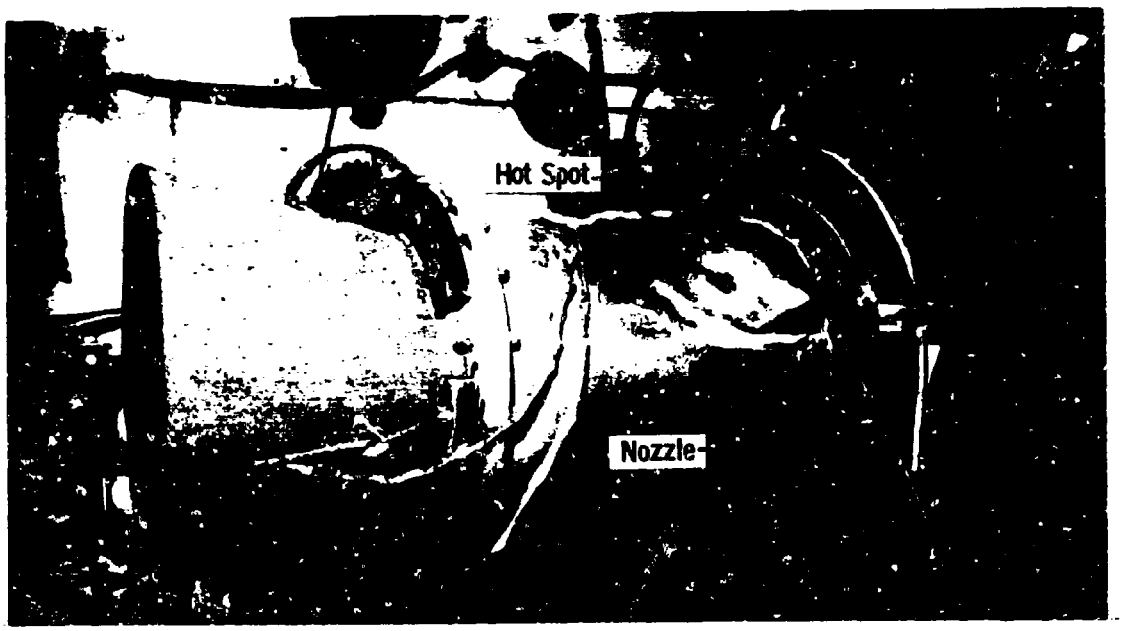

UNCLASSIFIED

Figure 40. Postfire Nozzle Condition

III, C, Demonstration Test Program (cont.)

(1) Deployment of Elastomeric Exit Cone

(u) As discussed previously, it was planned to deploy the elastomeric exit cones by pressurizing a rubber tube that was attached to the exterior surface of the cone near the exit plane. A variety of different tubes were tried as well as a variety of folding techniques in the order of accomplished deployment. Complete deployment was not achieved in any of these tests. A condition of partial deployment was achieved in many instances, a typical example of which is shown in Figure 41.

(u) It is believed that if the part were fired in this condition it would completely deploy under the internal gas pressure. However, no attempt was made to fire at a condition of potential deployment. On the first test of the elastomeric exit cone, the part was deployed before the test chamber was sealed.

(u) Subsequent to the first test another means of deployment was attempted. This scheme utilized a small trailer intertube as a bladder. The bladder was placed in the exit cone, and the V-44® exit cone was folded down on top of it and taped in place (Figure 42 and 43). The bladder was then pressurized, forcing the cone to open. A number of complete deployments were accomplished on a bench setup with this design, as well as one test on the motor at sea level (Figure 44).

(u) Nearly complete deployments were obtained with the exit cone in place on the motor at altitude (Figures 44, 45, and 46). This deployment had only a small kink in the cone when the deployment test ended, and it is quite certain that the exit cones would have completely opened during a motor firing. At any rate, it is evident that, with a properly designed bladder, an elastomeric cone of this size can be folded and deployed.

(u) The two V-44® exit cones that were tested were repeatedly folded into a shape in which the folded length was approximately one-half the free length (Figure 47).

(2) Erosion of V-44® Exit Cone

(u) V-44® performed exceptionally well as a high-expansion ratio exit cone material. A photograph of this component during firing is shown in Figure 48. The postfire condition of the two elastomeric exit cones (Figures 49 through 56) were nearly identical with regard to material loss.

(u) Erosion data was obtained by sectioning one of the exit cones and measuring the wall thickness with a micrometer at the various area ratios. The erosion rate varied from a maximum of 5.5 mils/sec at one point at an area ratio of 35 to an average rate of 1.6 mils/sec at the exit section at an area ratio of 50.

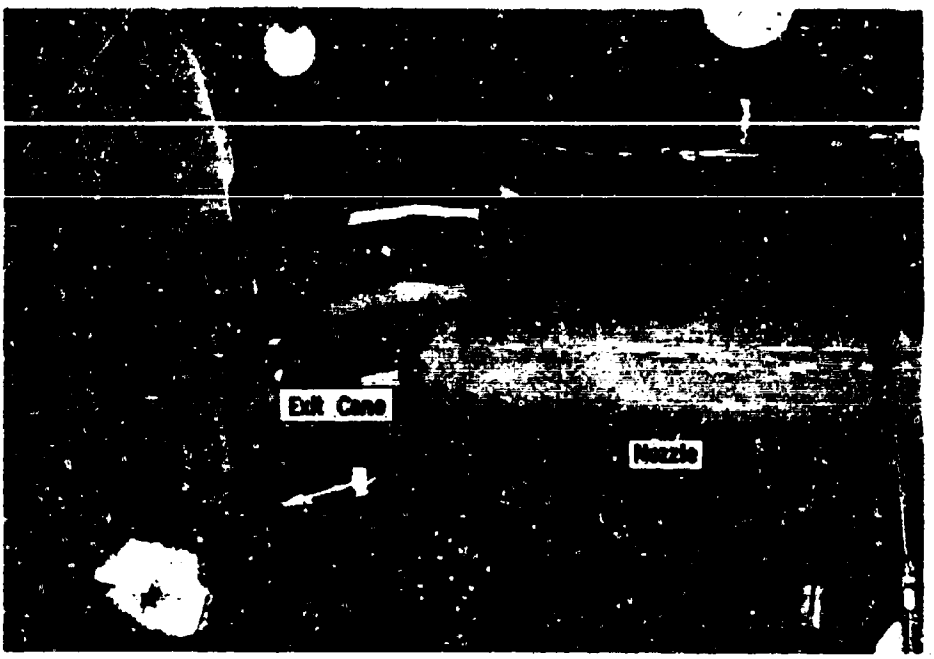

UNCLASSIFIED

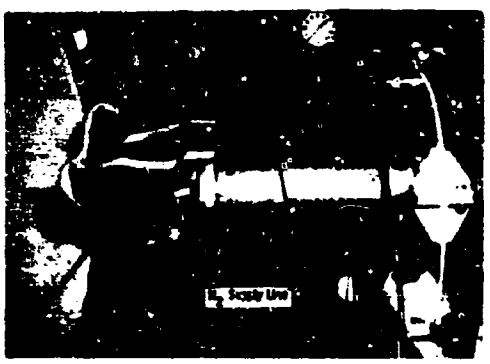

UNCLASSIFIED

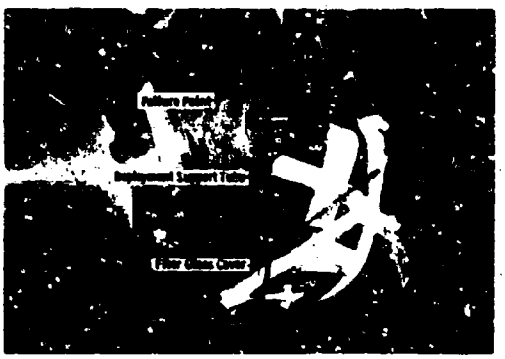

UNCLASSIFIED

Figure 41. Deployment of Demonstration V-44® Exit Cone with Circumferential Tube

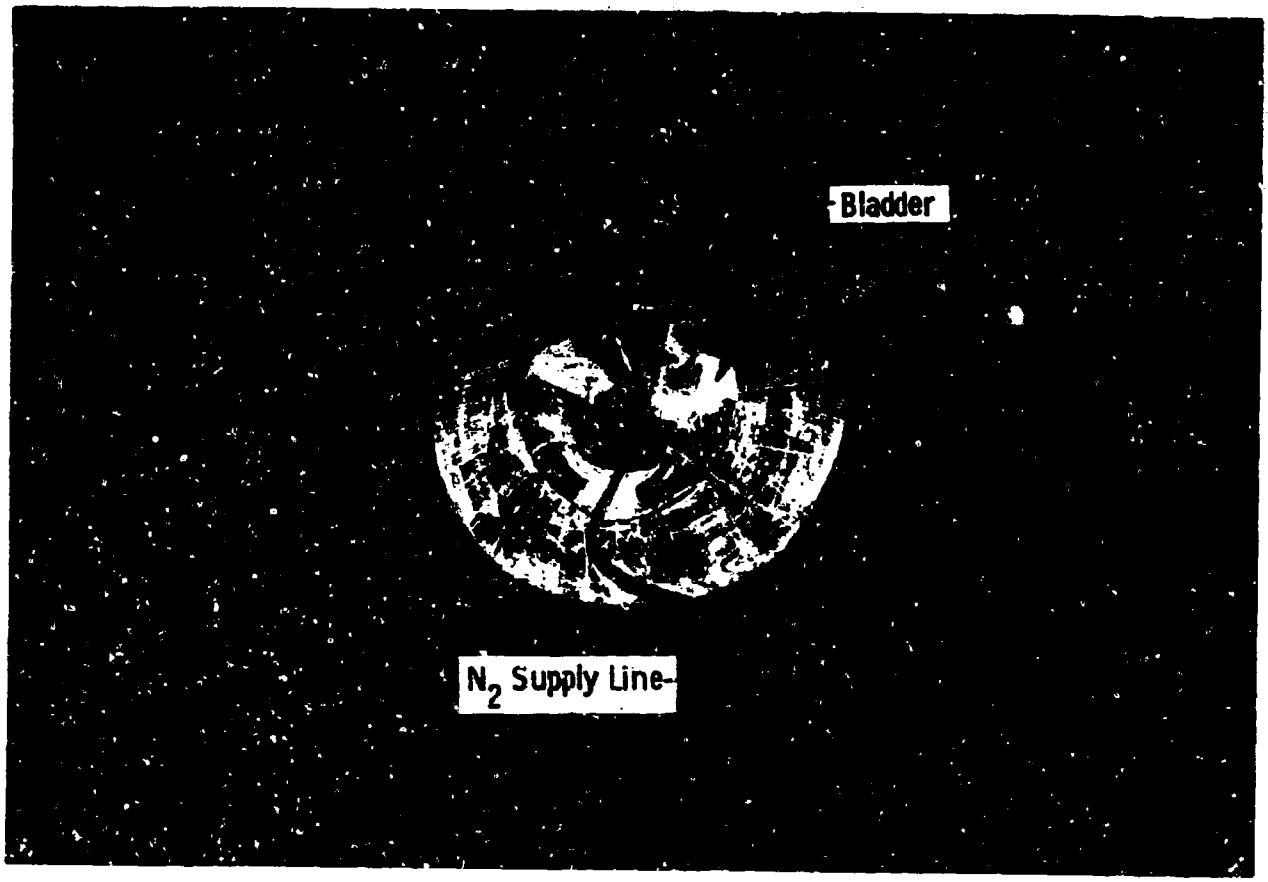

UNCLASSIFIED

Figure 42. Deployment of Demonstration V-44® Exit Cone, Bladder in Nozzle

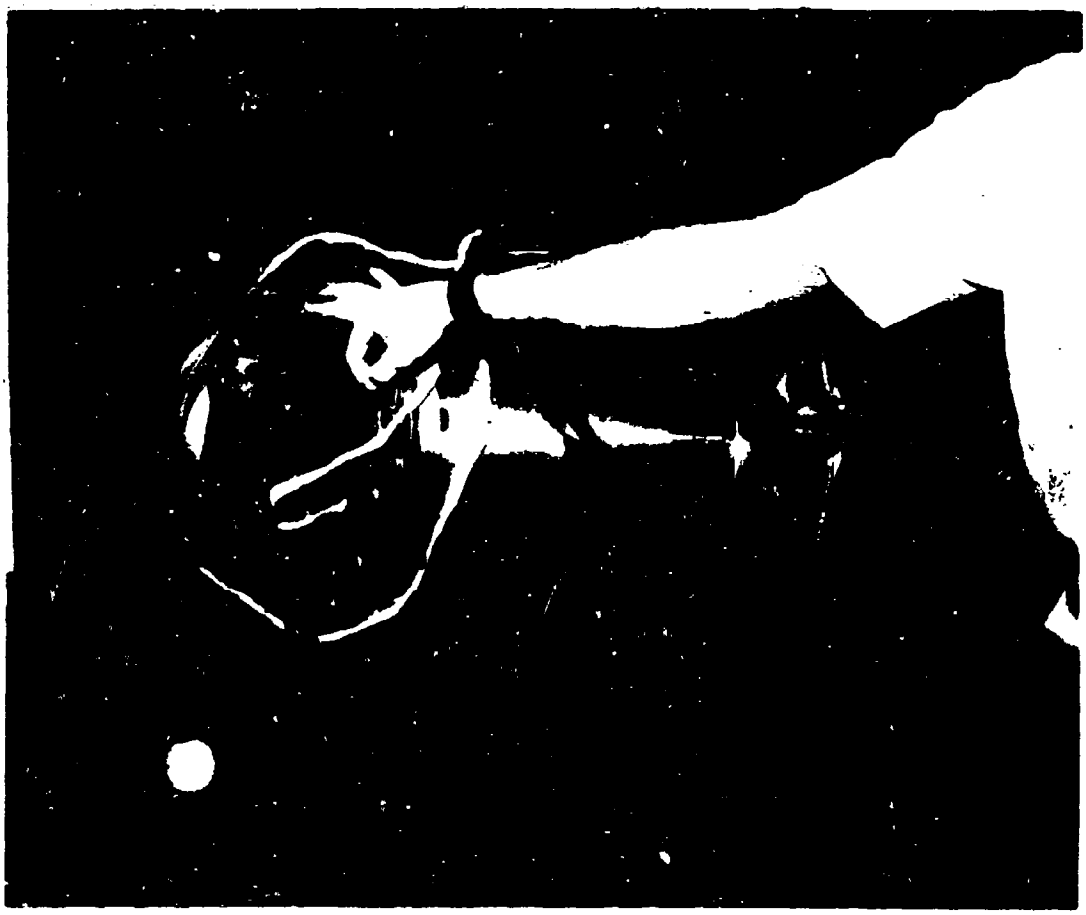

UNCLASSIFIED

Figure 43. Deployment of Demonstration V-44° Exit Cone, Using a Bladder at Sea Level

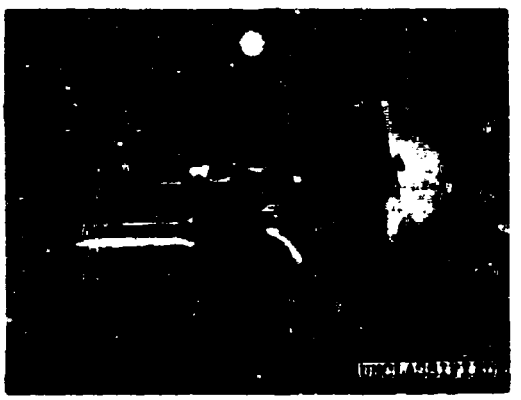

Application of Pressure, +0.1 sec

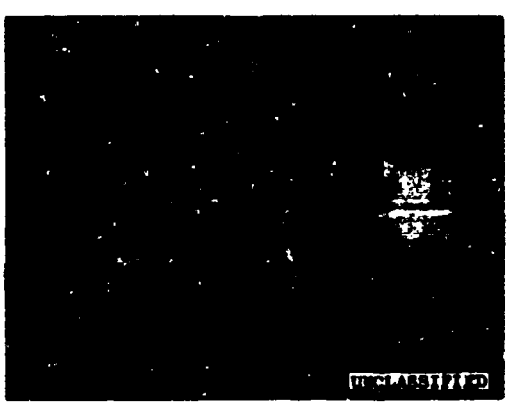

+8.3 sec

Full Deployment, +22.6 sec

Figure 44. Attempted Deployment of Demonstration V-44® Exit Cone at Sea Level Sequence 1

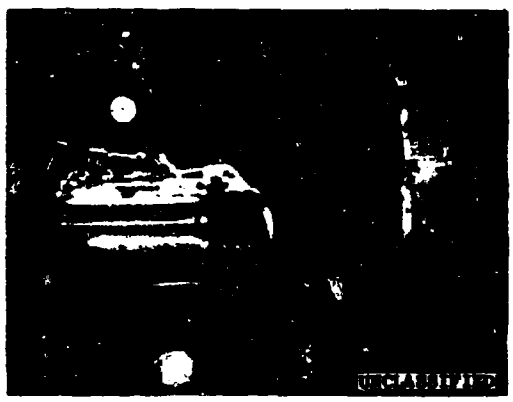

Pre-Test

Application of Pressure, +2.2 sec

Bladder Protruding, +9.2 sec

Figure 45. Attempted Deployment of Demonstration V-44B Exit Cone at Altitude, Sequence 2

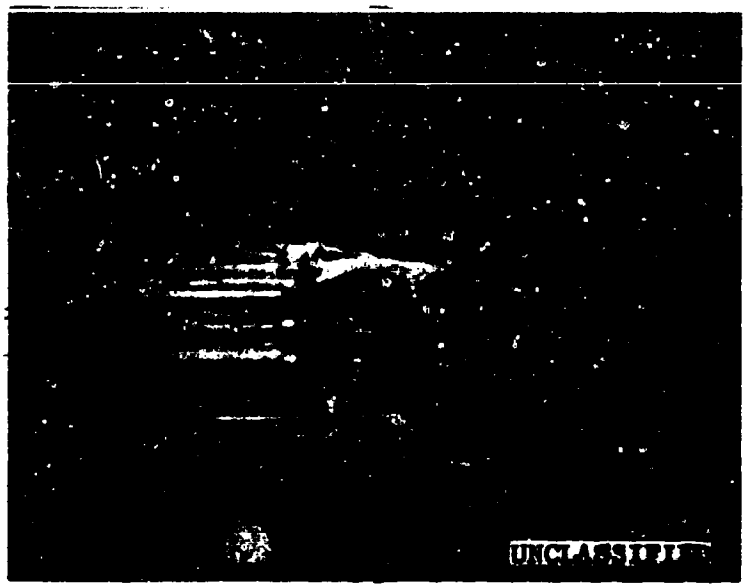

Bladder Burst, +9.208 sec

Maximum Deployment (Note Segment Folded Back), +9.7 sec

Figure 46. Attempted Deployment of Demonstration V-44(II) Exit Cone at Altitude, Sequence 3

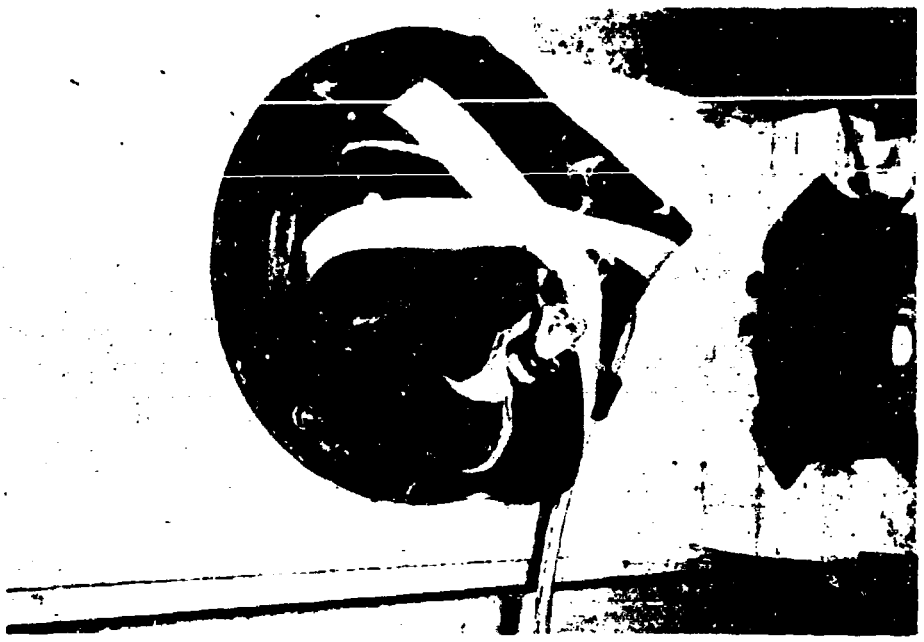

UNCLASSIFIED

UNCLASSIFIED

Figure 47. Folded Position of Demonstration V-44B Exit Cone

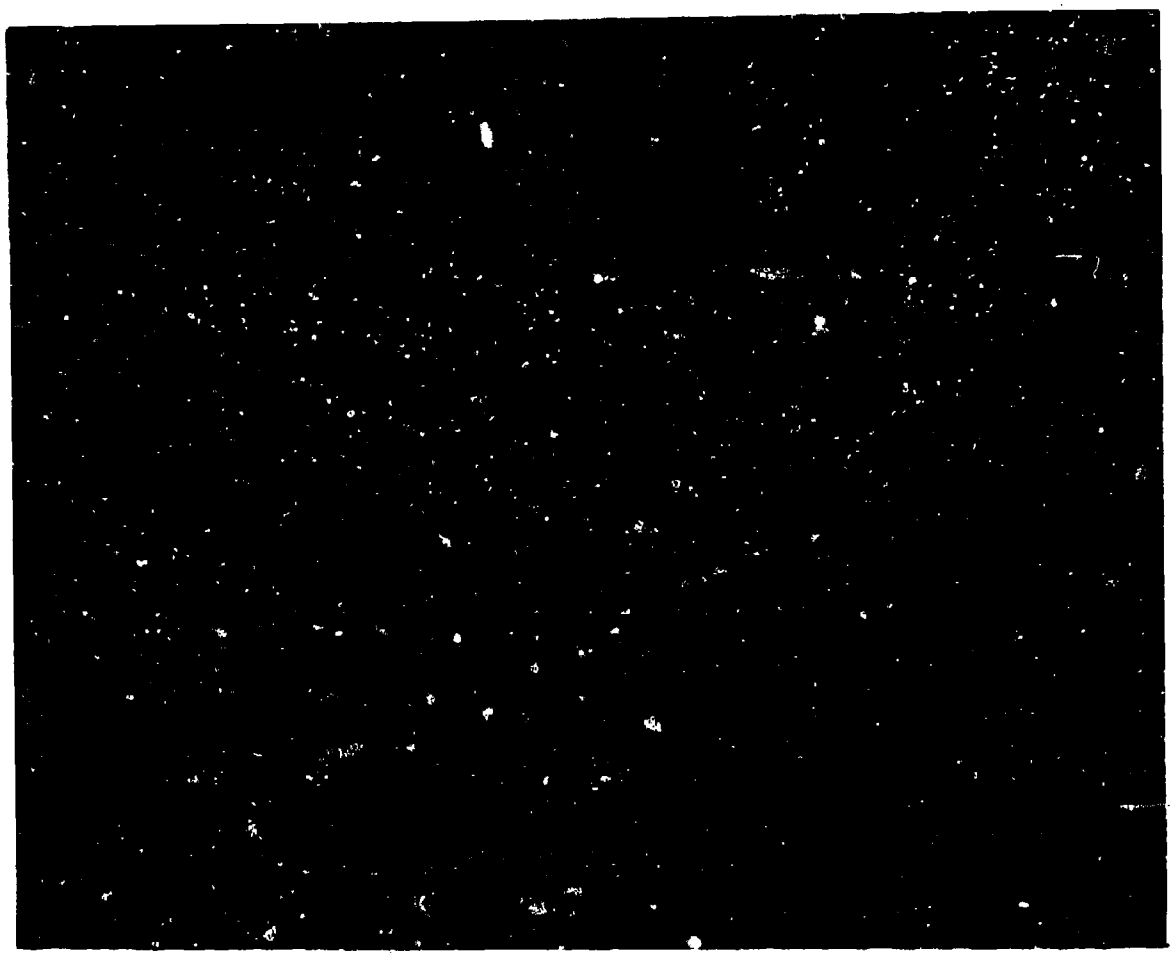

UNCLASSIFIED

Figure 48. Demonstration V-44® Exit Cone during Test at T + 6 sec

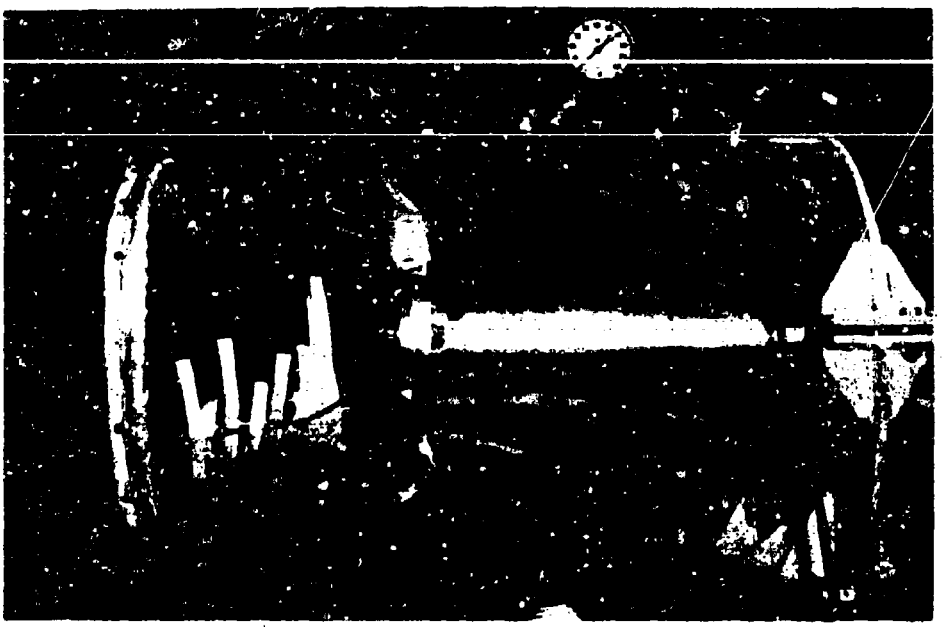

UNCLASSIFIED

Figure 49. Demonstration V-44® Exit Cone before First Firing, Overall View

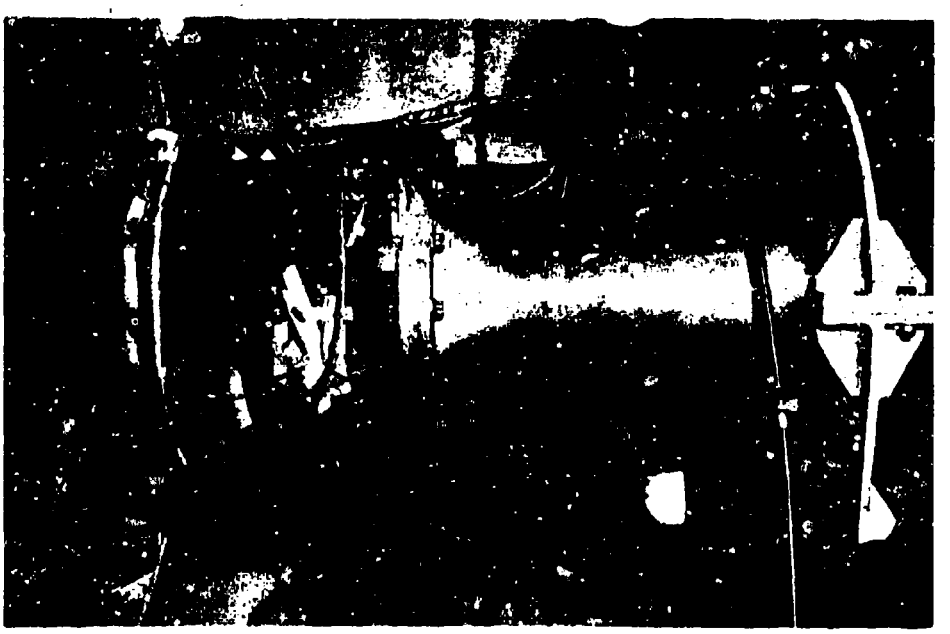

UNCLASSIFIED

Figure 50. Demonstration V-44® Exit Cone after First Firing, Overall View

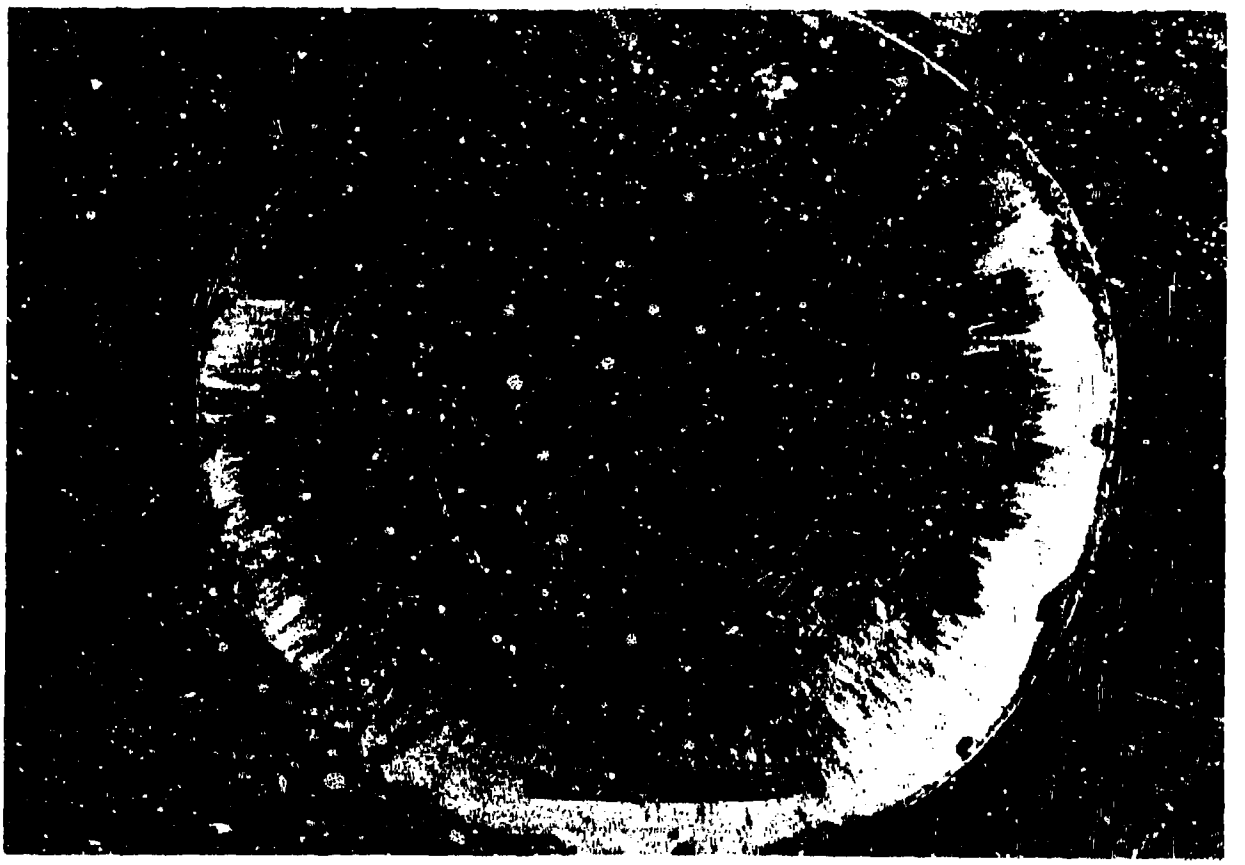

UNCLASSIFIED

Figure 51. Demonstration V-44® Exit Cone after First Firing

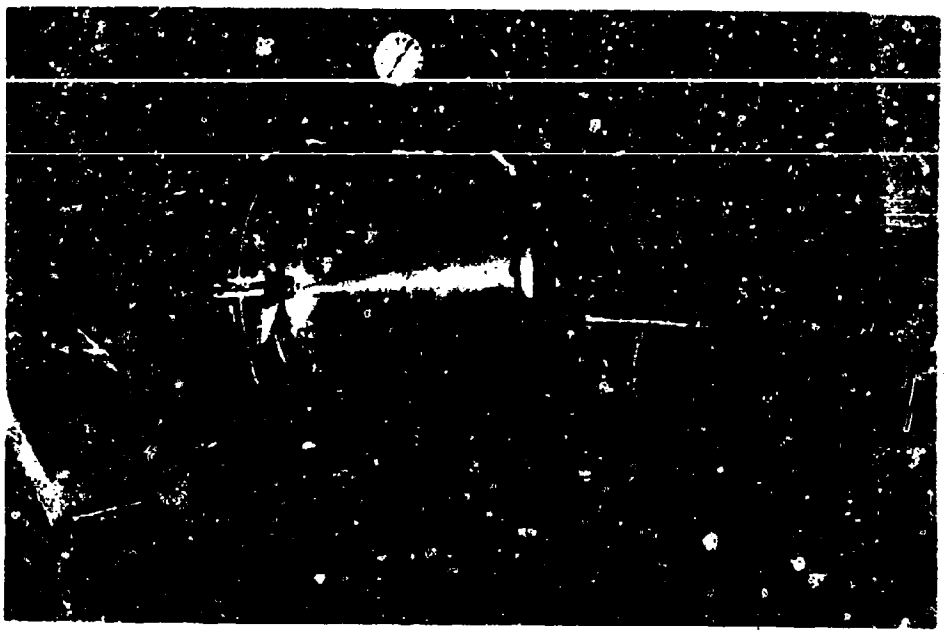

UNCLASSIFIED

Figure 52. Demonstration V-44® Exit Cone before Third Firing, Overall View

UNCLASSIFIED

Figure 53. Demonstration V-44® Exit Cone after Third Firing, Overall View

UNCLASSIFIED

Figure 54. Demonstration V-44B Exit Cone after Third Firing

UNCLASSIFIED

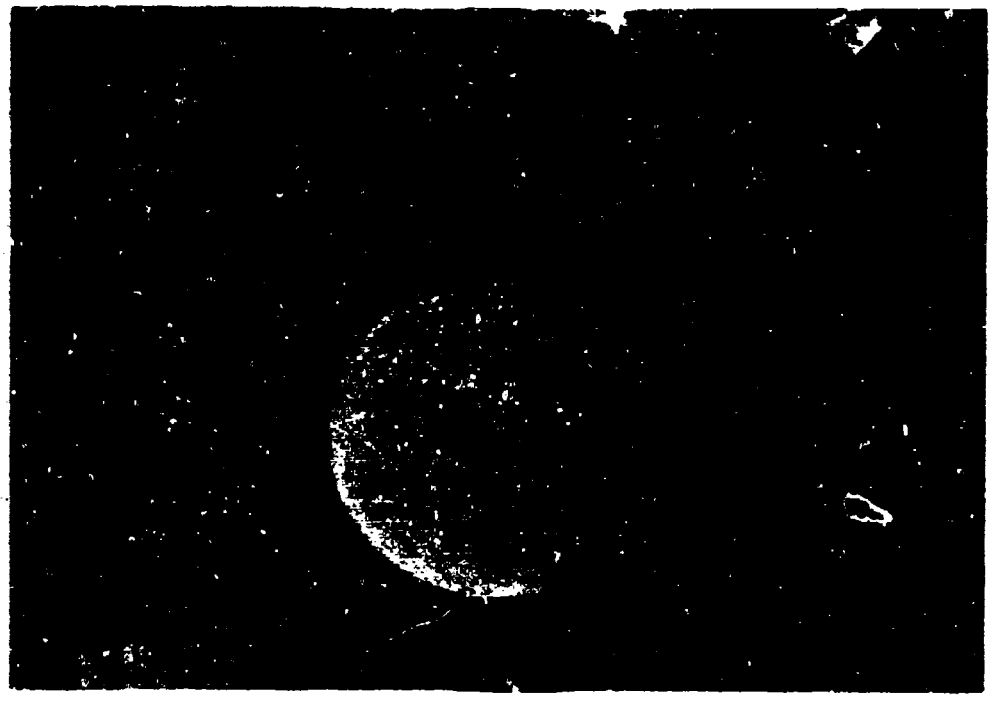

UNCLASSIFIED

Figure 55. Demonstration V-44® Exit Cone after First Firing, Comparison

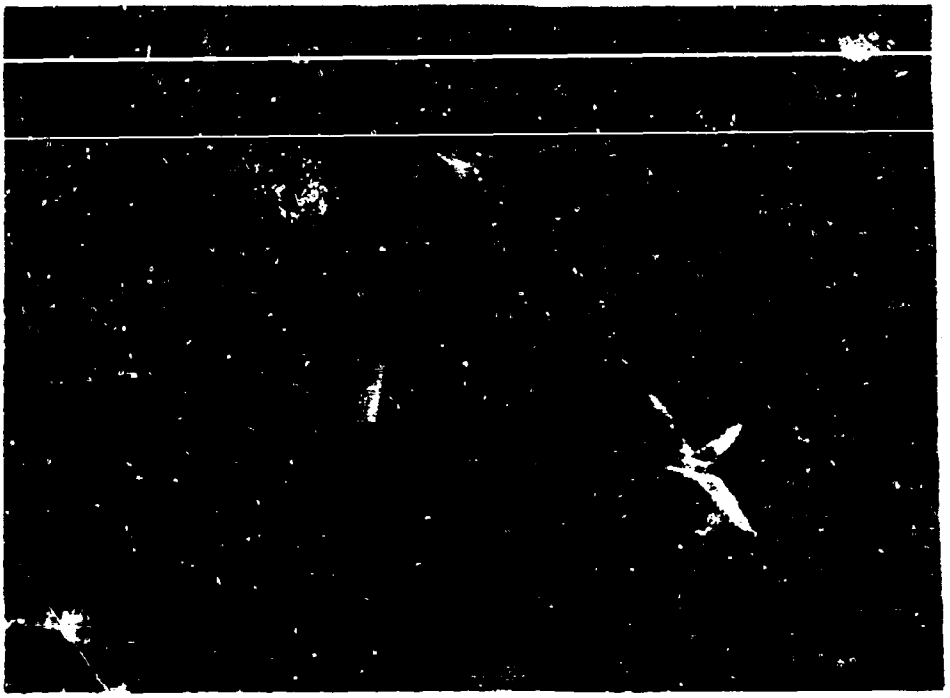

UNCLASSIFIED

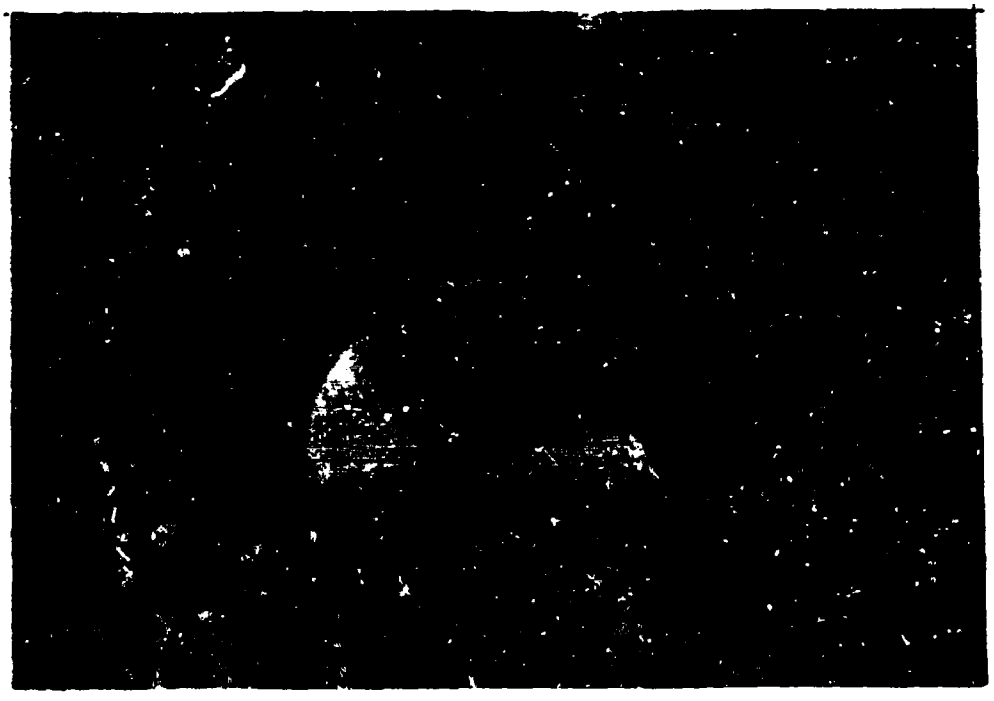

UNCLASSIFIED

Figure 56. Demonstration V-44® Exit Cone after Third Firing, Comparison

III, C, Demonstration Test Program (cont.)

(u) The demonstration exit cones did not exhibit the scalloped erosion pattern that was evident on the subscale cones. The material loss that occurred on these tests was 3.75 and 3.12 lb from an original prefire weight of approximately 11 lb. This weight loss averaged over the conical surface would amount to an average erosion of 120 mils (4 mils/sec). This average is somewhat higher than the true average erosion because some of the remaining V-44® liner wall decomposed resulting in a weight loss that would appear in this calculation of erosion. This partially decomposed V-44® is still an effective thermal barrier.

(u) Figure 57 presents the measured erosion at various stations in the exit cone, and Figure 58 shows the erosion of a typical longitudinal section. The predicted erosion (see Figure 8) from the thermal analysis agrees very well with the measurement made on the sectioned exit cone.

(u) The movies of these two tests do not indicate fluctuations in the V-44® exit cones at any time during the firings. The first test was with the circumferential external tube pressurized to 25 psia to provide additional stiffness. Because this did not appear to be necessary, the second V-44® exit cone was tested without this tube.

(u) The temperature histories for the two tests from backside thermocouples located at ℓ = 23.8 are shown in Figure 59. This included the 30-sec motor test and a 30-sec heat soak. Maximum temperature during motor operation was 90°F on the first test and 98°F on the third test.

(3) Columbium Exit Cone

(u) The columbium exit cone performed very well, as it did on the subscale tests. Unfortunately, the thermocouples broke loose very early on in the firing, and no more than 3.5 sec of temperature date were obtained. During this time, the maximum recorded reading was approximately 2200°F. A second thermocouple recorded a maximum reading of 4500°F at approximately 0.2 sec, but this thermocouple recorded wide fluctuations, casting doubt on all its measurements (see Figure 60).

(u) It is evident from the movies of both the subscale and the demonstration tests that the columbium exit cone ran much hotter on the demonstration test. The demonstration exit cone was white during the tests, while the subscale exit cone turned various shades of orange throughout the firing. There was no evidence of aluminum oxide deposits on the inner wall after the test (Figures 61 and 62), whereas the subscale exit cone was completely coated with aluminum oxide.

(u) The convolute opened during motor ignition and continued to open to a conic shape as the metal reached its peak temperature during the first few seconds of the firing (Figure 63). An examination of the pictures taken during

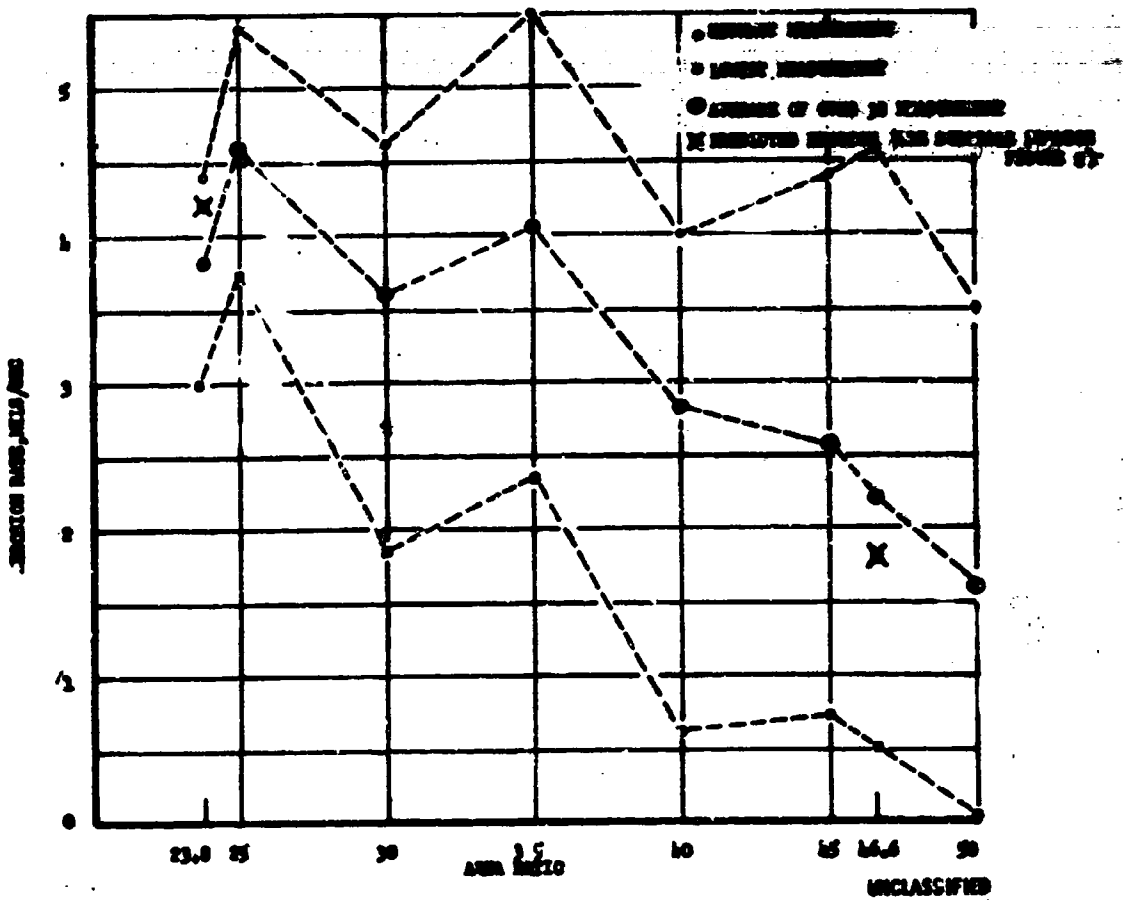

Figure 57. Erosion Rate Data for Demonstration V-44® Exit Cones

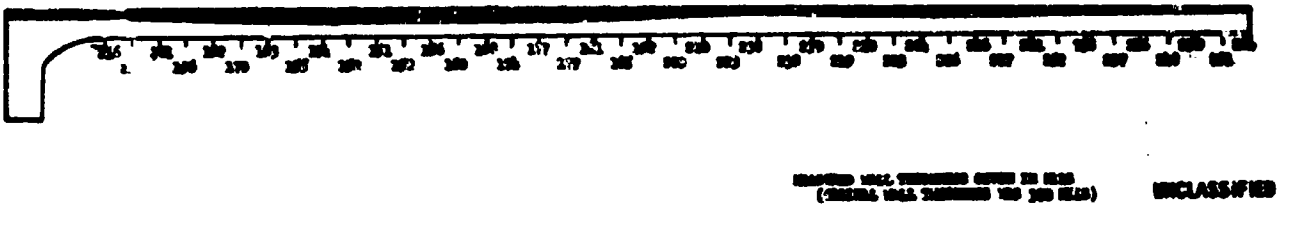

Figure 58. Typical Section of Tested Demonstration V-44® Exit Cone Showing Erosion

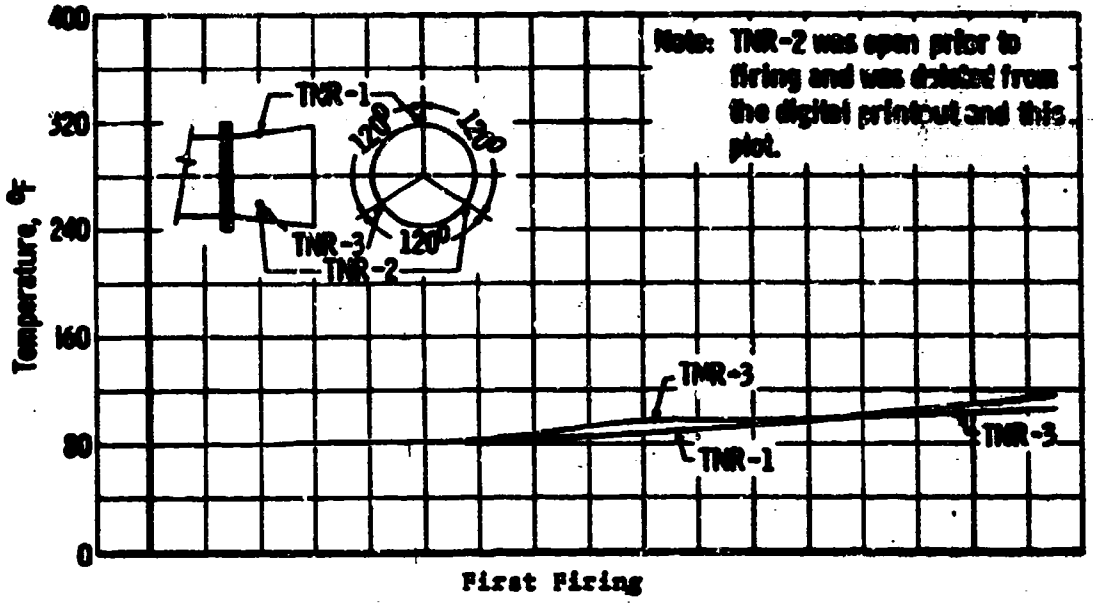

First Firing

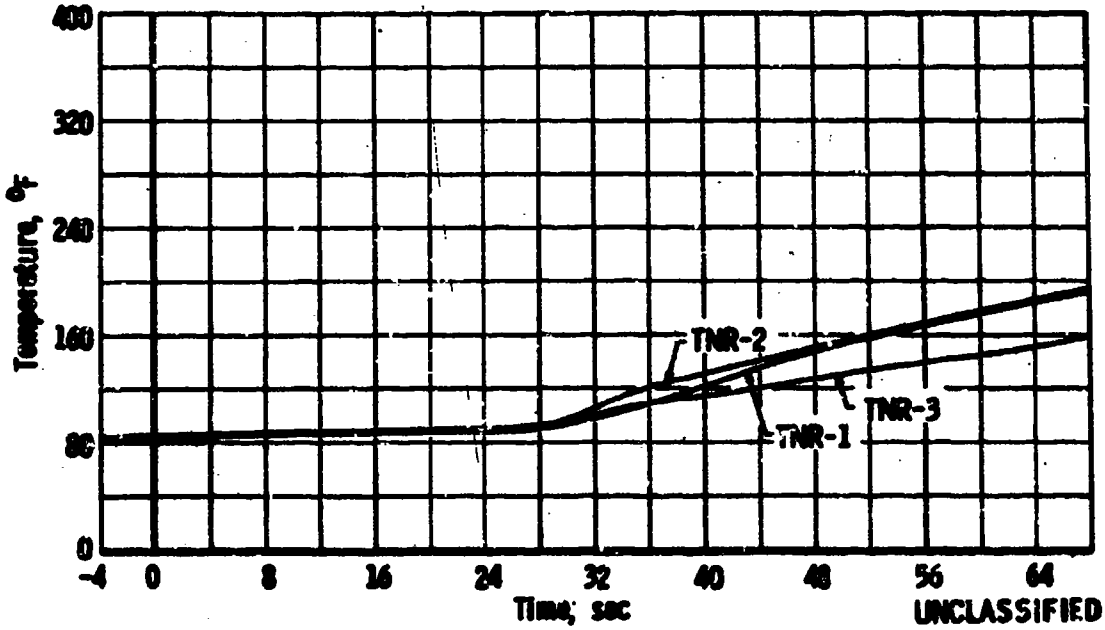

Third Firing

Thermocouple Data

Figure 59. Backside Temperature of Demonstration V-44® Exit Cones

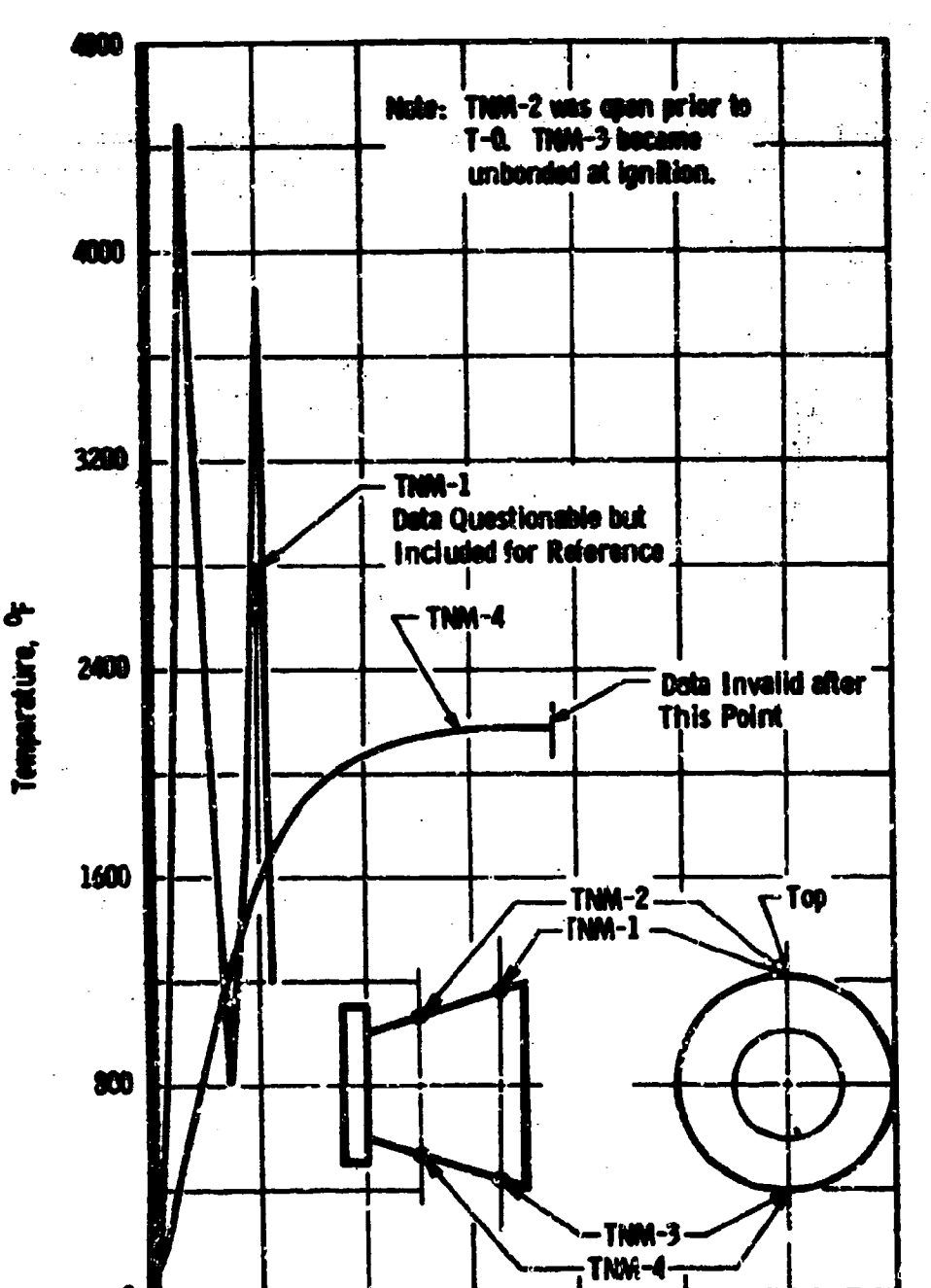

Figure 60. Backside Temperatures of Demonstration Columbium Exit Cone

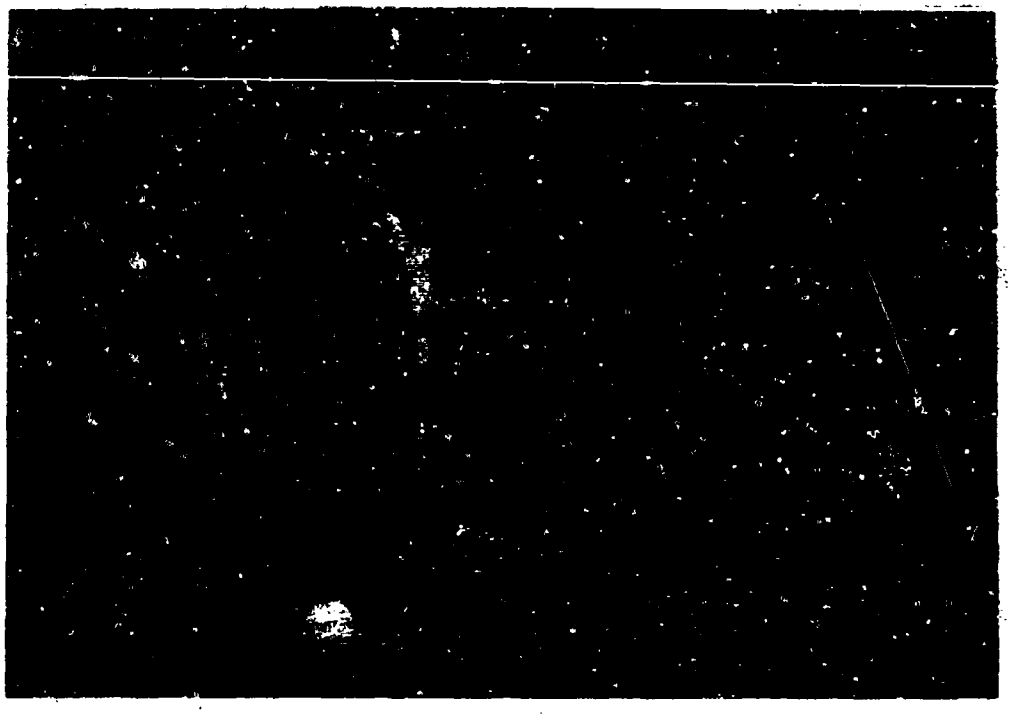

UNCLASSIFIED

Prefire

UNCLASSIFIED

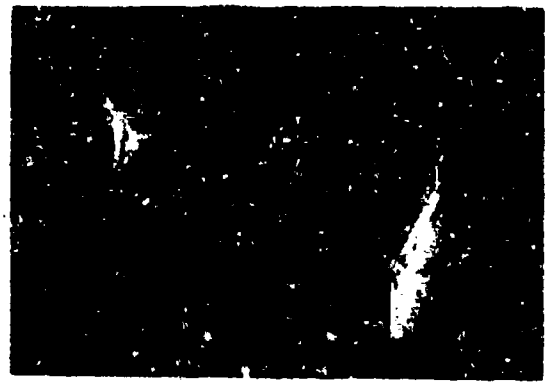

UNCLASSIFIED

Postfire

Figure 61. Demonstration Columbium Exit Cone. Overall View, Second Firing

UNCLASSIFIED

UNCLASSIFIED

Figure 62. Demonstration Columbium Exit Cone, Detailed Postfire View

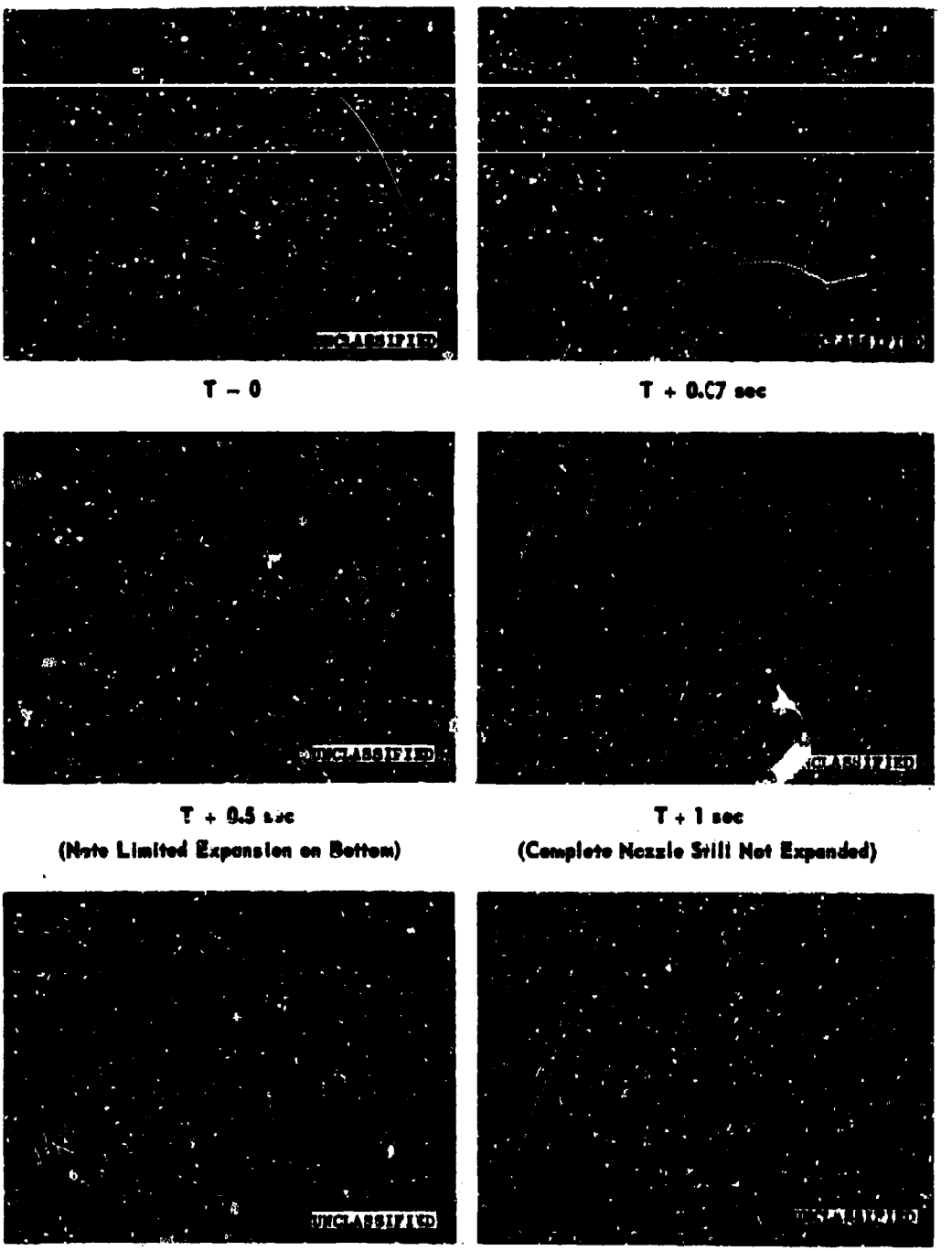

T - 0

T + 0.07 sec

T + 0.5 sec
(Note Limited Expansion on Bottom)

T + 1 sec
(Complete Nozzle Still Not Expanded)

T + 4.5 sec
(Maximum Expansion)

T + 22.3 sec

Figure 63. Deployment of Demonstration Columbium Exit Cone during Test Firing

III, C, Demonstration Test Program (cont.)

the firing indicates that the cone opened to an 11° half-angle. After the motor was shut down and the columbium exit cone had cooled to ambient temperature, the cone retracted to a 9.60° half-angle, (Figure 63). This corresponds to an exit area of 219 in.^{2} and an expansion ratio of 38.0. The convolutes did not expand uniformly, and the remaining corrugations had peak-to-trough variations from approximately 0.21 to 0.26 in.

(4) Motor Performance

(C) The performance of the three motors is summarized in Table 4. The total impulse for the three tests was 143,500, 142,000, 420,000, and 143,580 lbf-sec, respectively. The total impulse was calculated by correcting the thrust trace to vacuum conditions and integrating the resulting vacuum corrected thrust trace.

(C) The specific impulse values for the elastomeric exit cones, first and third tests, were 288.7 sec and 286.0 sec, respectively, whereas the specific impulse for the columbium exit cone, second test, was 284.8. These values for specific impulse were obtained from the stated total impulse calculations and the motor propellant weights. These motor propellant weights are accurate to approximately ± 2%; therefore, the calculated specific impulses contain a possible maximum 2% error due to uncertainty over the motor propellant weights.

(C) These measured specific impulse values corrected to standard sea level conditions (100-psi chamber pressure, optimum expansion, 15° conical half-angle) are 242.5 and 240.0 sec for the elastomeric exit cones and 239.5 for the columbium exit cone. The standard measured value for this propellant is 243.3, which was obtained from a series of standard test motor ballistic tests.

(U) All three test values of specific impulse are within 1.5% of the standard value, which is within the potential error in propellant weight. Thrust coefficients for the tests were computed from the vacuum corrected thrust measurements, measured chamber pressure, and motor throat area. For the two elastomeric cones, these measured thrust coefficients were 1.87 and 1.85, whereas the theoretical thrust coefficient for a 15° exit cone with an expansion ratio of 50 is 1.87. The measured thrust coefficient for the columbium exit cone was 1.85, as compared to a theoretical of 1.87 for a 9.6° exit cone at an expansion ratio of 38.

(U) A comparison of the four parameters (measured thrust coefficient, theoretical thrust coefficient, specific impulse from demonstration test, and specific impulse from 10-KS tests) indicates that they are within the stated accuracy of the motor propellant weights and the data acquisition system.

(C) The addition of an elastomeric or metallic nozzle extension (weighing 11 and 5-1/2 lb, respectively) results in a theoretical increase in motor performance of 4.5 %. For these motors, this increase is approximately

TABLE 4

SUMMARY OF DEMONSTRATION MOTOR PERFORMANCE (u)

Motor serial number	C	D	E
Igniter serial number	61	62	63
AEDC test number	RF0518-01	RF0518-02	RF0518-03
Test date	10-3-65	10-8-65	10-14-65
Motor environment during 16 hr prior to cell pumpdown, °F	83	83	83
Type of nozzle	Elastomeric	Metallic	Elastomeri
Ignition altitude, ft	100,000	103,000	107,000
Average altitude, ft	112,000	112,000	112,000
Propellant mass, lb	497	500	502
Prefire throat area, $in.^2$	5.76	5.76	5.743
Postfire throat area, $in.^2$	5.71	5.64	5.42
Prefire exit area, $in.^2$	290.1		290.1
Postfire exit area, $in.^2$*	289.2	219.0	281.7
Ignition delay, msec	36	44	36
Total burn time, sec	30.3	30.8	30.8
Total impulse, lbf-sec			
Measured	142,640	141,800	142,720
Vacuum	143,500	142,420	143,580
Percent vacuum correction	0.60	0.44	0.60
Specific impulse, sec	288.7	284.8	286.0
Specific impulse, sec**	242.5	240.0	239.5
Standard specific impulse	243.3	243.3	243.3
Measured thrust coefficient corrected to vacuum conditions	1.87	1.85	1.85
Theoretical vacuum thrust coefficient	1.87	1.87	1.87

*Based on measurement of circumference
**Corrected to standard condition (1000-psi chamber pressure, optimum expansion ratio, and 15° conical half-angle)

III, C, Demonstration Test Program (cont.)

6400 lbf-sec of total impulse. If overall system weight must be held constant, an equal decrease in propellant weight would reduce performance by 3100 and 1600 lbf-sec, respectively. Therefore, it can be seen that with no increase in system weight, motor performance could be increased by 3300 lbf-sec, 2.3% with the elastomeric nozzle (or 4800 lbf-sec), and 3.4 % with the metallic nozzle.

c. Conclusions

(u) The test program conducted at Arnold Engineering Development Center met the program objectives successfully:

(u) (1) Successful motor ignition, operation, and postfire heat soak for all three tests were conducted at a simulated altitude in excess of 100,000 ft.

(u) (2) Although an attempt to completely deploy the elastomeric exit cone from a folded position at altitude was successful, the principle of deployment was demonstrated by the successful deployments accomplished on sea level tests.

(u) (3) All three exit cones were stable during motor testing and were in excellent postfire condition, demonstrating the integrity of these materials for packageable exit cones.

(u) (4) Specific impulse data for the three motors demonstrated that the tested exit cone performance was close to theoretical.

(u) (5) The corrugated columbium exit cone deployed to an area ratio of 38.0 rather than the designed expansion ratio of 50:1. Still, the principle was successfully demonstrated and, with better design information on the high-temperature material properties of columbium, the required expansion ratio can be achieved.

SECTION IV

FUTURE WORK IN EXPANDABLE EXIT CONES

(u) The completion of the test series at AEDC supported the feasibility of using expandable exit cones on solid rocket motors. However, there remain certain areas that require further development: (1) deployment and support of elastomeric exit cones, (2) the analysis of external flow and aerodynamic heating on the exit cones, and (3) the analytical prediction of loadings and deflections of elastomeric exit cones under typical TVC loadings.

(u) The experimental work done to date with elastomeric expandable exit cones by both Liquid Rocket Operations and Solid Rocket Operations of Aerojet-General indicates the major problem to be one of deployment, with associated problems of folding and supporting the deployed cone. The subscale and demonstration test programs conducted on the expandable nozzle by Solid Rocket Operations definitely established that the tested elastomeric materials can withstand aluminized solid propellant gas flow when adequately supported.

(u) Liquid Rocket Operations has been working on the problems of deployment and exit cone support and is investigating a number of promising designs. These design concepts are readily adaptable to solid motors and should be investigated in sizes and thicknesses compatible with solid rocket motors.

(u) Expandable exit cones for solid rockets require thicker wall sections than for liquid rockets operating at the same chamber pressure and durations because solid propellant gases with metal or oxide particles are much more erosive.

(u) In general, the expandable exit cone sections for solid rockets are smaller than those that have been tested for liquid rockets. Thus, folding and deployment of solid expandable exit cones differ from those that are being tested for liquid rockets because of the higher ratio of wall thickness-to-cone diameter.

(u) The effect of this difference cannct be evaluated analytically because of the complexity of the problem and must be determined by testing in the solid rocket configuration.

(u) There are a number of deployment methods to be considered. One such deployment method is the pressurized tube concept shown in Figure 30. A series of flexible tubes are attached longitudinally to the exterior of the exit cone surface and are manifolded at the top and bottom. The bottom manifold is a steel torus fixed to the nozzle attachment flange, and the top manifold is a flexible tube. The complete tube assembly is bonded to the exit cone and sprayed with a silicone-base rubber material.

IV, Future Work in Packageable Exit Cones (cont.)

(u) A second concept utilizes an inflatable bladder. Exit cone deployment and structural stability are provided by a fibrous cloth-reinforced pneumatic jacket. The expandable exit cone and an outer bladder are stitched together by glass fibers, and the entire assembly is vulcanized into one integral unit. Deployment and stability are obtained when the jacket is inflated. The advantages of this technique are a lightweight deployment structure and a continuous uniform gas pressure in the supporting jacket.

(u) Another concept proposed by Liquid Rocket Operations is a combination of a metallic exit cone structure and a foldable elastomeric exit cone. The metallic cone structure backs up the elastomeric exit cone when it is deployed by either mechanical actuators or a pneumatic system.

(u) Each of these concepts appears promising and should be investigated for use with solid rockets.

(u) The use of a metallic radiation-cooled exit cone appears most promising. The testing done to date has established the feasibility of metallic radiation-cooled exit cones on both liquid and solid rockets, with either a fixed cone or a convoluted cone. Additional information is needed on material properties of columbium and tantalum alloys in the high operating temperatures of radiation-cooled exit cones to consummate these designs. Also required is additional analysis and testing of the opening of the convoluted cylinder during motor operation.

APPENDIX I

DERIVATION OF LIQUID ROCKET OPERATIONS' MATERIAL EFFECTIVENESS PARAMETER

APPENDIX I

DERIVATION OF LIQUID ROCKET OPERATIONS' MATERIAL EFFECTIVENESS PARAMETER

A. ANALYSIS

(u) This appendix presents a heat transfer analysis of the ablative materials tested on the liquid Lark engine; the original analysis was presented in Ref 2. Symbols used herein are defined in Section B of this appendix.

(u) It is assumed that the heat flux into the rubber wall produces a corresponding increase in material ablation rate, neglecting any blocking effects. The heat balance on the wall element is

$$\Delta H \frac{\dot{dm}}{da} = h_c (T_{aw} - T_w) \qquad \text{(Eq 1)}$$

The recovery temperature, wall temperature, and heat of decomposition are taken as constant and relatively independent of nozzle area ratio. The heat transfer film coefficient is predicted by the Bartz equation

$$h_c = \left[\frac{0.026}{D_*^{0.2}} \frac{C_p \mu^{0.2}}{Pr^{0.6}} \left(\frac{\dot{W}}{A_t} \right)^{0.8} \right] \frac{1}{\rho^{0.9}} \qquad \text{(Eq 2)}$$

If it is assumed that the heat transfer film coefficient depends only on the diameter, the expression reduces to

$$h_c = K_1 \frac{D_*^{1.6}}{D^{1.8}} \qquad \text{(Eq 3)}$$

If this expression is substituted into the heat balance equation and integrated over the conic divergent nozzle, the result is given below:

$$H = K_2 \left[\frac{t_b}{\Delta M} D_*^{1.8} (T_{aw} - T_w) (\varepsilon_e^{0.1} - \varepsilon_a^{0.1}) \left(\frac{\dot{W}}{A_t} \right)^{0.8} \right] \frac{0.026}{\sin \alpha} \qquad \text{(Eq 4)}$$

(u) The factor outside the brackets is a nozzle geometry parameter, whereas the factor inside includes both a material ablation rate and heat transfer environment factors. The larger the factor, the higher the heat of decomposition of the material. The factor inside the bracket will be used as a material effectiveness parameter for comparison of one material to another. It is described as an effectiveness parameter, ξ.

$$\xi = \frac{t_b}{M} D_*^{0.2} (T_{aw} - T_w) (\varepsilon_e^{0.1} - \varepsilon_a^{0.1}) (\dot{W})^{0.8} \qquad \text{(Eq 5)}$$

A, Analysis (cont.)

(u) In the test series, the total expansion ratio and attachment area ratio are varied by the nozzle redesign as well as the total propellant weight flow rate. The throat diameter also varies. The wall temperature is taken as 500°F for all materials tested. This was obtained from the 1961-62 test series for Gen-Gard V-44® rubber material.

(u) It is realized that for materials containing asbestos the wall temperatures would be higher, but the asbestos does not ablate. The temperature that should be used is the decomposition temperature of the material that ablates away. Combustion efficiencies were used in the determination of the recovery temperature. The recovery temperature is related to the static gas temperature and combustion temperature by

$$\frac{T_{aw} - T_{\infty}}{T_{stag.} - T_{\infty}} = \sqrt[3]{Pr} \qquad \text{(Eq 6)}$$

The stagnation temperature is corrected for combustion efficiency by

$$T_{\substack{stag. \\ actual}} = T_{\substack{stag. \\ theor.}} \left(\frac{C^*_{actual}}{C^*_{theor.}} \right)^2 \qquad \text{(eq 7)}$$

(u) A tabulation of the effectiveness parameters for the materials tested on the Lark engine is presented in Table 5.

TABLE 5

MATERIAL EFFECTIVENESS PARAMETERS

Vendor	Compound Designation	Composition-Major Ingredients*	Effectiveness** Parameter
General Tire & Rubber Co.	Gen-Gard V45	NBR, Silica	172/421
	Gen-Gard V44	NBR, Silica, Asbestos	255/1400
	Gen-Gard V50	NBR, Silica, Low-Temperature Plasticizer	291/415/665
	Gen-Gard V52	NBR, Silica, Asbestos, Low-Temperature Plasticizer	472/540
	9790-IV-29C	SBR, Silica, Asbestos	539/900
	9790-IV-31C	SBR, Silica, Asbestos, Phenolic	323/580
	Gen-Gard V62	SBR, Silica, Asbestos, Phenolic	342/525
	Gen-Gard V63	SBR, Silica, Asbestos, Phenolic	490/741
	9790-IV-138D	XP-139, Silica	220/298
	7409-II-39C	EPT, Silica	930
	7242-I-114X	Butyl, Silica, Asbestos	506/935
	9790-IV-144A	Epoxy, Silica, Asbestos	172/459
	7242-III-10A	Silicone Rubber, Silica	214/245
	9790-IV-126A	NBR, Phenolic, Silica, Asbestos	99
	7242-III-41C	Silicone Rubber, Silica, Asbestos	901
	9790-IV-146A	Silicone Rubber, Silica	157
Raybestos-Manhattan	RL-2061A	Asbestos-Coated Inconel Wire Aluminum-Coated Silica-Filled Buna-N	280
	RL-2061B	Same as above but no coating	286
	RL-2061C	Silicone Rubber, Asbestos and Wire Cloth	449
	RL-2061D	Proprietary Material	312
	2169-14	Proprietary Material	224
	CL 8575-8	Proprietary Material	400
	CL 8575-7	Proprietary Material	830
	RL 2403	Proprietary Material	566
	CL 8575-7-F	Proprietary Material	481
	CL 8575-7-E	Proprietary Material	580
	CL 8576-7-D	Proprietary Material	812
American Poly-Therm Co.		Refrasil-Filled Polyuretane	419
Nobel Research Laboratory		Modified Phenolic	350

* General Tire and Rubber exit cones were reinforced with nylon cord.

** Where data for more than one test was available, the effectiveness parameter for each test is given.

Legend: NBR - Nitrile Butadiene Rubber
SBR - Styrene Butadiene Rubber
EPT - Ethylene Propylene Rubber

B. NOMENCLATURE

Symbol	Definition
A_t	Throat area, $in.^2$
C*	Characteristic velocity, ft/sec
C_p	Specific heat at constant pressure, Btu/lb°F
D	Local diameter, in.
D_*	Throat diameter, in.
H	Total heat flux, Btu
h_c	Convective heat transfer, Btu/ft^2-hr-°F
ΔM	Material weight loss, gm
Pr	Prandtl number
Taw	Adiabatic wall temperature, °F
T_w	Wall temperature, °F
T_{stag}	Stagnation temperature, °F
$T\infty$	Free stream temperature, °F
t_b	Test duration, sec
$\dot{w}$	Motor mass flow, lb/sec
d_m/d_a	Elemental material loss per unit area
α	Exit-cone half-angle, degree
ε	Expansion ratio
ε_a	Expansion ratio at cone entrance
ε_e	Expansion ratio at cone exit
μ	Absolute viscosity, lb/ft-hr

APPENDIX II

THERMAL ANALYSIS PROCEDURES

APPENDIX II

THERMAL ANALYSIS PROCEDURES

A. DESCRIPTION

(u) This appendix contains a discussion of the heat transfer to the internal surfaces of the nozzle design that was generated during the design phase of this program. It is included in this report to show how the resulting transient temperatures of the pertinent nozzle components are calculated.

(u) Symbols used in the calculations are defined in portions of the text.

B. METHOD OF ANALYSIS

1. Convection

(u) The thermal analysis of the expandable nozzle consists of predicting the transient and steady-state temperature distribution in the various nozzle components. This analytical prediction requires the evaluation of the surface heat flux, which subsequently is used to evaluate the boundary conditions necessary for solution of the transient-conduction equation.

(u) The surface heat flux due to convection is governed by the relation

$$\dot{q} = h_c (T_{aw} - T_w) \qquad \text{(Eq 1)}$$

where

$\dot{q}$ = Convective heat flux, Btu/sq ft hr

h_c = Convective heat transfer coefficient, Btu/sq ft hr °F

T_{aw} = Adiabatic wall temperature, °R

T_w = Wall temperature, °R

(u) During this thermal analysis, the Colburn equation, originally developed for fully developed flow in circular ducts, was used to evaluate the convective-heat-transfer coefficient of Equation 1. Although the flow in nozzles does not correspond to the flow in constant-area circular ducts, previous experience with numerous motors with nozzles geometrically similar to the nozzle design considered here has shown that accurate results are obtained by using the Colburn equation to evaluate the convective-heat-transfer coefficient.

(u) The dimensionless form of the Colburn equation corresponding to Reynolds analogy is

$$\frac{h_c}{\rho u C_p} \, Pr^{2/3} = 0.023 \left(\frac{\rho u D}{\mu} \right)^{-1/5} \qquad \text{(Eq 2)}$$

B, Method of Analysis (cont.)

where

ρ = Local propellant gas density, lb/cu ft

u = Local free stream velocity, ft/hr

C_p = Specific heat at constant pressure

Pr = Prandtl number

D = Local nozzle diameter, ft

μ = Absolute viscosity, lb/ft hr

(u) The mass flux in Equation 2, at the throat of a nozzle (*), is given by

$$(\rho u)^* = C_w P_c \qquad \text{(Eq 3)}$$

where

C_w = Propellant mass flow coefficient, hr^{-1}

P_c = Absolute chamber pressure, lb/sq ft^2

(u) When the equation of continuity is used, the local mass flux (δ) at any location in the nozzle becomes

$$(\rho u)_\delta = C_w P_c \frac{A^*}{A} \qquad \text{(Eq 4)}$$

where

A = Local nozzle area, sq ft

A* = Throat area, sq ft

(u) Equation 4 can be substituted in Equation 2 and simplified to obtain the relationship

$$h_c = \frac{0.023\, C_w P_c C_p}{\left(\frac{P_c C_w D^*}{\mu}\right)^{1/5}} \, Pr^{-2/3} \left(\frac{A^*}{A}\right)^{0.9} \qquad \text{(Eq 5)}$$

(u) Analytical and experimental studies of motors with conventional nozzles similar to the configuration in this study has indicated that particle impingement and radiation are negligible contributions to the surface heat flux, as compared with the convective contribution. Based on this finding, Equation 1 was used to approximate the total heat flux.

B, Method of Analysis (cont.)

(u) The adiabatic wall temperature, T_{aw}, contained in Equation 1, is given by the relationship

$$T_{aw} = T_c \left(\frac{2 + (\gamma - 1) R M^2}{2 + (\gamma - 1) M^2} \right) \qquad \text{(Eq 6)}$$

where

R = Recovery factor

γ = Isentropic coefficient

M = Local Mach number

T_c = Chamber gas temperature, °R

(u) The recovery factor for a turbulent boundary layer is obtained from the Seban equation

$$R = \sqrt[3]{Pr} \qquad \text{(Eq 7)}$$

(u) Total heat flux to the nozzle interim wall is then obtained by substituting Equations 5 and 6 in Equation 1.

2. Transient Conduction

(u) As noted earlier, the thermal-response character of the nozzle components is obtained by solution of the transient-conduction equation with the appropriate boundary conditions. The general transient conduction equation, expressed in cylindrical coordinates, is

$$W C_p \frac{\partial T}{\partial \theta} = \frac{\partial}{\partial r} \left(k \frac{\partial T}{\partial r} \right) + \frac{k}{r} \frac{\partial T}{\partial r} \frac{\partial}{\partial z} \left(k \frac{\partial T}{\partial z} \right) \qquad \text{(Eq 8)}$$

where

k = Thermal conductivity, Btu/hr ft °F

r = Radial coordinate, ft

z = Axial coordinate

W = Material density, lb/cu ft

C_p = Specific heat, Btu/lb °F

θ = Time, hr

B, Method of Analysis (cont.)

(u) The boundary conditions used in the solution of Equation 8 are obtained from an energy balance at the heated surface. At this surface, the heat flux to the surface is equal to the heat flux leaving the surface in the absence of ablation, or

$$\dot{q} = h_c (T_{aw} - T_w) = -k \left(\frac{\partial T}{\partial r}\right)_{r = r_i} \qquad \text{(Eq 9)}$$

where

k = Thermal conductivity of the surface material, Btu/hr ft °F

r_i = Radius of internal nozzle surface, ft

When the surface material is known to erode, the surface boundary conditions now become

$$\dot{q} = h_c (T_{aw} - T_a) = k \left(\frac{\partial T}{\partial r}\right)_{r = r_i} + h_{eff} \left(\frac{\partial r}{\partial \theta}\right)_{r = r_i} \qquad \text{(Eq 10)}$$

where

T_a = Effective ablation temperature, °F

h_{eff} = Effective heat of ablation, Btu/lb

(u) With the heating rates and boundary conditions as noted above, the data presented in the appendix were calculated by a general thermal analyzer program written for the IBM 7094 computer. A modification of the Dusinberre explicit finite difference technique for heat flow in multilayer solids is used in this solution.

(u) The difference equations are described to incorporate variable thermal properties, multidimensional heat flow, and boundary conditions required to predict any transient or steady-stage temperature environment.

3. Radiation Equilibrium

(u) For a thin metallic wall, the temperature at which the net internal heat transfer is equal to the external radiation heat flux is defined as the radiation equilibrium temperature, T_{eq}. The value is estimated by trial and error from an equation of the form

$$h_c (T_{aw} - T_{eq}) = \varepsilon_w \sigma \left(\frac{T_{eq}}{100}\right)^4 \qquad \text{(Eq 11)}$$

where

ε_w = Wall emissivity

σ = Radiation constant

Conventional methods are used to evaluate the internal heat imput.

APPENDIX III

GENERAL DESCRIPTION OF AEROJET-GENERAL IBM 7094 DIGITAL COMPUTER PROGRAMS

APPENDIX III

GENERAL DESCRIPTION OF AEROJET-GENERAL IBM 7094 DIGITAL COMPUTER PROGRAMS

(u) The general approach to the thermal analysis of a specific configuration consists first of defining all local boundary heating conditions. When the proper heat input parameters have been established, transient and/or steady-state temperatures for the given configuration are predicted by one of two general heat conduction solutions to the Fourier equation that have been programed on the IBM 7094 computer.

(u) These programs vary in complexity and include multidimensional heat flow, variable thermal properties, and moving boundaries. While both programs solve the same basic equation, the choice of program depends primarily on the material and complexity of the heat flow path.

(u) All boundary conditions are known, and only the temperature distributions in a given configuration are desired. A discussion of the different available computer programs follows; the well-known transient conduction differential equations and boundary conditions given in Appendix II are not described.

(u) If a simple one-dimensional solution to the Fourier conduction equation is adequate, the first of the two programs will be used. This program is capable of calculating the one-dimensional temperature distribution in any multilayer composite. The particule method of solution is numerical, wherein the given configuration is divided into a large number of individual small elements. Each element is small enough that accuracy and convergence of the numerical solution is achieved. These criteria are built into the program so that the same high degree of accuracy is always achieved.

(u) Also, the heat capacity is considered concentrated at the center of each element, while the thermal conductivity is calculated as the average value between adjacent modes. Thus, a temperature variation of these thermal properties can be incorporated. Output format allows each calculated temperature to be printed at any desired time interval.

(u) Because the configuration details of the nozzle throat region analyzed for this program are such that multidimensional heat flow exists, the General Thermal Analyzer Program, Program 278, was used. This particular program considers each node as part of an analogous electrical network.

(u) Thus, the region to be analyzed is again divided into a large number of small elements or nodes. The heat capacity is concentrated at the center of each node, and together with the volume, defines a relative electrical capacity. The resistances between adjacent nodes are lumped to define the relative heat flow paths. A program solution calculates the temperature at each node at the end of a series of finite time steps. Output data includes the temperature at any node for any desired time interval.

(u) In addition to the conduction network solution, the program is capable of computing special functions at each time step. These include:

(u) (1) Cathode Follower: This function substitutes the temperature of any specific node for that of any second node at the end of each time interval.

(u) (2) Radiation Resistance: This function computes a pseudo-radiation resistance which may be used as a simple conduction resistance in the temperature solution.

(u) (3) Phase Transition: This function handles phase transition of any specific node.

(u) (4) Convenction Resistance: This function expresses the film resistance for convection heat transfer as a simple conduction resistance.

(u) (5) Arbitrary Heating: This function computes an arbitrary heat rate for any specified interior node.

(u) (6) Arbitrary Functions: Provisions are made for the tabular dependency of any of the individual members of the four primary variables in the network (resistance, capacitance, temperature, time) on any other member of the network.

(u) (7) Contact Resistance: This function handles any temperature drop at the boundary of the dissimilar solids.

(u) Thus, from the above description, the temperature response of any physical n-dimensional system that can be expressed as an electrical analog can be predicted. The major disadvantage of this program, primarily because of its versatility, is the excessive quantity of required input parameters. To this end, a setup program which eliminates all hand calculation of resistance, capacitance, etc., and punches input cards for the main program has been developed.

(u) To illustrate this input procedure, a sample program is presented: The detail of the present nozzle configuration is presented in Figure 64. Figure 65 shows the sample section laid out on an X-Y grid. This section is then broken into several areas, each containing a temperature point or node. Each node and all corner points of each node are then assigned a consecutive number.

(u) This coordinate description and input numbering system, together with appropriate input parameters, thus defines completely the conduction problem to be solved. With this input format, the time required to set up a typical transient conduction problem has been reduced from several days to a few hours.

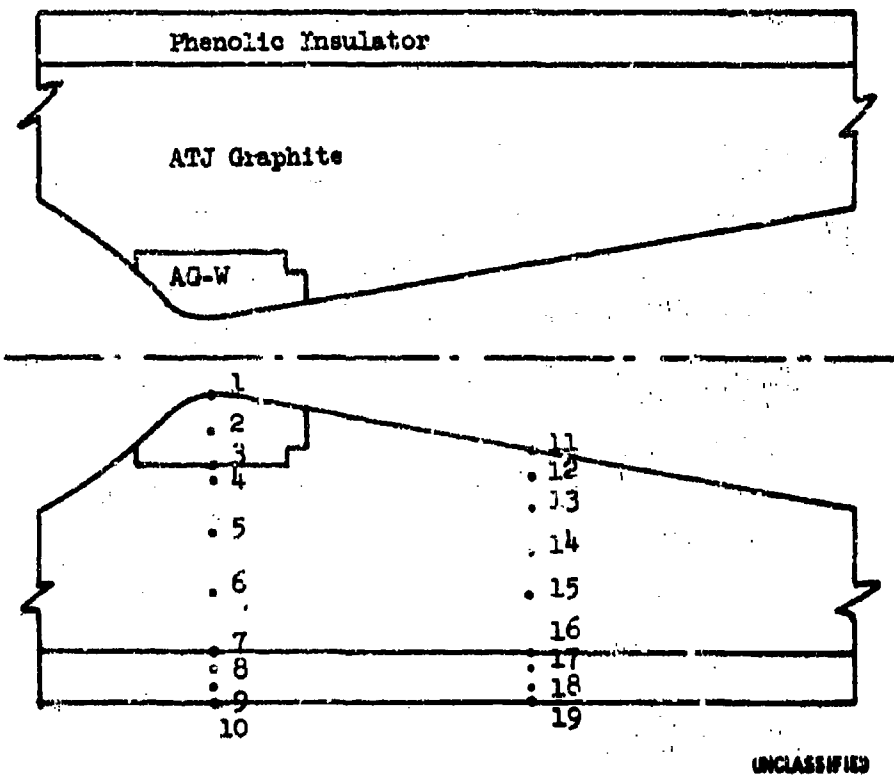

Figure 64. Nozzle Configuration

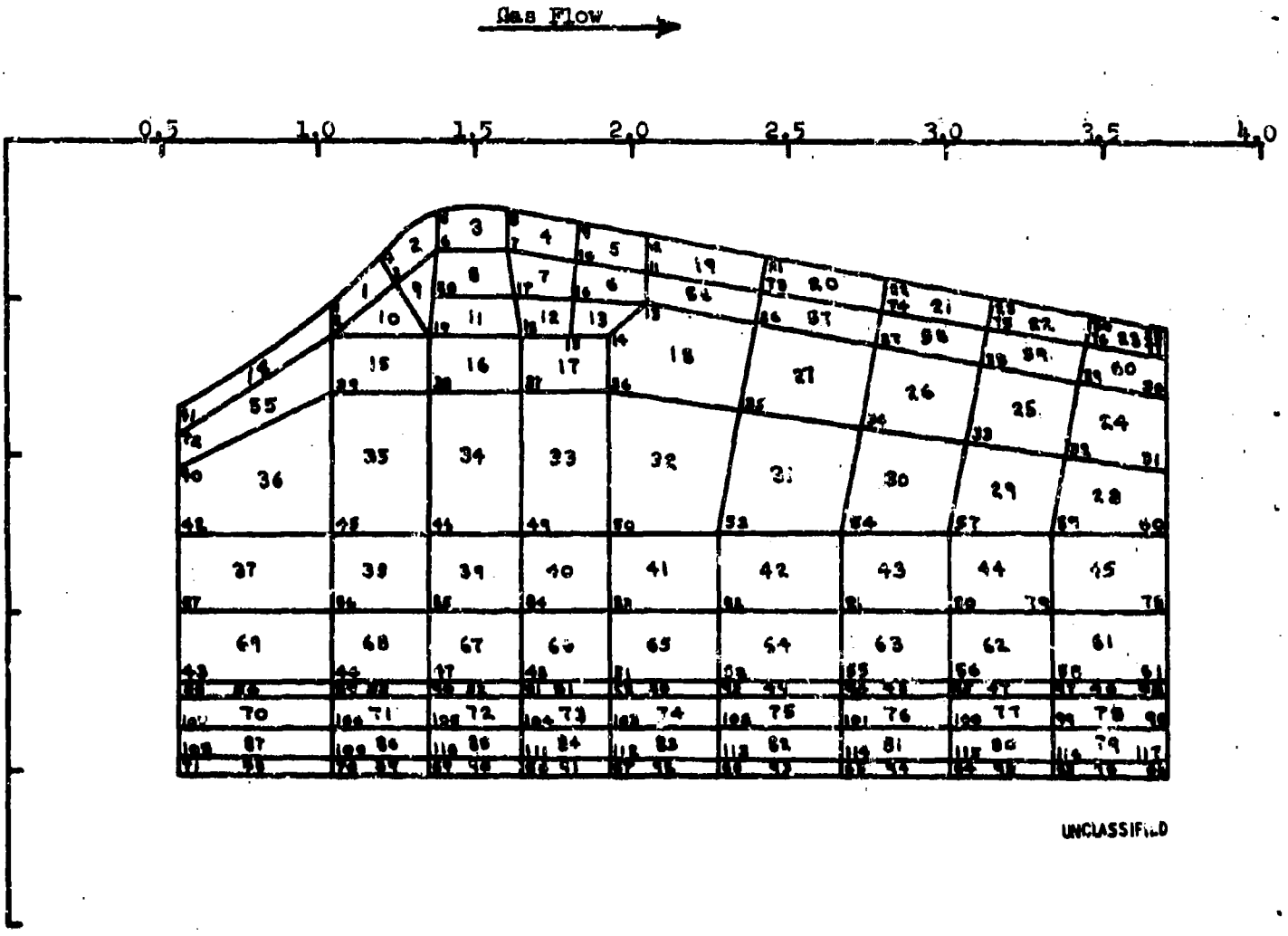

Figure 65. Temperature Node Layout for Input to Thermal Analyzer Program

APPENDIX IV

STRESS ANALYSIS FOR EXPANDABLE EXIT CONE MOTOR

APPENDIX IV

STRESS ANALYSIS FOR EXPANDABLE EXIT CONE MOTOR

A. SUMMARY

This appendix presents the structural analysis of the motors to be used in the expandable exit cone program. It includes an analysis of the modified 30KS-5000 chamber that will be used for the demonstration firing, as well as the analysis of the nozzle and exit cone for both the subscale and demonstration motors. The chamber for the subscale motor is an off-the-shelf item; therefore, the structural analysis of this chamber is not included in this report.

The maximum duration of the subscale motor will be 60 sec, while that for the demonstration motor will be 30 sec. The design criteria for both motors is presented in Section C of this appendix. The results of the structural analysis are presented below. Symbols for the analysis are shown in Section F.

Summary of Stresses

Item	Stress	Type of Stress	M.S.
Subscale			
Nozzle	*	*	*
Nozzle support	3.917 psi	Tension	0.22
Exit cone	760 psi	Tension	1.63
Demonstration			
Chamber	91 ksi	Hoop	0.32
Nozzle	*	*	*
Nozzle support	118.3 ksi	Bending	0.37
Exit cone	1262 psi	Tension	0.58

*See Section E,9.

B. DESCRIPTION

1. Chambers

The chamber that will be used for the subscale firings is an off-the-shelf heavy-wall test motor.

B, Description (cont.)

(u) The chamber that will be used for the demonstration motor is basically a 30KS-5000 chamber that has been lengthened and has had a flange provided at the aft end for attaching the closure. The chamber is now 76 in. long, with an OD of 15 in. and a thickness of 0.113 in.

2. Throats

(u) The throats of both motors are very similar and consist of a silver-infiltrated tungsten throat inserted in a large block of ATJ graphite that forms the entrance to the throat and the forward portion of the exit cone. The graphite is then wrapped by a silica insulating material, which is backed up with a steel sleeve.

3. Exit Cones

(u) The exit cones for use on the subscale motor are truncated cones with a flange at the smaller end. One design is based on the use of elastomeric material to make the cone, and the other designs use either 90Ta - 10W or columbium foil.

(u) The exit cones for the demonstration firings are made from the same materials as those used in the subscale firing. However, these exit cones will be much larger than the subscale exit cones, and the metallic cones will have their free ends corrugated so that initially they will be cylindrical.

C. DESIGN CRITERIA

(u) The expandable exit cone program is a feasibility program designed to determine the characteristics of such an exit cone. The pressures and temperatures for which the motor hardware are designed are shown below for both the subscale and demonstration motors.

1. Pressures (Both Motors)

Item	Maximum Expected Chamber Pressure, psi	Factor of Safety, psi	Design Yield Pressure, psi	Hydrotest Pressure, psi
Chamber	500	2.5	1250	1200
Throat	500	1.0	500	---
Throat Backup	500	1.5	750	---
Exit Cone	500	1.5	750	---

C, Design Criteria (cont.)

2. Temperatures

(u) Both the nozzle and exit cone were designed for use at elevated temperatures. The temperature distributions for which they were designed are given in III,B,2,a(2) and Figures 5, 6, and 30 of this report.

3. Thrust

(u) The demonstration motor is designed for an axial thrust of 5400 lb.

(u) The material properties of silver-infiltrated tungsten, columbium, and 90Ta - 10W used in the stress analysis in this appendix are shown in Figures 66 through 70.

D. THERMAL STRESS ANALYSIS PROGRAM, PROGRAM 878

(u) The thermal stress analysis program, Program 878 (Ref 7), for the IBM 7097 computer is used for the analysis and design of nozzle configurations, with particular application to regions where a large thermal gradient exists in the radial direction.

(u) In this program, the throat is divided into a series of concentric shells which are assumed to be of infinite length. The material properties and nozzle geometry are put into the computer which then computes the stresses in the radial, longitudinal, and tangential directions.

$$f_r = A_r \varepsilon_r + B_r \varepsilon_\theta + B_x \varepsilon_x - KT \qquad \text{(Eq 1)}$$

$$f_\theta = B_r \varepsilon_r + A_r \varepsilon_\theta + B_x \varepsilon_x - KT \qquad \text{(Eq 2)}$$

$$f_x = E_x (\varepsilon_x - \alpha_x T) + \nu_x (f_r + f_\theta) \qquad \text{(Eq 3)}$$

where

$$A_r = \frac{1 - \nu_x^2 E_r}{(1 + \nu_r)(1 - \nu_r - 2\nu_x^2)}$$

$$B_r = \frac{\nu_r + \nu_x^2 E_r}{(1 + \nu_r)(1 - \nu_r - 2\nu_r^2)}$$

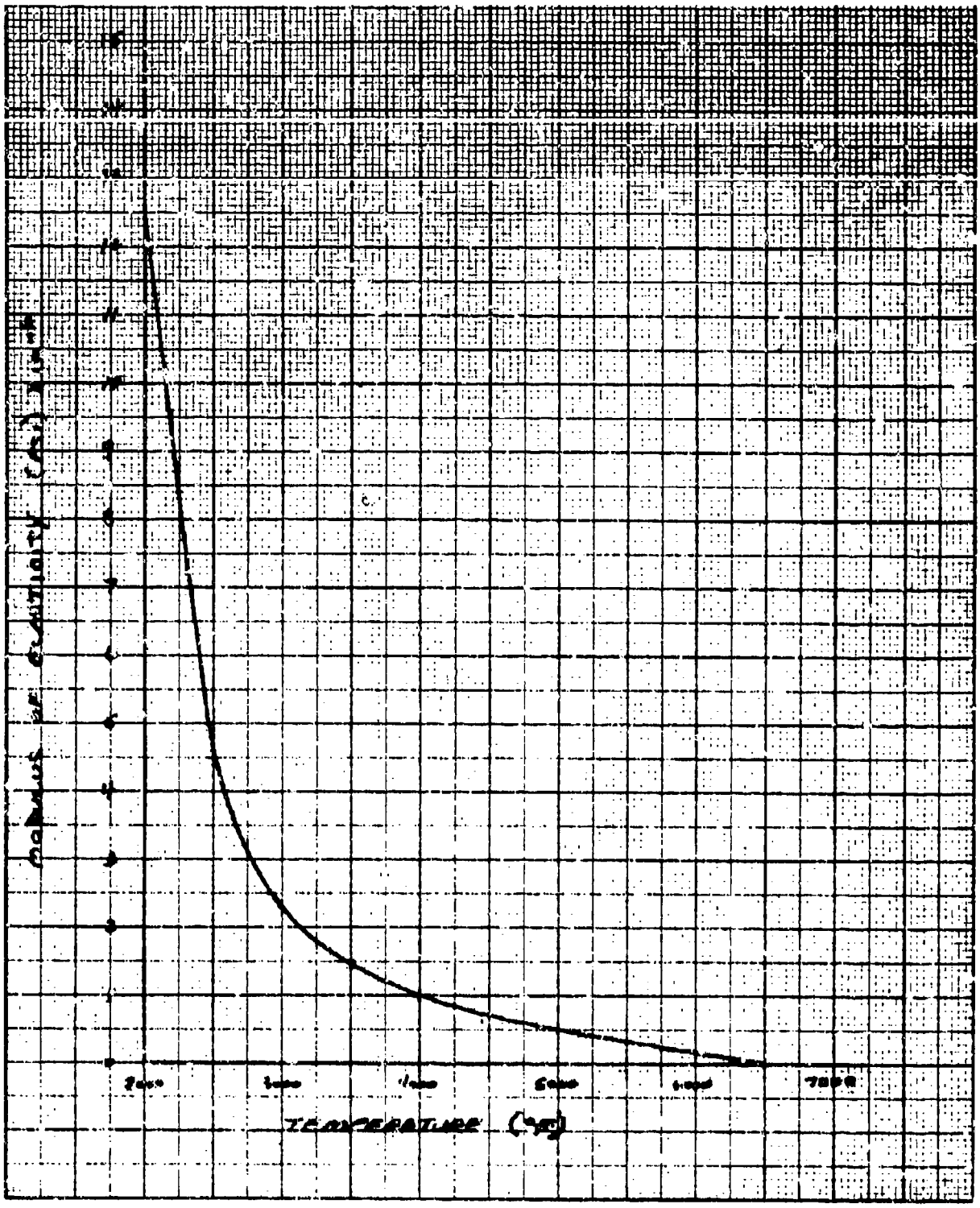

Figure 66. Silver-Infiltrated Tungsten

UNCLASSIFIED

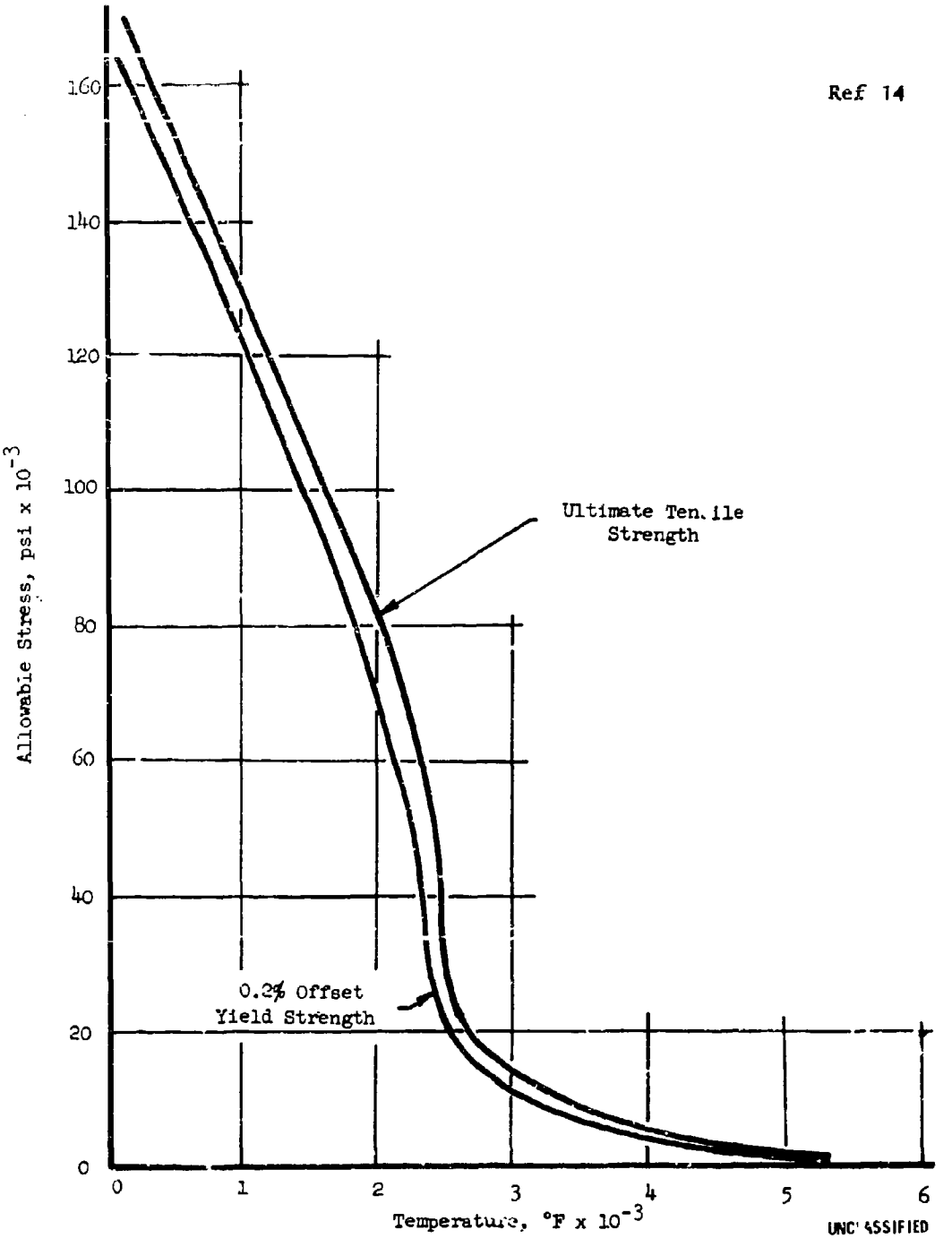

Figure 67. Allowable Stress vs Temperature, 90 Ta - 10W

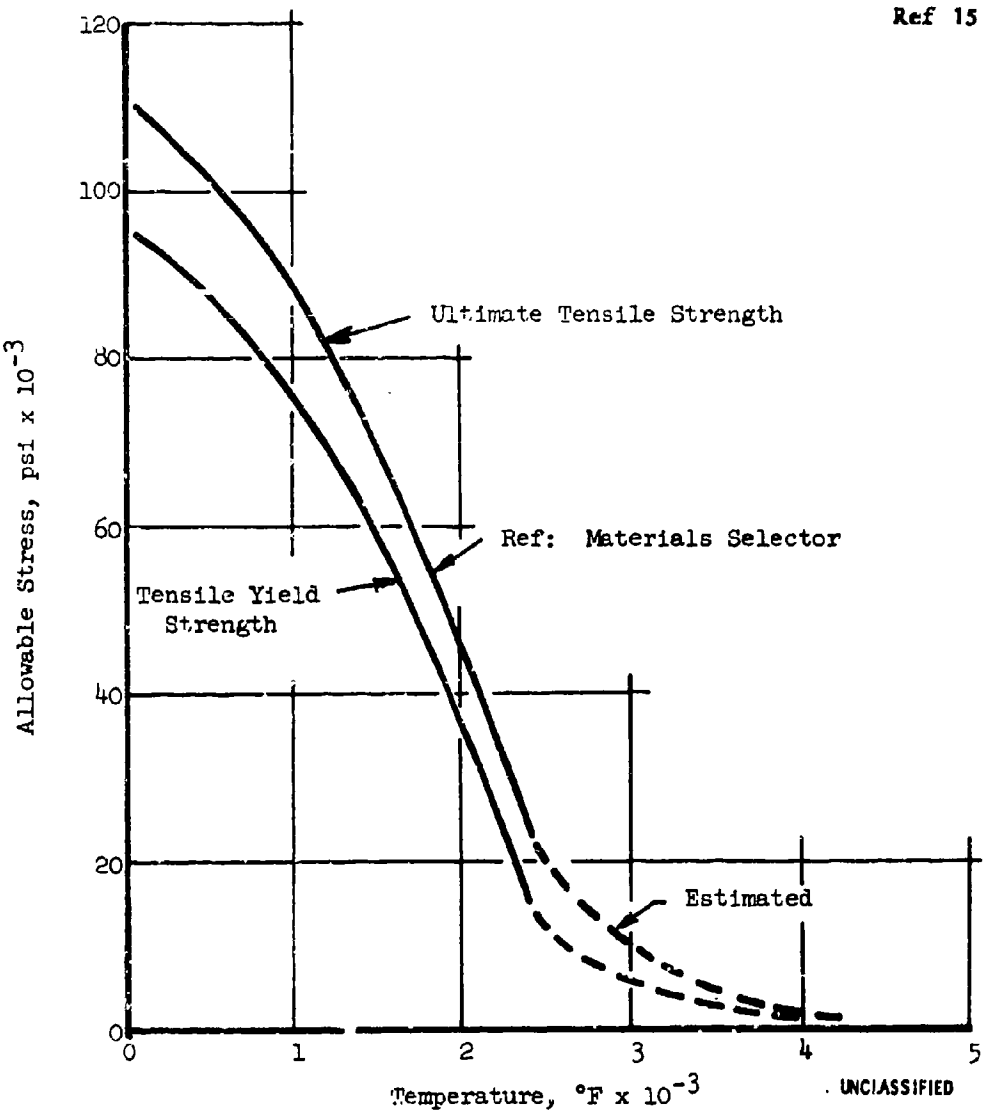

Figure 68. Tensile Properties vs Temperature, Columbium

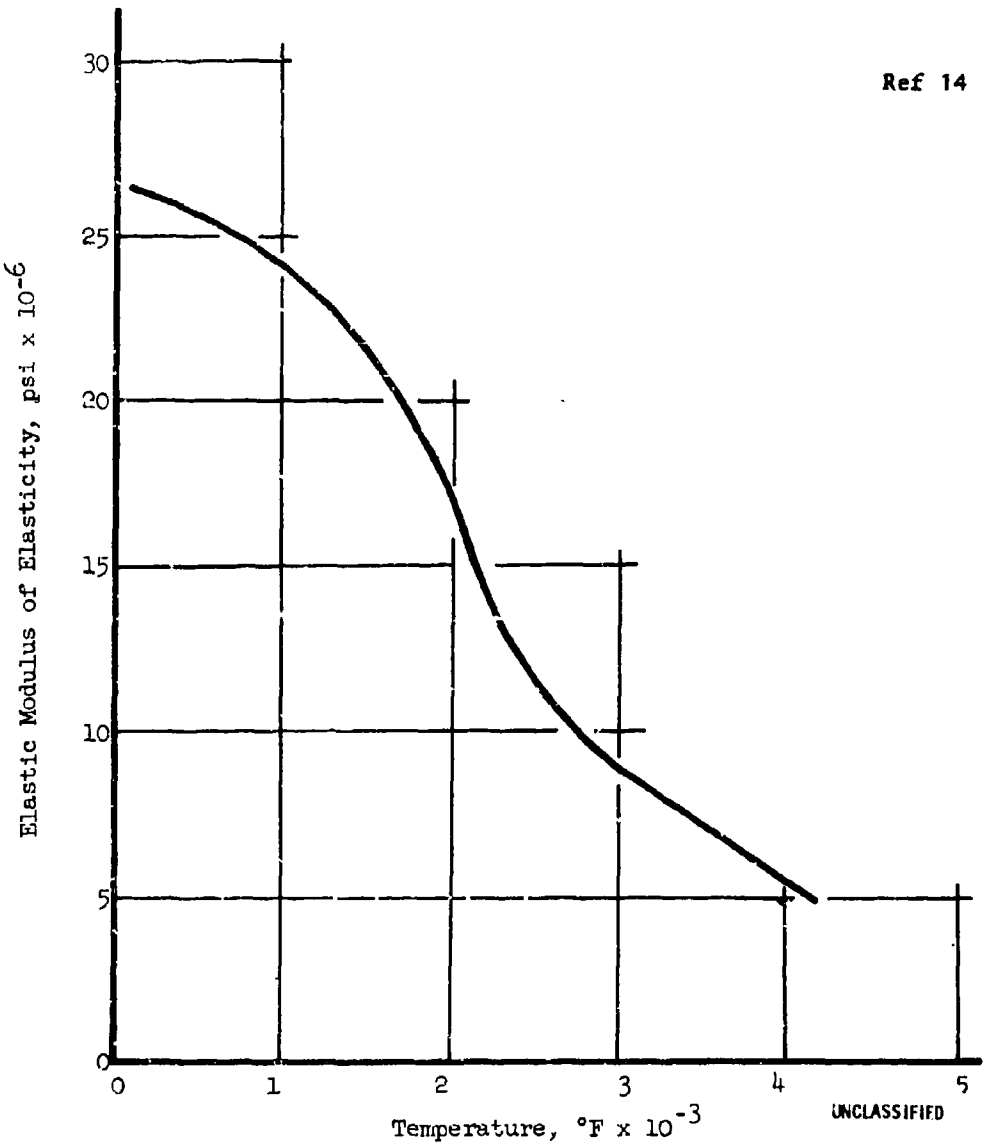

Figure 69. Modulus of Elasticity vs Temperature, 90 Ta - 10W

Ref 15

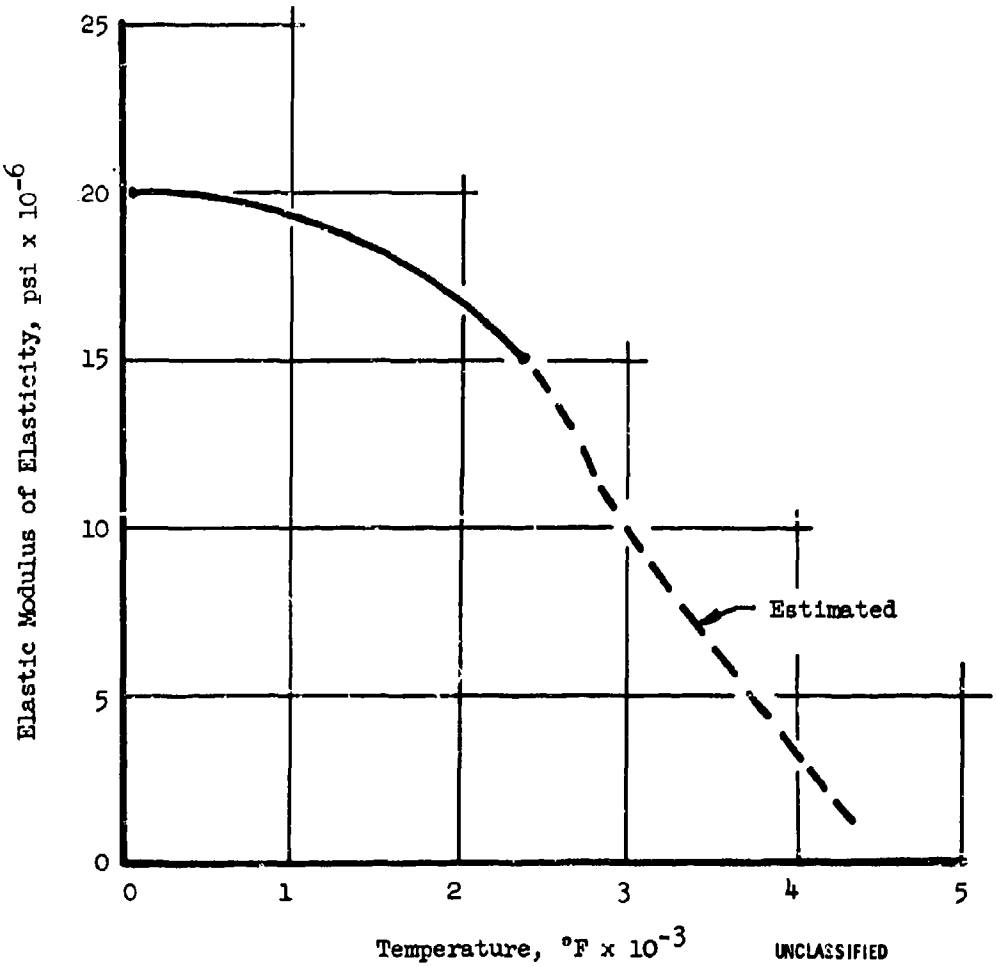

Figure 70. Modulus of Elasticity vs Temperature, Columbium

D, Thermal Stress Analysis Program, Program 878 (cont.)

$$B_x = \frac{\nu_x \, E_r}{1 - \nu_r - 2\nu_x^2}$$

$$K = (A_r + B_r)\alpha_r + B_x\alpha_x$$

$$= \frac{E_r}{E_x}$$

f_p = Stress in radial direction
f_θ = Stress in tangential direction
f_x = Stress in axial direction
ϵ_r = Strain in radial direction due to f_r
ϵ_θ = Strain in tangential direction due to f_r
ϵ_x = Strain in axial direction due to f_x
T = Temperature differential between time being analyzed and time zero
E_x = Modulus of elasticity in x direction
$E_r = E_\theta$ = Modulus of elasticity in radial or tangential direction
ν_x = Poisson's ratio in longitudinal direction
$\nu_r = \nu_\theta$ = Poisson's ratio in radial or tangential direction

(u) After the computer has found the stresses at each interface, it prints out both the original input information and the derived stresses for the radial, tangential, and longitudinal stresses at each interface.

E. STRUCTURAL ANALYSIS

1. Chamber

(u) The chamber that will be used in the subscale firings is an off-the-shelf heavy-wall test motor for which no stress analysis is included in this report. The demonstration motor uses a modified 30KS-5000 chamber, and the stress analysis for this chamber is presented in this section.

E, Structural Analysis (cont.)

2. Geometry

(u) Design Yield Pressure = 1250 psi

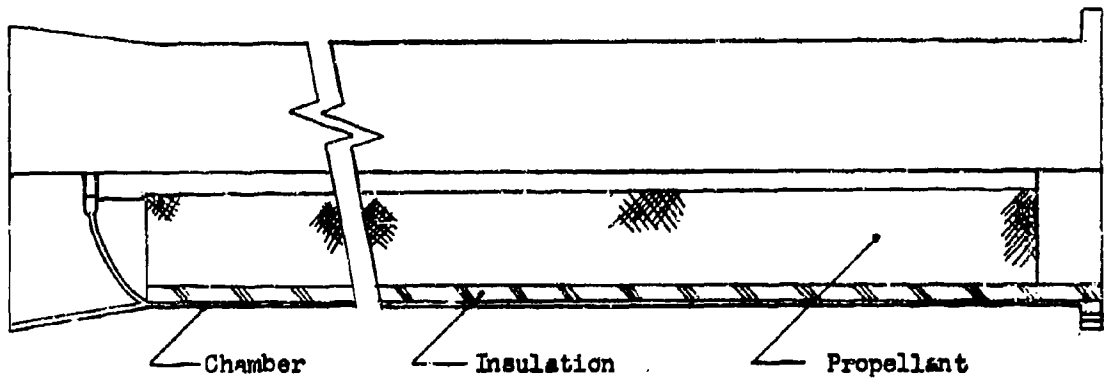

Material: 4130 steel

F_{tu} = 140 ksi min

F_{ty} = 120 kis (Ref 8)

3. Cylindrical Section

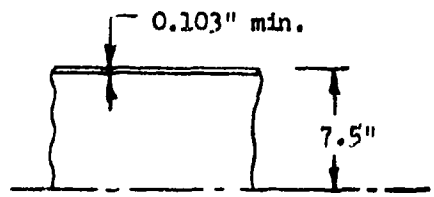

$$\sigma_{Hoop} = \frac{PR}{t} = \frac{1250 \times 7.5}{0.103}$$

$$= 91{,}000 \text{ psi}$$

$$M.S._{yield} = \frac{120}{91} - 1 = 0.32$$

4. Aft Closure Joint (Hydrotest)

Plate

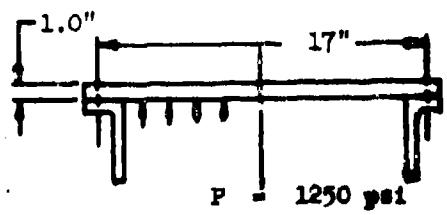

E, Structural Analysis (cont.)

(u) Conservative values for the stresses in the plate can be found by using Case 1, Page 194, of Roark (Ref 9).

$$\sigma_{max} = \frac{3\,w\,(3m + 1)}{8\pi m\,t^2} = 112{,}000 \text{ psi}$$

$$w = \pi R^2 p = 284{,}000 \text{ lb}$$

$$m = \frac{1}{\nu} = 3.33$$

$$\text{M.S.} = \frac{120}{112} = 0.07$$

5. Aft Closure Joint

Bolts

(u) A conservative value for the moment at the bolt circle can be found by assuming the plate is fixed at the bolt circle. This moment can then be reacted by a couple located at the bolt circle and the edge of the plate. From Roark, Page 195, Case 6 (Ref 9), the stress at the bolt circle (edge of a fixed plate) is:

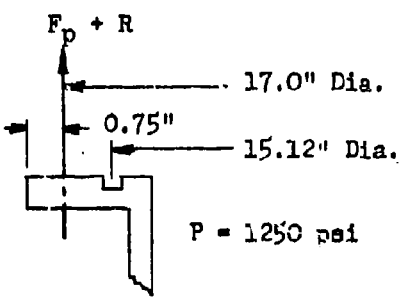

$$\sigma_{max} = \frac{3\,w}{4\pi t^2}$$

This stress is also equal to $\frac{6\,M}{t^2}$

$$\therefore M = \frac{w}{8\pi} = 5170 \text{ in. lb/in.} \quad P_c = 750 \text{ psi}$$

$$\text{Bolt Load} - F_p + R = \left(\frac{PR}{2} + \frac{M}{0.75}\right) \text{bolt spacing}$$

$$= 32{,}400 \text{ lb}$$

E. Elasticity of Acrylic (cont.)

P_{all} 48,700 lb ultimate or 43,200 lb yield = P_{ult} (Ref 10)

$$M.S._{yield} = \frac{43.2}{32.4} - 1 = 0.33$$

6. Aft Closure Joint

(u) Section Between Bolts

M = 8950 in. lb/in.

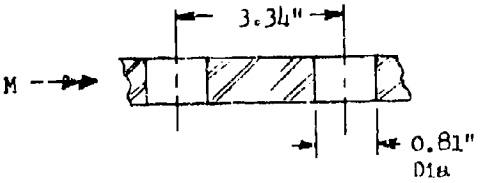

$$\sigma = \frac{6\,M}{t^2} \times \frac{3.34}{2.53} = 70{,}800 \text{ psi}$$

$$M.S._{yield} = \frac{120}{70.8} - 1 = .70$$

(u) Junction of Flange and Barrel

M = 0.304 PRt

(Ref 9, Roark, Page 270, Case 9)

M = 810 in. lb/in.

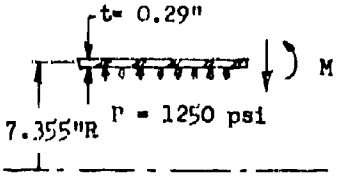

$$\sigma_{merid} = \frac{PR}{2t} + \frac{6M}{t^2} = 74{,}000 \text{ psi}$$

$$M.S._{yield} = \frac{120}{74} - 1 = 0.62$$

*Based on 16 bolts

4. Structural Analysis (cont.)

7. Forward Closure

(u) Membrane

(u) The surface of the forward closure is generated by a 2:1 ellipse having a semi-major axis of 7.46 in. The thickness of the forward closure is 0.104 in. for this ellipse:

$$\sigma_{hoop} = \sigma_{merid} = \frac{pr}{t} = 90{,}000 \text{ psi}$$

$$\text{M.S.} = \frac{120}{90} - 1 = 0.33$$

(u) Igniter Boss

The igniter boss was analyzed here by using Ref 11.

A = 0.28 Available

a = 7.46

t = 0.104

R_B = 1.75

A_B = Optimum boss area

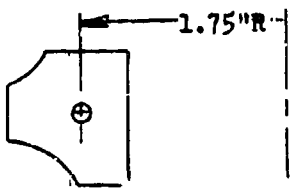

$$\frac{R_b}{a} = 0.29$$

$$\frac{A_b}{R_b t} = 1.51$$

$$A_b = 1.75 \times 0.104 \times 1.51 = 0.27$$

Because $A > A_B$ the boss is satisfactory.

8. Forward Skirt

(u) The forward skirt will be checked for stability under a thrust load of 5400 lb, assuming it is a cylinder.

E, Structural Analysis (cont.)

l = 8.0 in.
$\bar{R}$ = 8.1 in.
t = 0.4 in.
L/R ≈ 1.0
R/t = 202

$$\frac{\sigma_{cr}}{E} \ (x\ 10^3) = 1.4 \qquad \text{(Ref 12)}$$

$$\sigma_{cr} = 1.4 \times 29{,}000 = 40{,}500 \text{ psi}$$

The compressive stress due to the thrust load is

$$\sigma_c = \frac{5400}{\pi \times 16.1 \times 0.04} = 2680 \text{ psi}$$

$$\text{M.S.} = \frac{40.5}{2.68} - 1 = \text{High}$$

9. Thermal Stress Analysis

(u) A thermal stress analysis (Computer Program 878) (Ref 7) was performed on both the subscale and demonstration motor throat inserts using the temperature profiles described in III,B,2,a,(2) and Figures 5, 6, and 30.

(u) The results of the two analyses are very similar. Both are structurally adequate with similar margins of safety.

(u) Detailed results of the throat insert analyses for the subscale motor are presented in Figures 77 through 79 and for the demonstration motor in Figures 80 through 84.

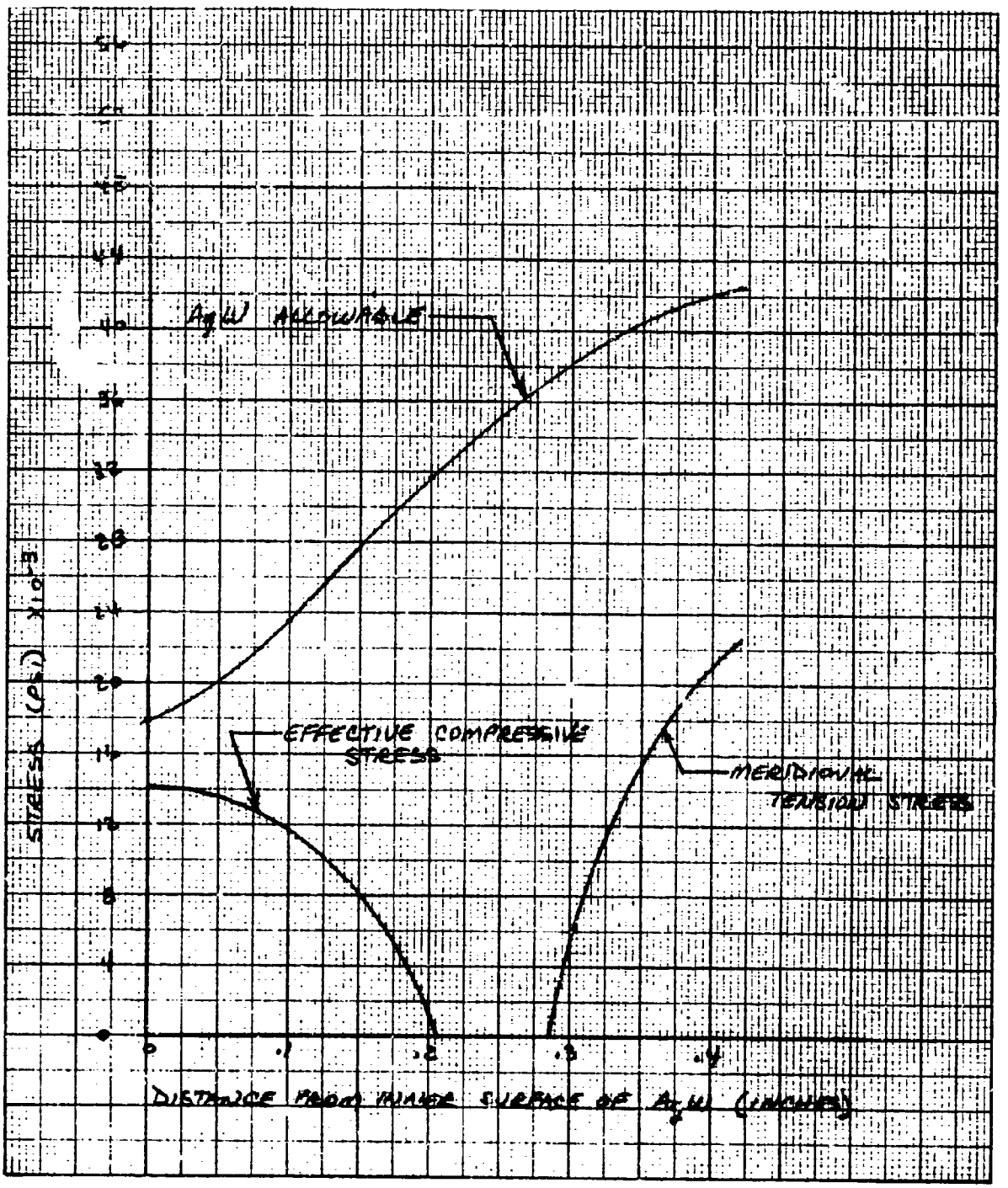

UNCLASSIFIED

Figure 71. Subscale Expandable Exit Cone Motor Throat (D_t = 0.4.) at 5 sec Ag W

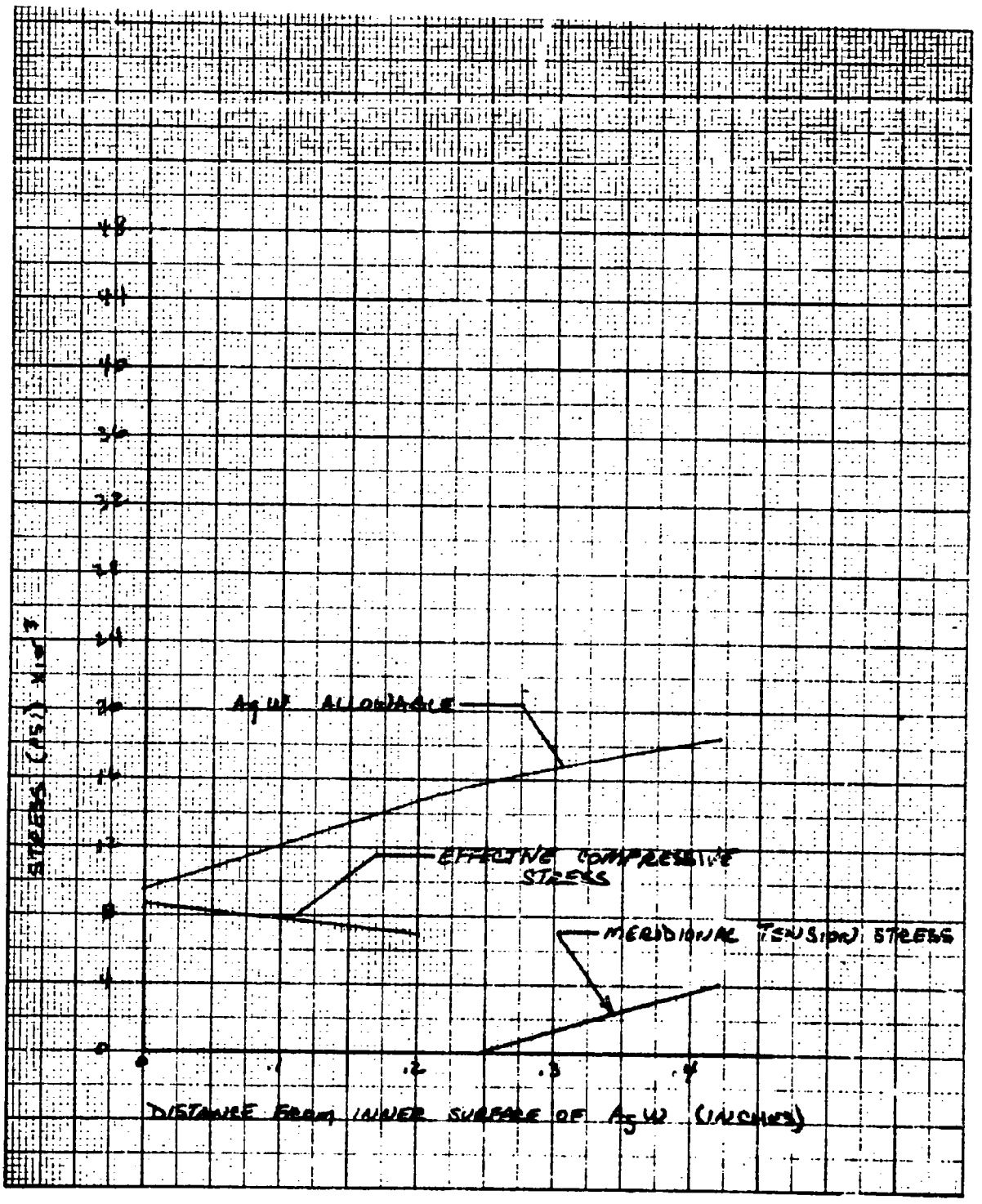

Figure 72. Subscale Expandable Exit Cone Motor Throat at 20 sec Ag W

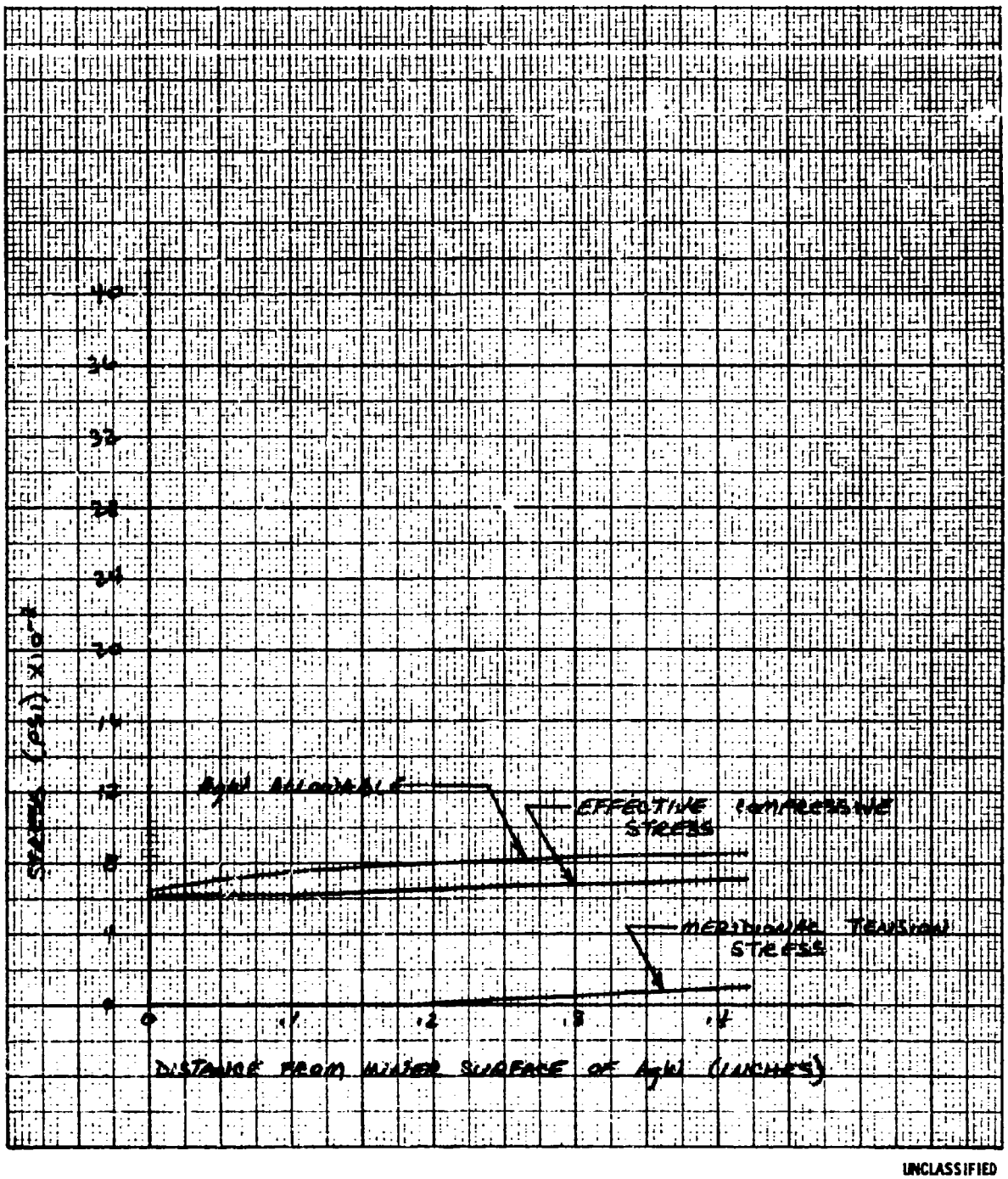

UNCLASSIFIED

Figure 73. Subscale Expandable Exit Cone Motor Throat at 60 sec Ag W

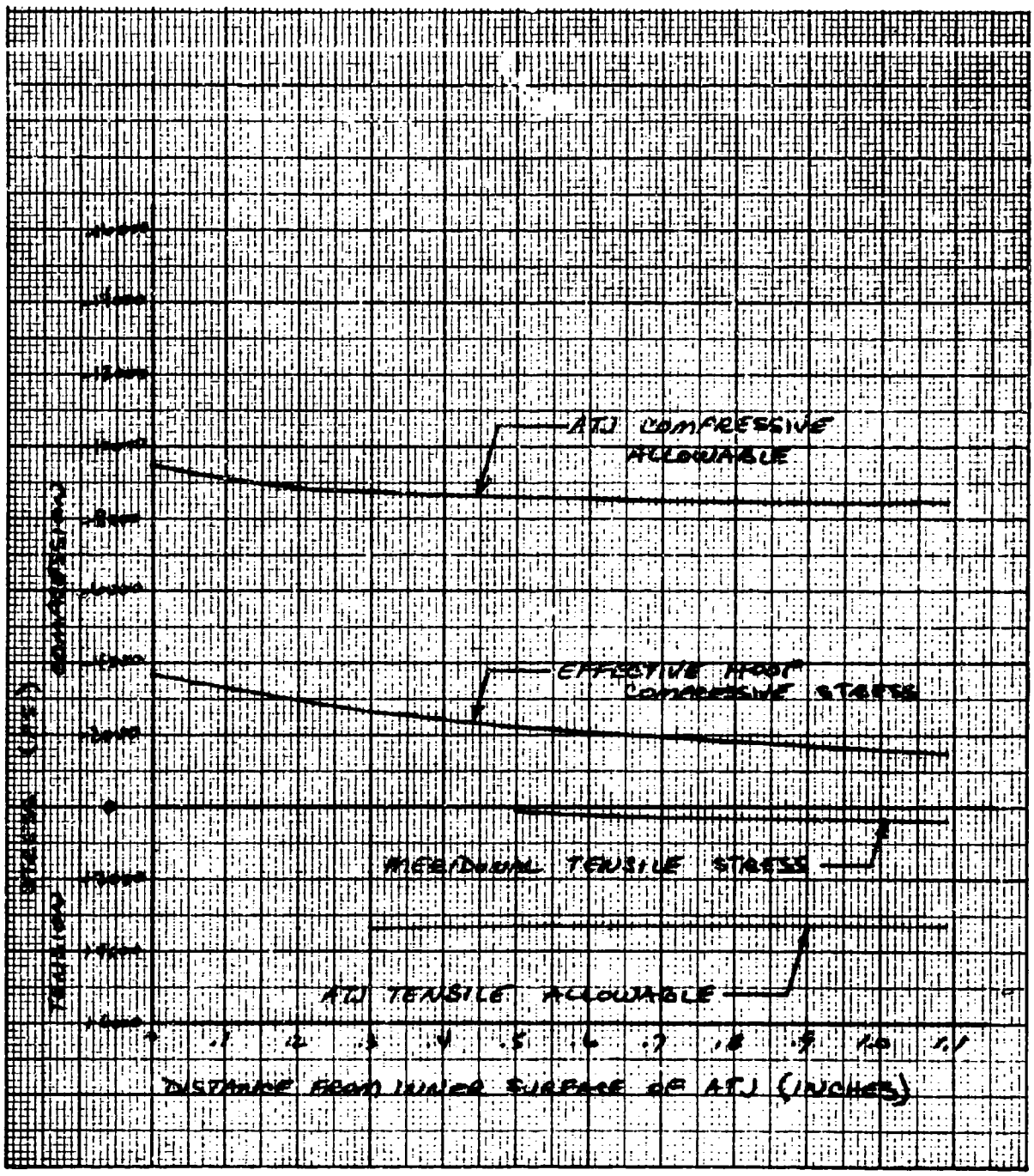

UNCLASSIFIED

Figure 74. Subscale Expandable Exit Cone Motor Throat at 5 sec ATJ

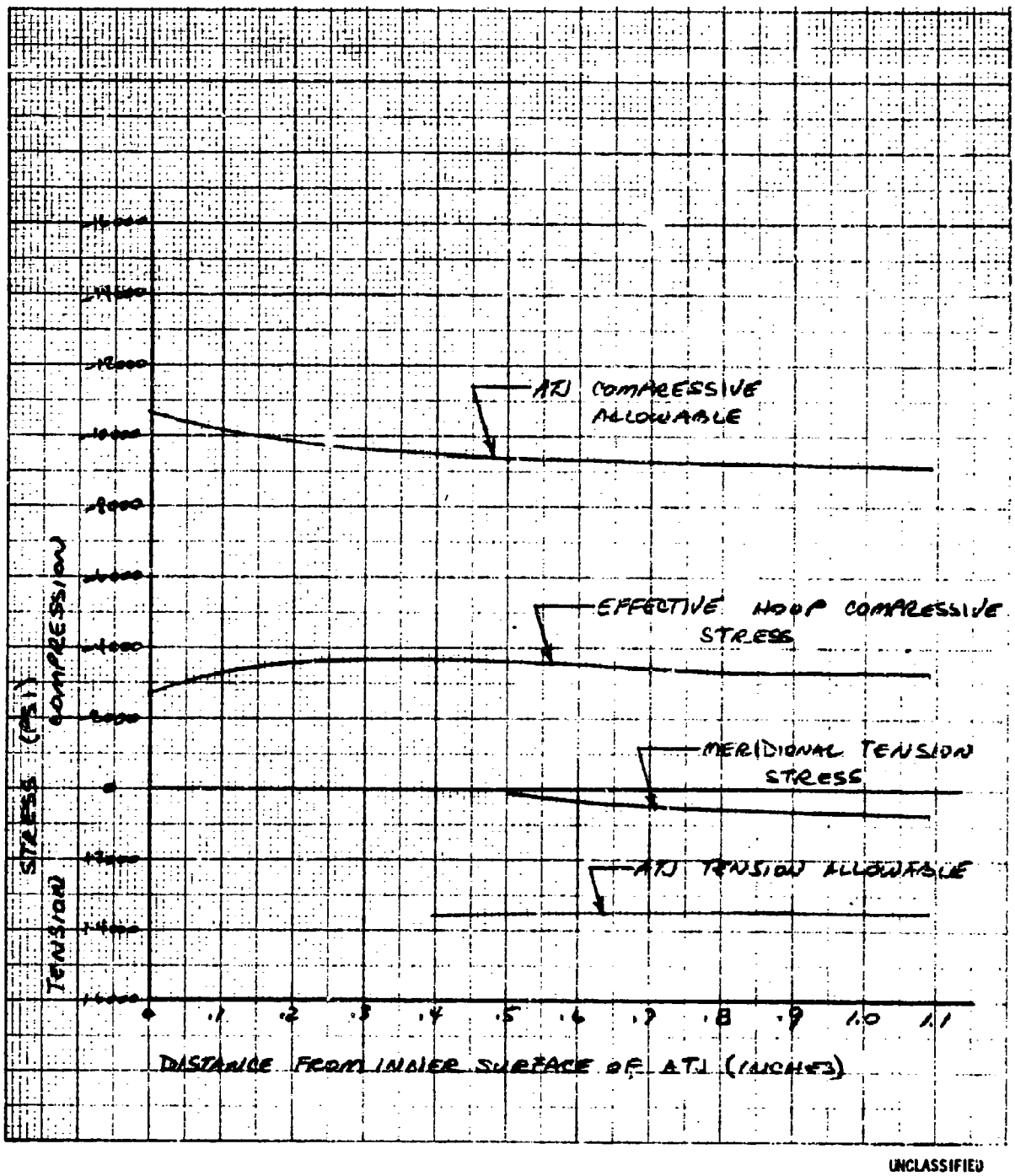

Figure 75. Subscale Expandable Exit Cone Motor Throat at 20 sec ATJ

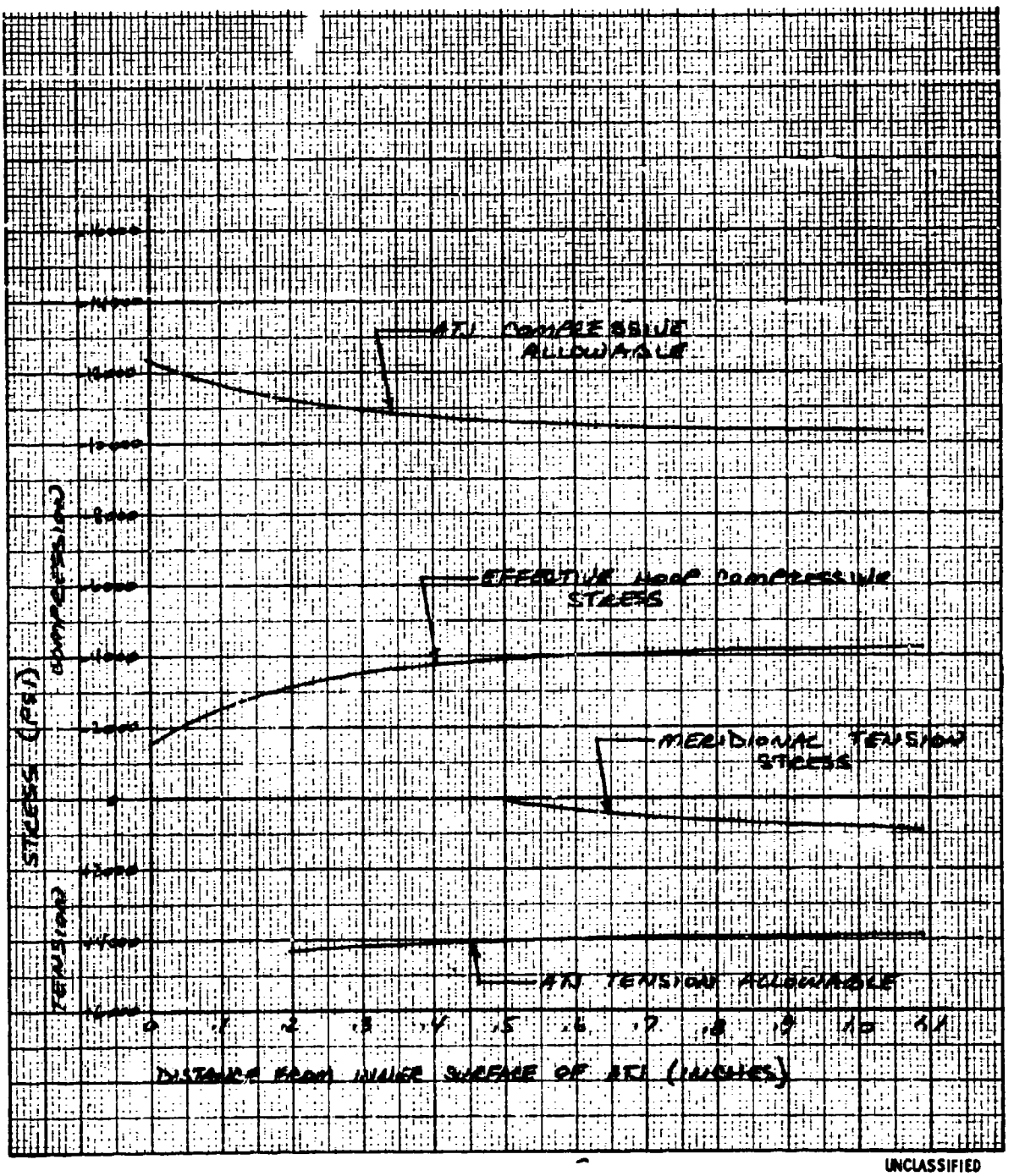

Figure 76. Subscale Expandable Exit Cone Motor Throat at 60 sec ATJ

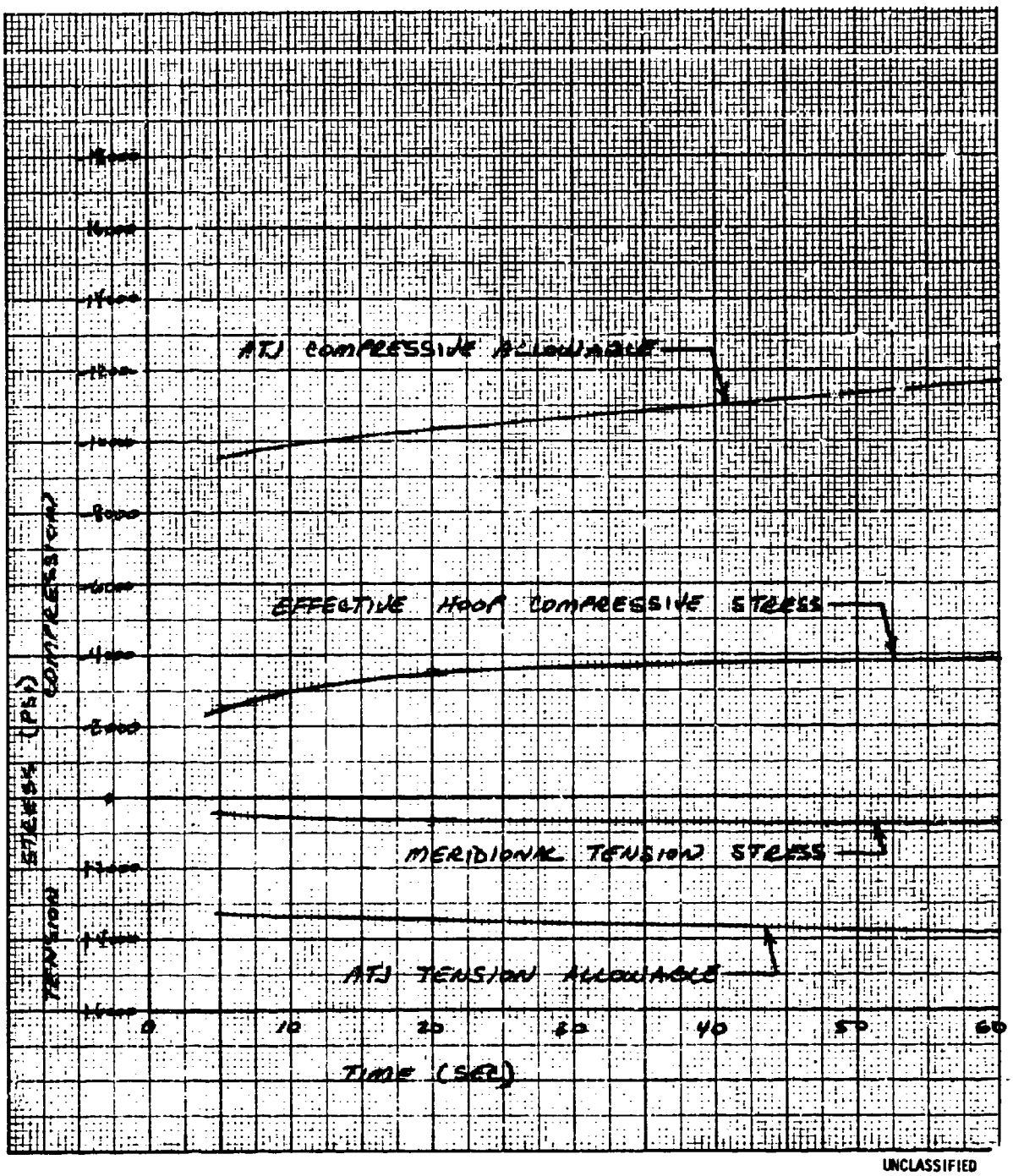

Figure 77. Subscale Expandable Exit Cone Motor Exit Cone ATJ

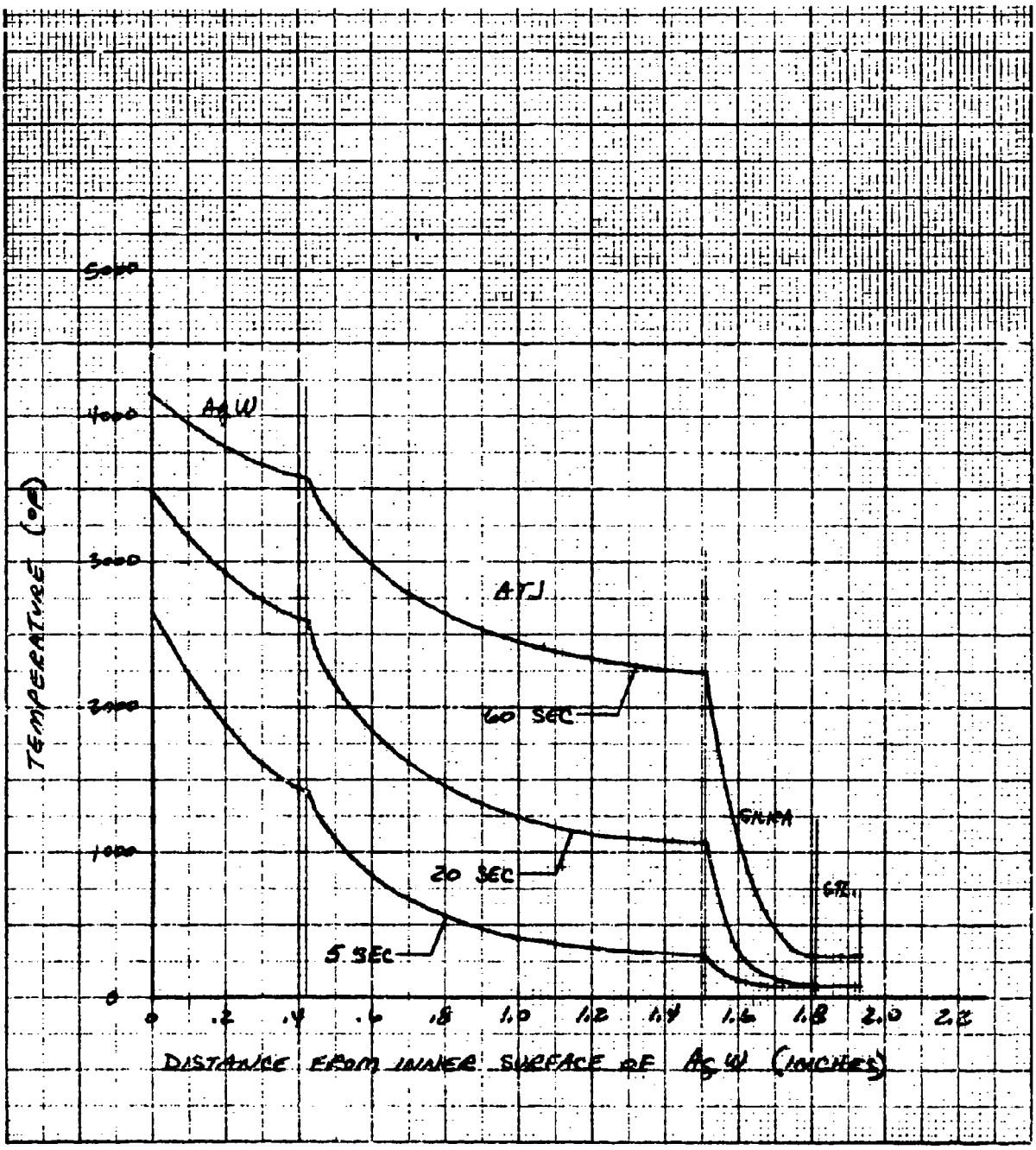

Figure 78. Subscale Expandable Exit Cone Motor Throat

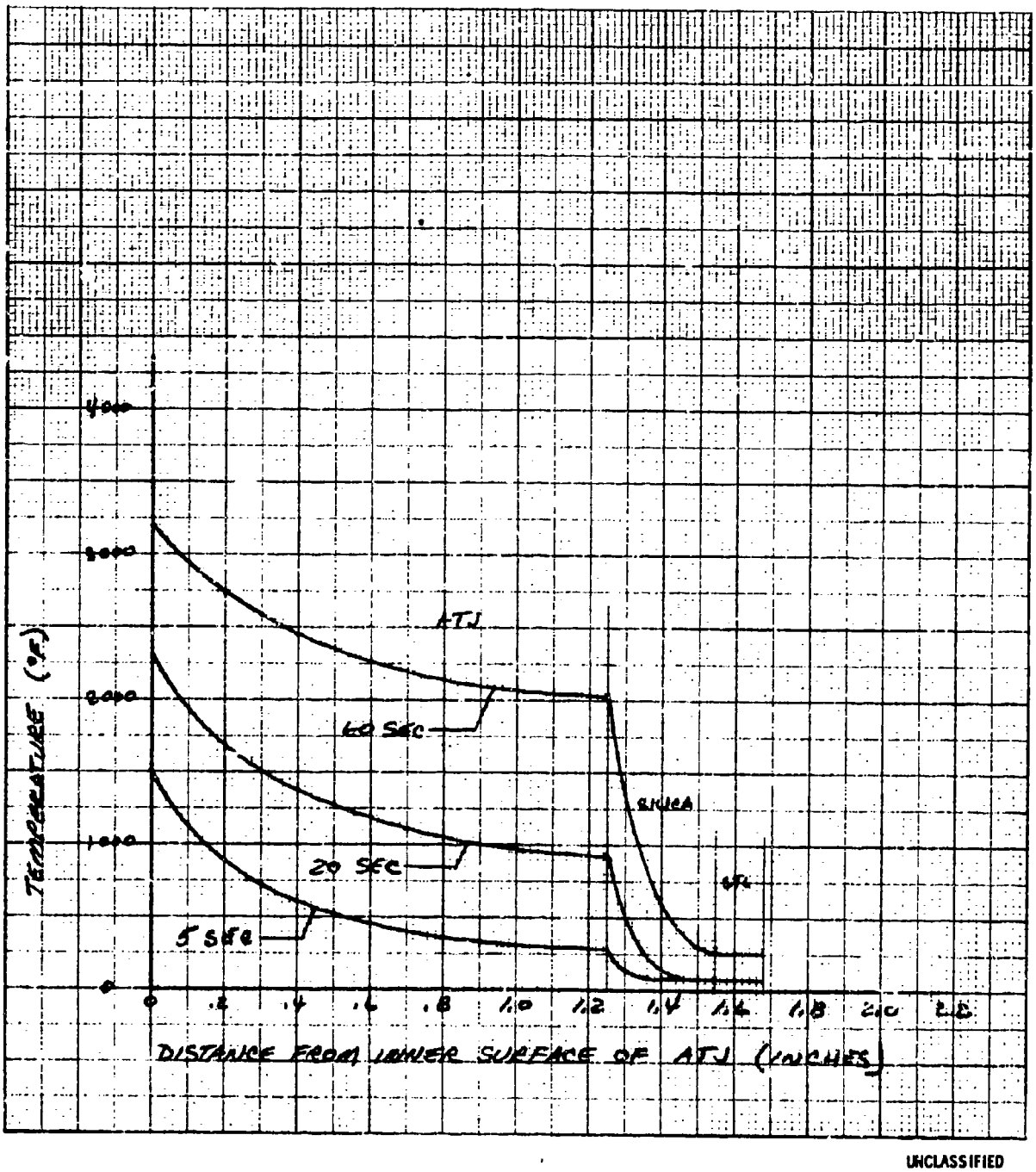

Figure 79. Subscale Exit Cone Motor Exit Cone

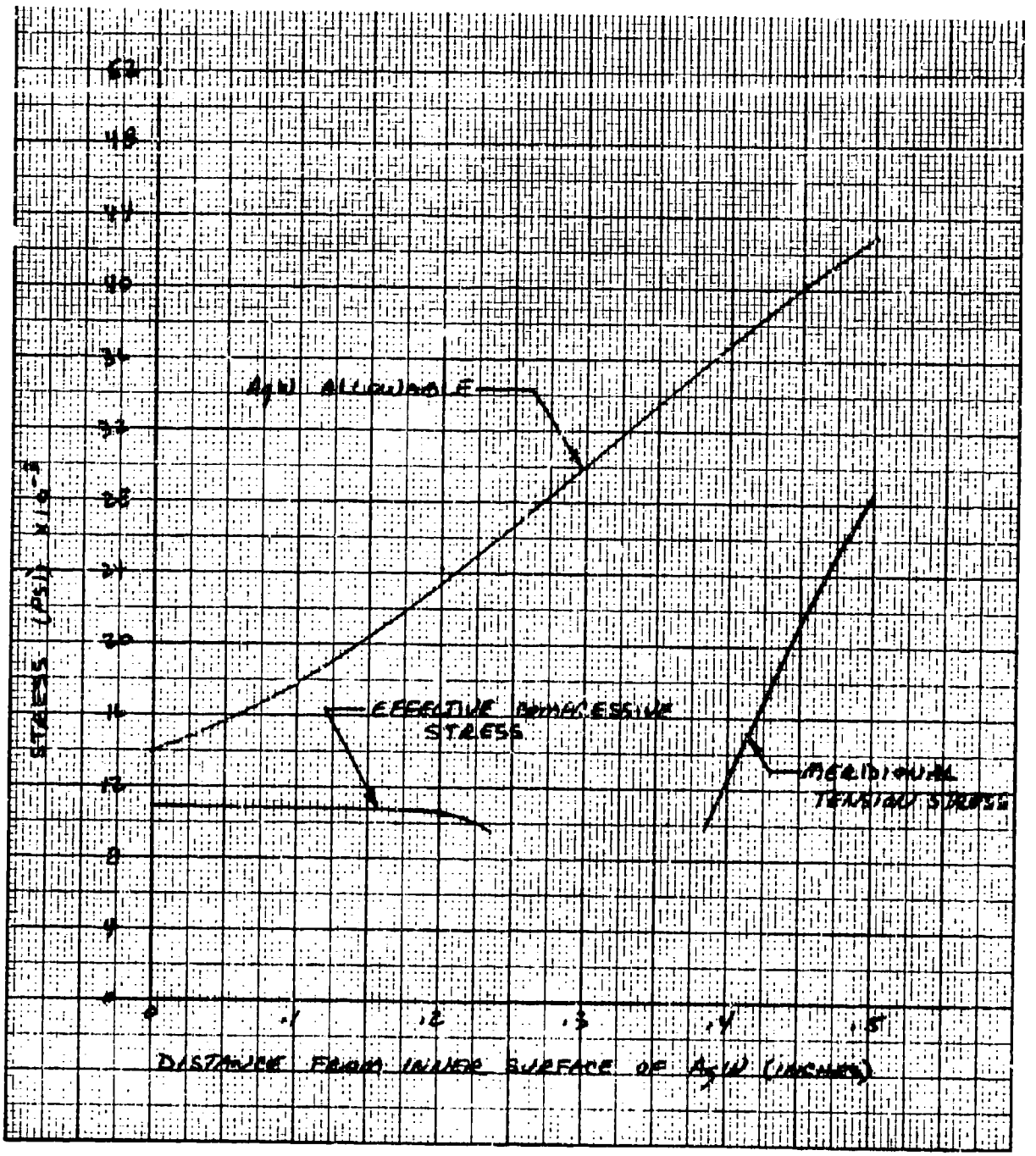

UNCLASSIFIED

Figure 80. Demonstration Motor Expandable Exit Cone Motor Throat (D_t = 2.72) at 5 sec Ag W

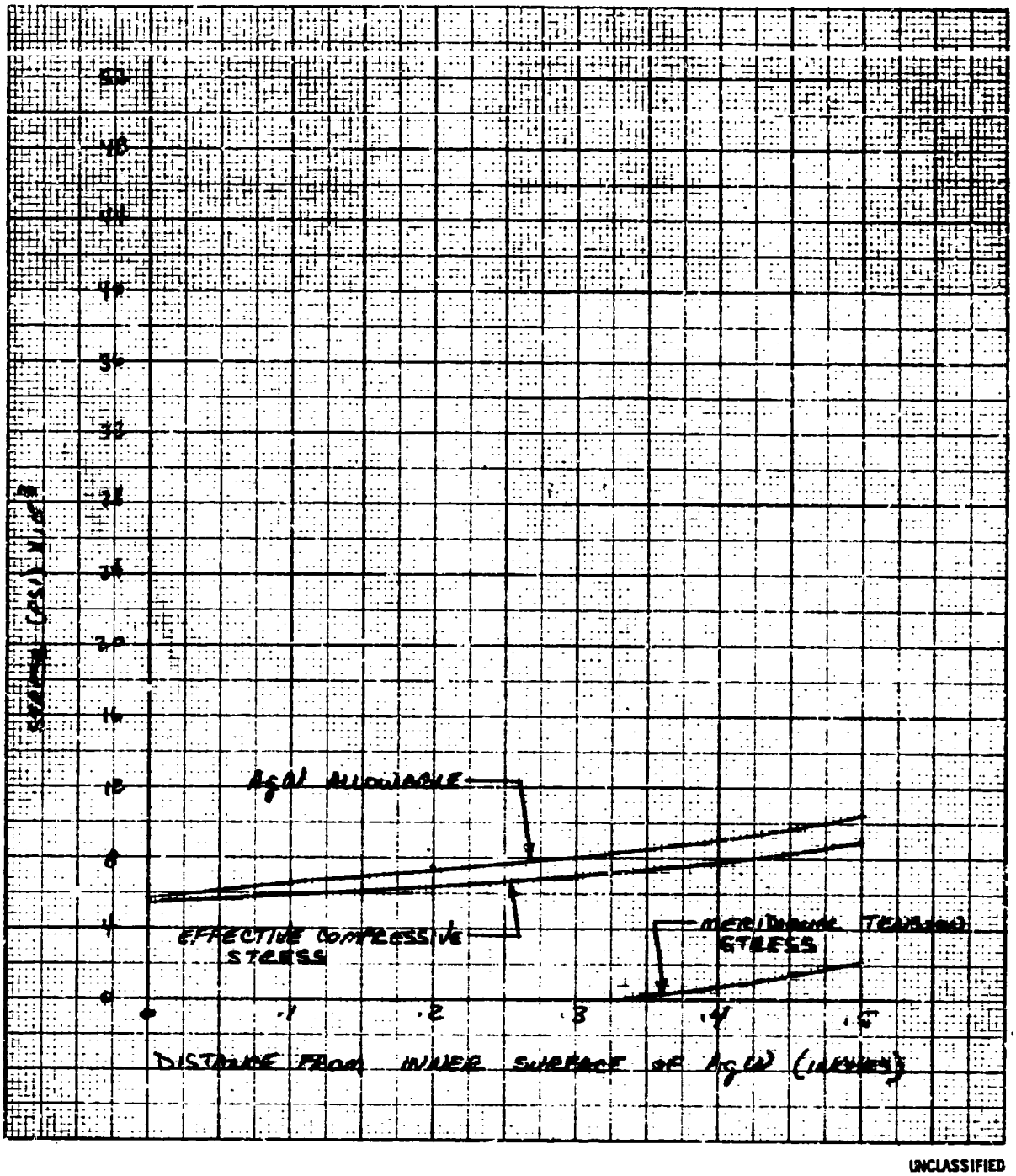

UNCLASSIFIED

Figure 81. Demonstration Motor Expandable Exit Cone Motor Throat at 30 sec Ag W

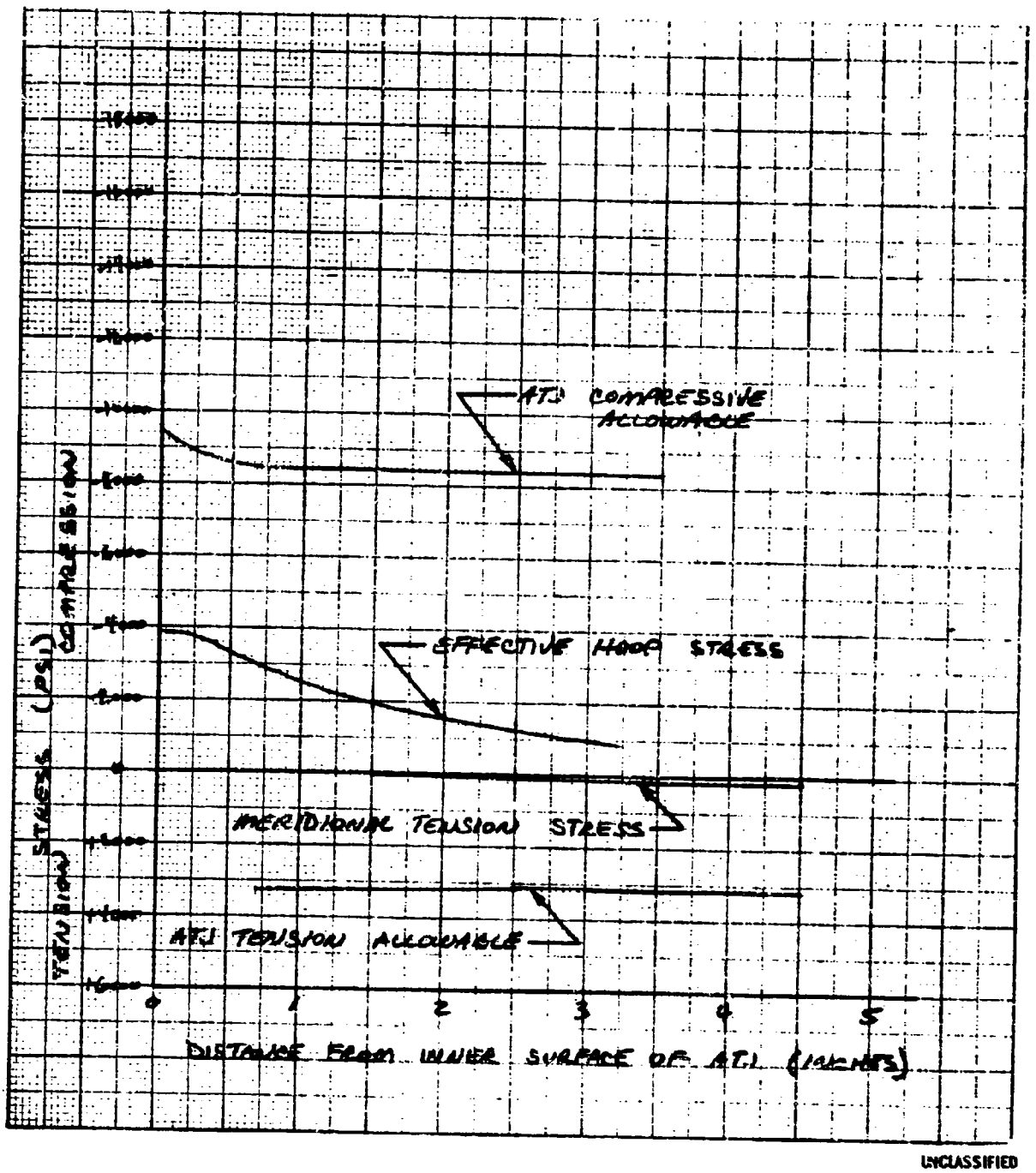

Figure 82. Demonstration Motor Expandable Exit Cone Throat at 5 sec ATJ

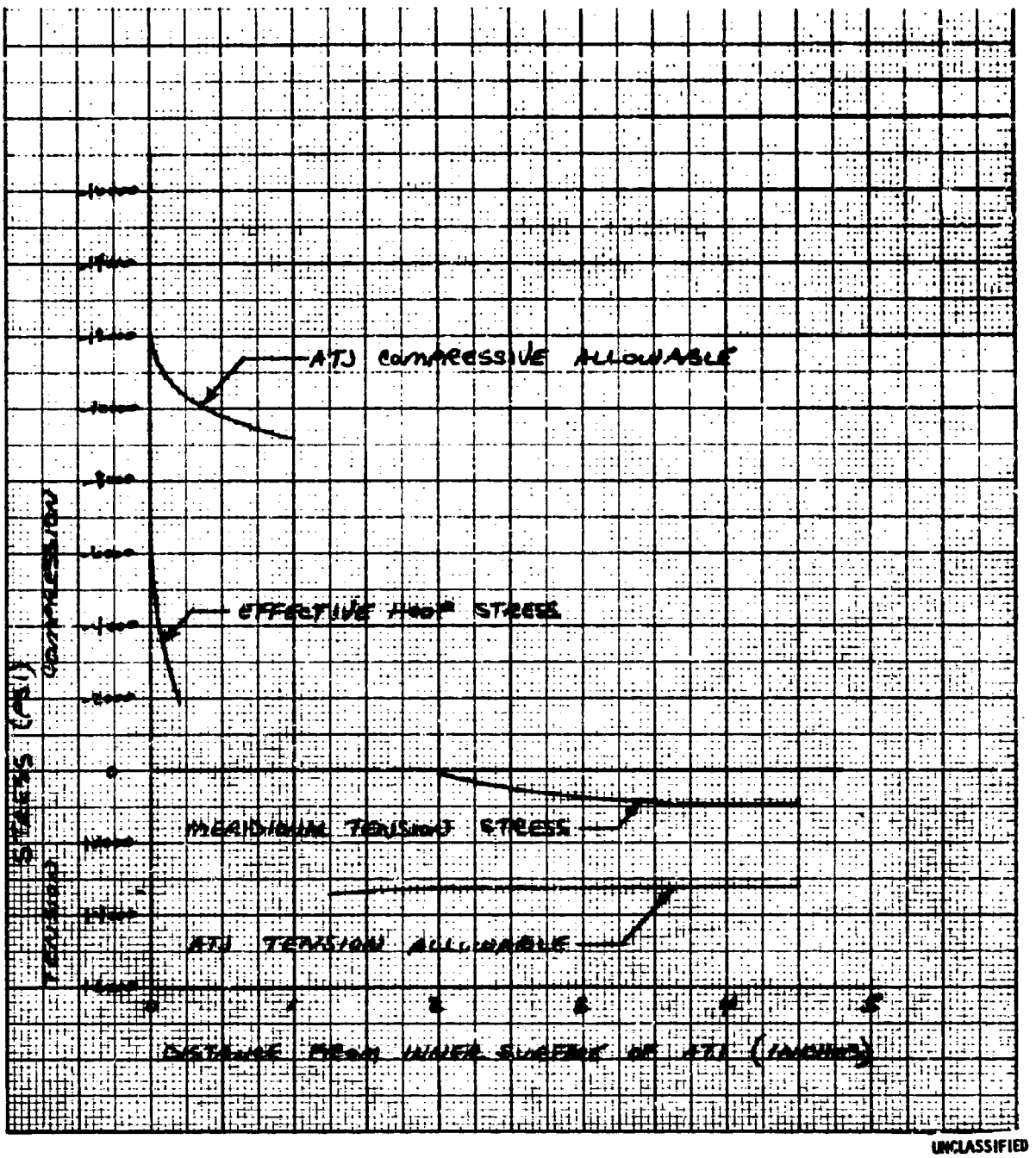

Figure 83. Demonstration Motor Expandable Exit Cone Motor Throat at 30 sec ATJ

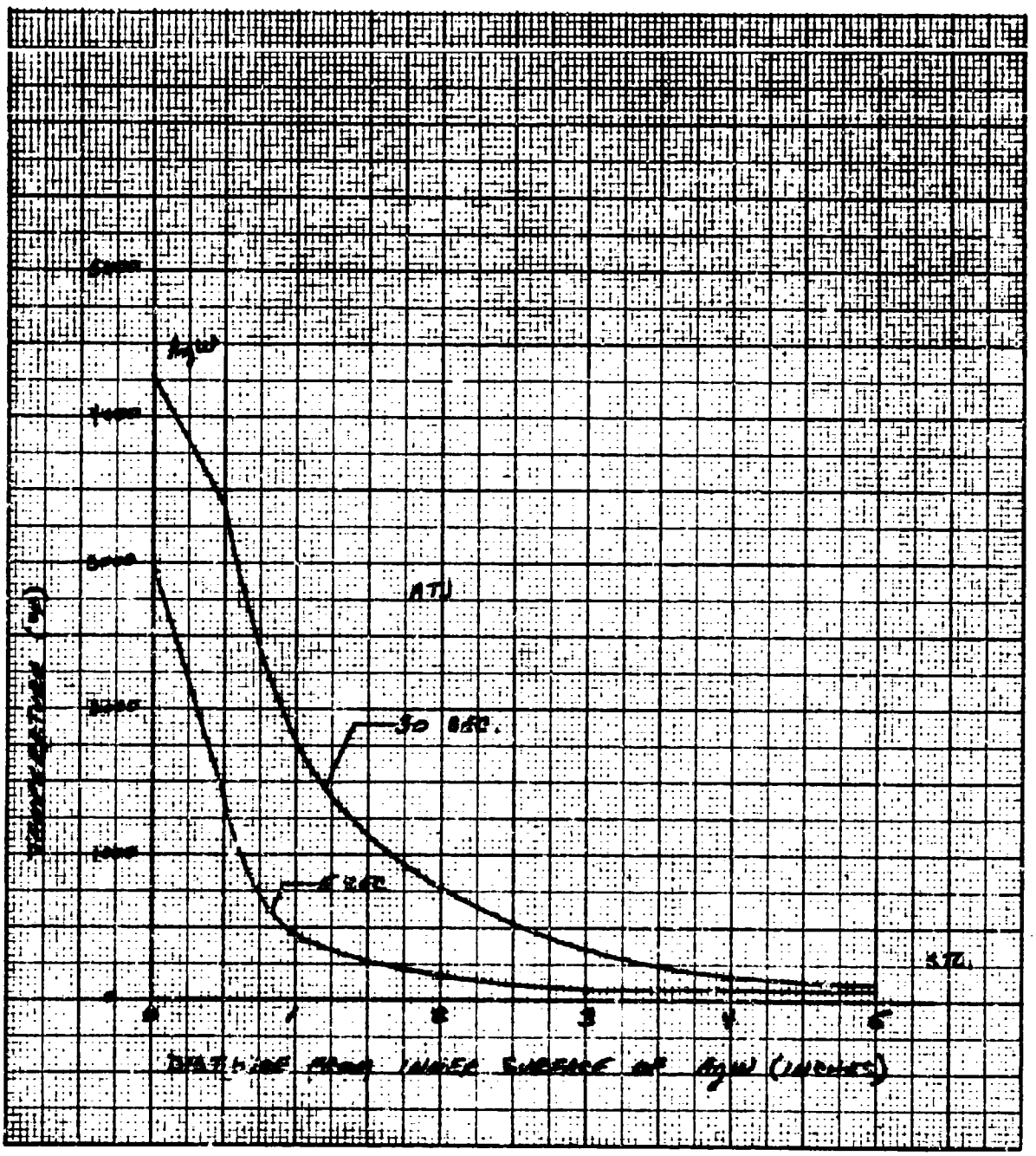

Figure 84. Demonstration Motor Expandable Exit Cone Motor Throat

E, Structural Analysis (cont.)

10. Nozzle Support

a. Subscale Motor

(u) (1) Design Condition

(u) The nozzle support structure for the subscale motor is designed to keep the nozzle in place when the chamber pressure is 750 psi.

General Configuration Subscale Nozzle Support

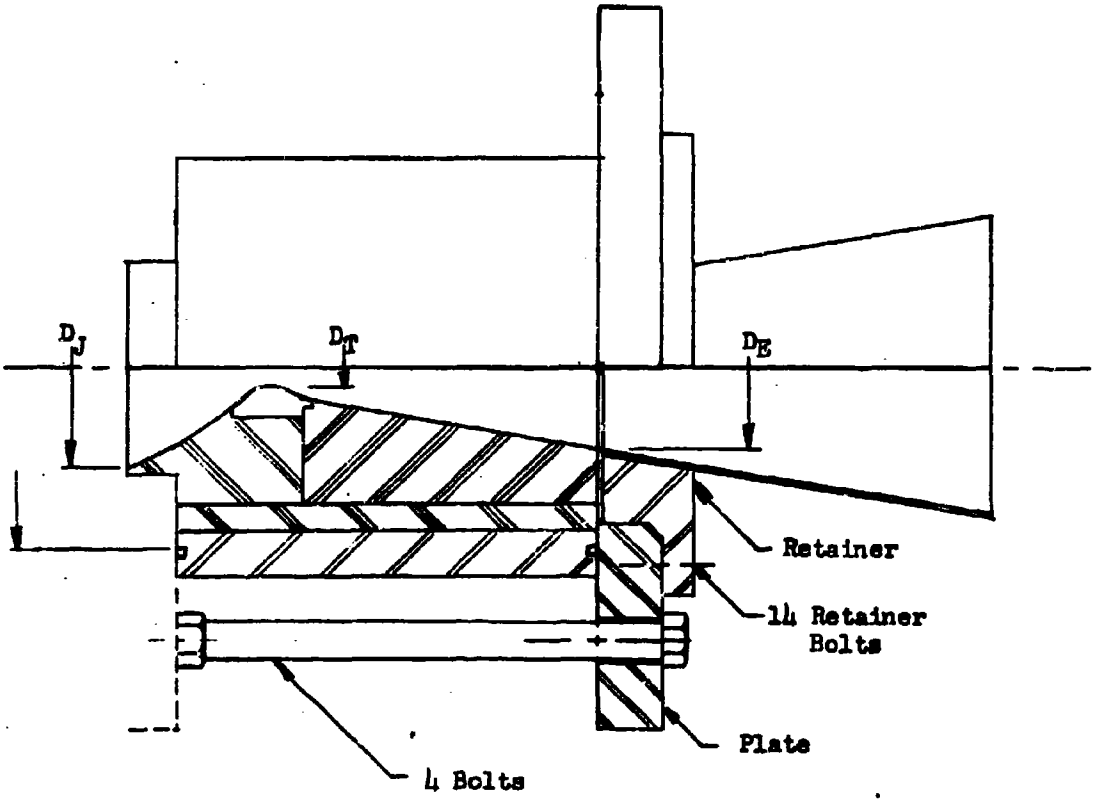

E, Structural Analysis (cont.)

(2) Analysis ~ Ejection Loads

(u) In computing the ejection loads on the support structure, the expendable section of the exit cone will be conservatively neglected.

$$F_{eJ} = P_J A_J [1 + \gamma M_J^2] - P_E A_E [1 + \gamma M_E^2] + P_J (A_s - A_J)$$

where

F_{EJ} = Ejection load on the nozzle (lb)
P = Pressure (psi)
A = Cross-sectional Area ($in.^2$)
γ = Coefficient of specific heats
M = Mach number

Subscripts

J = Nozzle entrance section
T = Throat section
E = Exit section
S = Seal

$$A_J = \frac{\pi}{4} \times 2.44^2 = 4.676 \text{ in.}^2$$

$$A_T = \frac{\pi}{4} \times 0.427^2 = 0.143$$

$$A_E = \frac{\pi}{4} \times 1.82^2 = 2.601$$

$$A_S = \frac{\pi}{4} \times 4.325^2 = 14.691$$

$$\frac{A_J}{A_T} = 32.6$$

$$\frac{A_E}{A_T} = 18.2$$

E, Structural Analysis (cont.)

(u) Using the above area ratios and Ref 13, and assuming that $\gamma = 1.2$, gives the following values for pressure and Mach number at the entrance and exit sections, respectively:

$$P_J = 1.00\ P_c$$
$$P_E = 0.005761\ P_c$$
$$M_J = 0.0$$
$$M_E = 3.693$$

Therefore

$$F_{eJ} = P_J A_s - P_E A_E (1 + \gamma M_E^2)$$

$$= 14.691\ P_c - 0.260\ P_c = 14.431\ P_c$$

(3) Analysis ~ Retainer

(u) The retainer will be analyzed conservatively, assuming all of the ejection force on the nozzle is reacted at a radius of 1.42 in.

AGC Sketch SK-0874-8
Material: 4130 Annealed
F_{ty} = 55 ksi
(Ref 8)

Therefore

$$F_p = \frac{14.431\ P_c}{2 \times \pi \times 1.42} = 1.617\ P_c$$

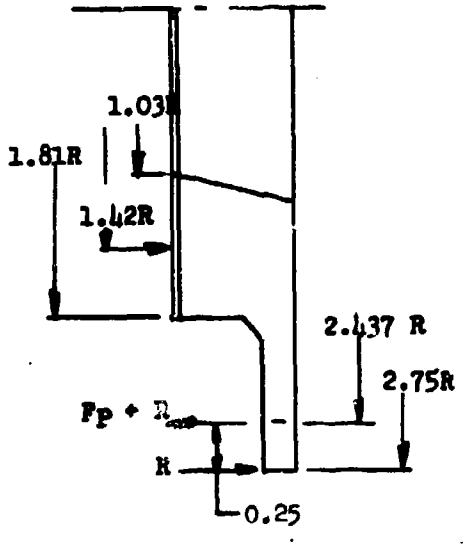

E, Structural Analysis (cont.)

(u) The bending moment at the bolt circle is:

$$M = 1.617\ P_c \times (2.437 - 1.42)\ \frac{1.42}{2.437} = 0.9582\ P_c$$

$$\therefore \sigma_b = \frac{6\ M}{t^2} \times \frac{\pi(\text{bolt circle dia})}{\pi(\text{bolt circle dia}) - n\ (\text{bolt dia})}$$

$$= \frac{6\ (0.9582\ P_c}{0.3752} \times \frac{2\pi\ 2.437}{2\pi\ 2.437 - 14\ (0.28)}$$

$$= \frac{88.032\ P_c}{1.6020} = 54.951\ P_c$$

$$\text{M.S.} = \frac{55\ \text{ksi}}{54.951 \times 750} - 1 = 0.33$$

(u) The load in the retainer bolts is due to the ejection load plus the reaction to the moment at the bolt circle

$$P_{bolt} = \frac{14.431\ P_c}{14} + 0.9582\ P_c \times 2\pi \times 2.437/14 \times 0.25$$

$$= (1.0308 + 4.1920)\ P_c$$

$$= 5.2228\ P_c$$

$P_{allowable}$ for 1/4-in. socket-head cap screw is 4800-lb yield strength

$$\text{M.S.} = \frac{4800}{5.2228\ (750)} - 1 = 0.22$$

E, Structural Analysis (cont.)

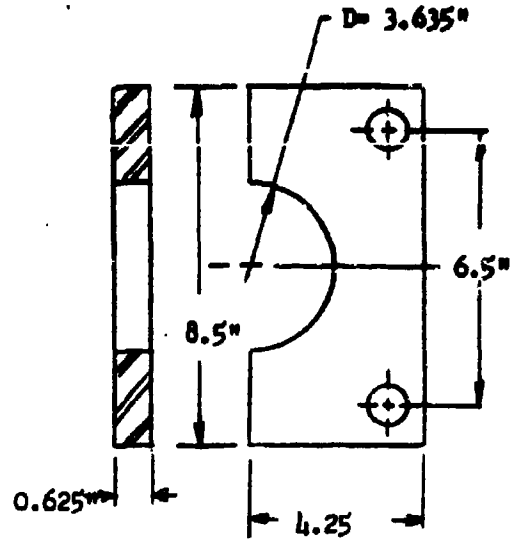

(4) Analysis - Plate

(u) A conservative analysis of the plate will be made by assuming it is a simply supported beam.

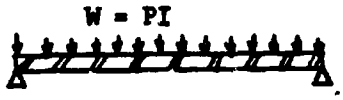

Material: 4130 Annealed
F_{ty} = 55 ksi (Ref 8)

The maximum moment is

$$w = 14.691 \times 750 = 11.018 \text{ lb}$$

$$M = \frac{wl}{8} = \frac{11,018 \times 6.5}{8} = 8952 \text{ in. lb}$$

$$\sigma_b = \frac{6M}{b\,t^2} = \frac{6 \times 8952}{(8.5 - 3.635)\ 0.625^2} = \frac{53,712}{1.900} = 28,300 \text{ psi}$$

$$M.S._{yield} = \frac{55}{28.3} - 1 = 0.94$$

(5) Main Bolts

(u) The four main bolts not only hold the nozzle on the closure, but they also hold the forward and aft closures. In computing the ejection load on these bolts, it will be assumed (conservatively) that the nozzle is plugged and that the motor is sealed at a radius of 4 in.

E, Structural Analysis (cont.)

$$F_{eJ} = 750\pi 4^2 = 37,699 \text{ lb}$$

The stress on each of the 1-in. bolts is

$$T = \frac{37,699}{4 \times 0.785} = 12,000 \text{ psi}$$

(u) Using a yield strength of 30 ksi for the bolts gives the following margin of safety

$$M.S. = \frac{30}{12} - 1 = 1.5$$

b. Demonstration Motor

(u) (1) Design Condition

The nozzle support structure for the subscale motor is designed to keep the nozzle in place when the chamber pressure is 750 psi.

E, Structural Analysis (cont.)

(u) (2) Ejection Load ~ Exit Cone Corrugated

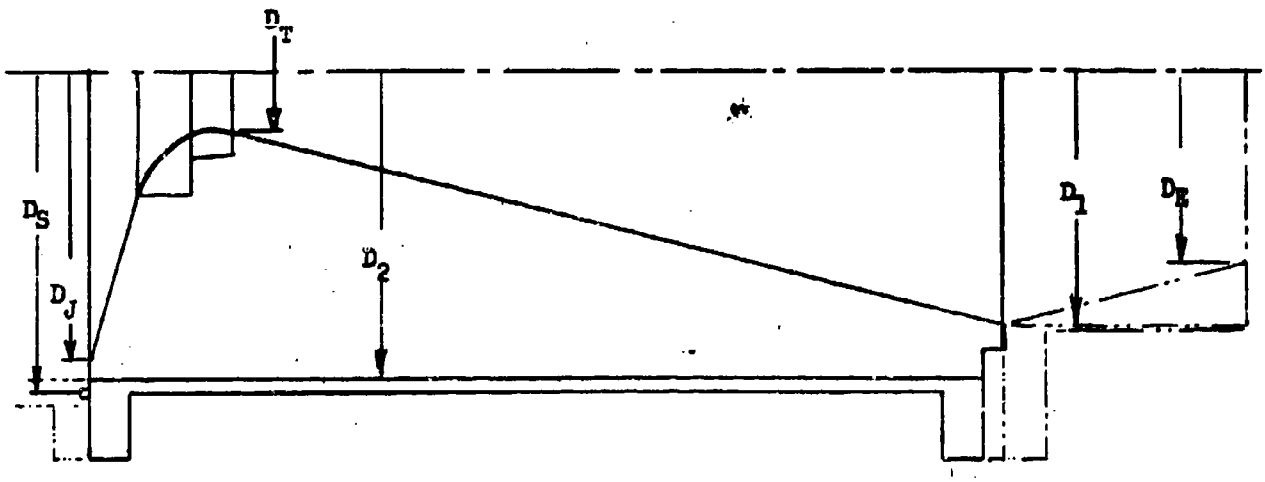

D_J = 12.9

D_T = 2.72 in.

D_E = 11.15 in.

D_S = 15.12 in.

$\frac{P_J}{P_c}$ = 1.0

$\frac{P_E}{P_c}$ = 0.00633

A_J = 130.7 in.^{2}

A_T = 5.81 in.^{2}

A_E = 97.64 in.^{2}

A_S = 179.55 in.^{2}

M_J = 0

M_E = 3.64

$\frac{A_J}{A_T}$ = 22.49

$\frac{A_E}{A_T}$ = 16.8

P_J = 750 psi

P_E = 4.7475 psi

E, Structural Analysis (cont.)

$$F_{eJ} = F_J A_J (1 + 1.2 M_J^2) - F_E A_E (1 + 1.2 M_E^2) + F_J (A_S - A_T)$$

$$= 750 (130.7) - 4.7475 (99.64) (1 + 1.2 \times 3.64^2) + 750 (179.55 - 130.7)$$

$$= 98,025 - 7994 + 36.637 = 126.668 \text{ lb}$$

(u) (3) Stresses

(a) Cylindrical Section

Material: 4130 Normalized
F_{ty} = 70 ksi (Ref 8)

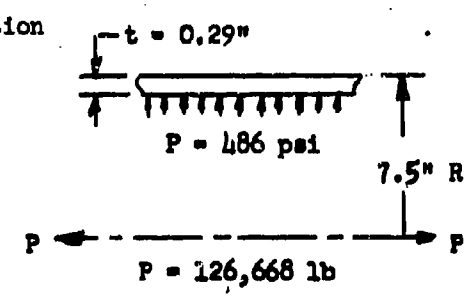

(u) The thermal analysis discussed previously indicated the maximum interface pressure between the insulation and the steel was 486 psi. Therefore, the hoop stress in the cylinder is

$$\sigma_{hoop} = \frac{PR}{t} = \frac{7.35 \times 486}{0.29} = 12,300 \text{ psi}$$

Meridional Stress

(u) The ejection force "P" on the nozzle is 126,668 lb. Therefore, the meridional stress in the nozzle shell is:

$$\sigma_{merid} = \frac{126,668}{2\pi (7.35) (0.29)} = 9458 \text{ psi}$$

$$M.S._{hoop} = \frac{70}{12.3} - 1 = 4.7$$

E, Structural Analysis (cont.)

(b) Aft Flange

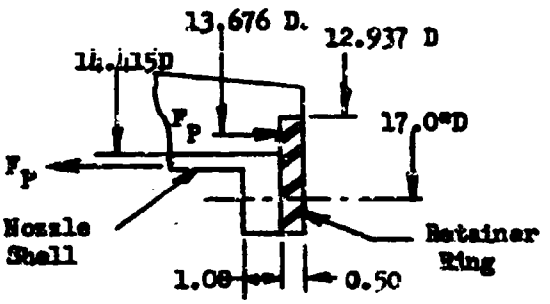

Material:

Nozzle Shell

4130 Cond A

F_{ty} = 55 ksi (Ref 8)

Retainer Ring

4130 Cond

F_{ty} = 163 ksi (Ref 8)

(u) The maximum moment on the retainer ring and the flange occurs at the bolt circle

$$F_p \text{ (bolt circle)} = \frac{126{,}668}{\pi \times 17} = 2371 \text{ lb/in.}$$

$$M_{\text{bolt circle}} = 2{,}371 \times \frac{(17 - 13.676)}{2} = 3{,}940 \text{ in.-lb/in.}$$

The circumference at the bolt circle is

$$C = \pi \times 17 = 53.4 \text{ in.}$$

The material removed for bolts is

$$d = 16 \times 0.670 = 10.7$$

The stress in the retainer ring at the bolt circle is

$$\sigma_b = \frac{6\,M}{t^2} \times \frac{c}{c-d} = \frac{6 \times 3940}{0.25} \times \frac{53.4}{53.4 - 10.7}$$

$$\sigma_b = 118{,}855 \text{ psi}$$

$$M.S._{\text{yield}} = \frac{163}{118.3} - 1 = 0.37$$

The stress in the flange is

$$\sigma_b = \frac{6 \times 3940}{1} \times \frac{53.4}{42.7} = 29{,}564$$

$$M.S._{\text{yield}} = \frac{55}{29.6} - 1 = 0.85$$

E, Structural Analysis (cont.)

The bolt load is $F_R + F_P$.

f_p = 2371 lb/in.

$F_R = \frac{3940}{0.7}$ = 5629 lb/in.

P_{bolt} = 8000 lb/in.

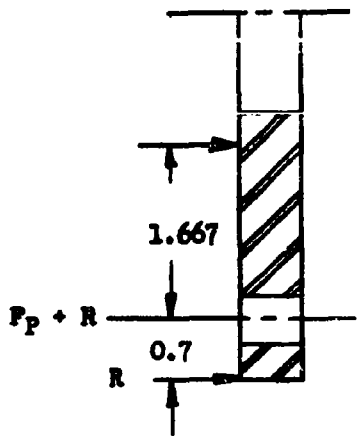

Bolt spacing is

$S = \frac{53.4}{16}$ = 3.34 in.

Total bolt load is 26,720 lb/bolt

The allowable bolt load for a 5/8-in. bolt with an allowable strength of 180 ksi is

P_{all} = 48,700-lb ultimate or 43,200-lb yield (Ref 10)

$$M.S._{yield} = \frac{43.2}{26.7} - 1 = 0.61$$

E, Structural Analysis (cont.)

11. Exit Cone

a. Subscale Motor

(u) The exit cone of the subscale motor is designed to operate when the chamber pressure is 750 psi. The exit cone may be made from F85 columbium, 90Ta - 10W, or elastomeric material. This analysis considers the first two materials, whose material properties are given in Figures 67 through 70.

(1) Geometry

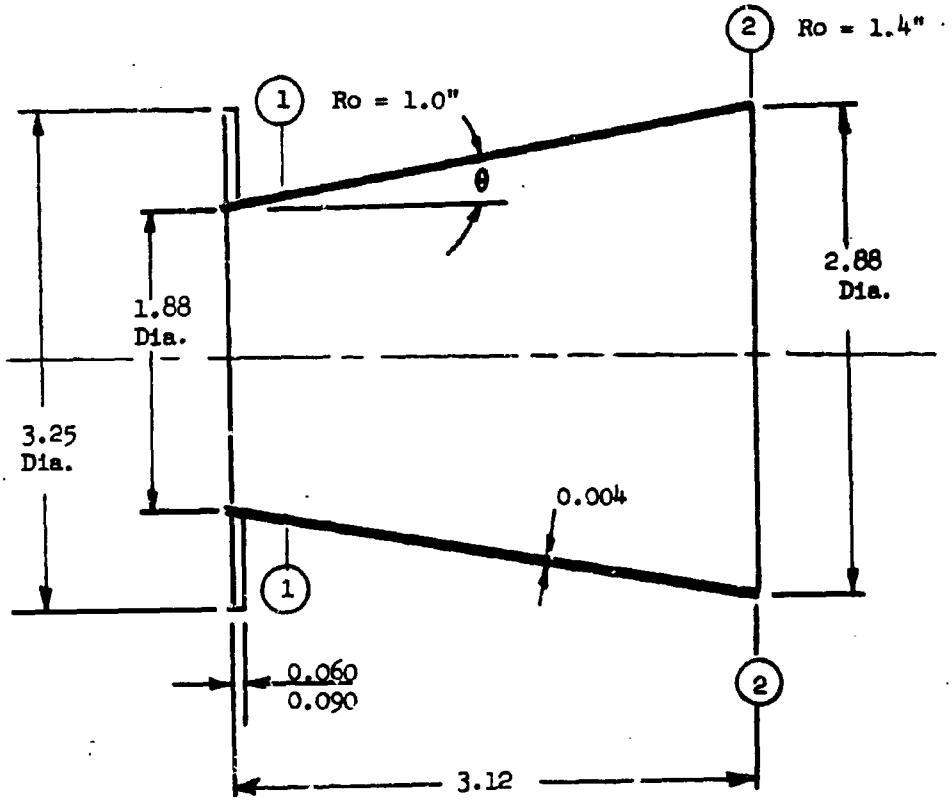

E, Structural Analysis (cont.)

$$\tan \theta = \frac{0.5}{3.125} = 0.16$$

$$\theta = 9.1°$$

$$\cos \theta = 0.987$$

P = 2 psi at Section 1, R_2 = 1.013 in., A = 3.14 in.^{2}

P = 0.85 psi at Section 2, R_2 = 1.420, A = 6.15 in.^{2}, F.S. = 1.5P

(2) Hoop Stress

Section 1

$$\sigma_h = \frac{PR_2}{t} = \frac{1.5 \times 2 \times 1.013}{0.004} = 760 \text{ psi}$$

Section 2

$$\sigma_h = \frac{PR_2}{t} = \frac{1.5 \times 0.85 \times 1.42}{0.004} = 453 \text{ psi}$$

(3) Allowable Tensile Stress 0.2% Offset

90Ta - 10W at 3560°F = 6000 psi

F-85 columbium at 3800°F = 2000 psi

$$\text{M.S.}_{\text{yield}} = \frac{2000}{760} - 1 = \underline{1.63}$$

(4) Meridional Stress

Section 1

The compressive load on the exit one at Section 1 is:

$$P_c = \left\{ P_1 A_1 \left[1 + \gamma M_1^2 \right] - P_2 A_2 \left[1 + M_2^2 \right] \right\} \text{ F.S.}$$

$$= 1.5 \left\{ 2(3.14) \left[1 + 1.2(3.88)^2 \right] - 0.85(6.15) \left[1 + 1.2(4.35)^2 \right] \right\}$$

$$= -6.3 \text{ lb}$$

E, Structural Analysis (cont.)

Section 2

The compressive stress at Section 2 is:

$$c = \frac{-6.3}{2 \times 1.013 \times 0.004} = -247 \text{ psi}$$

The compressive allowable will found by using Ref 12:

$R/T = 200$

$L/R = 2$

E for 90Ta - 10W at 3560°F = 7×10^6 psi

E for F-85 columbium at 3800°F = 4×10^6 psi

$$\frac{\sigma_{cr_{p=0}}}{E} \times 10^3 = 1.0$$

$$\sigma_{cr_{p=0}} = 4 \times 10^3 \times 1.2 = 4800 \text{ psi}$$

$$\text{M.S.} = \frac{4000}{247} - 1 = \underline{\text{High}}$$

b. Demonstration Motor

(u) The exit cone of the demonstration motor is designed to withstand a chamber pressure of 750 psi. This exit, like that listed on the subscale motor, may be made from F-85 columbium, 90Ta - 10W, or rubber. This analysis considers the first two materials, whose mechanical properties are shown in Figures 67 through 70. This exit cone differs from the subscale exit cone in that it is initially convoluted so that the outer surface is cylindrical. The rubber exit cone will be analyzed at a later date.

E, Structural Analysis (cont.)

(1) Geometry

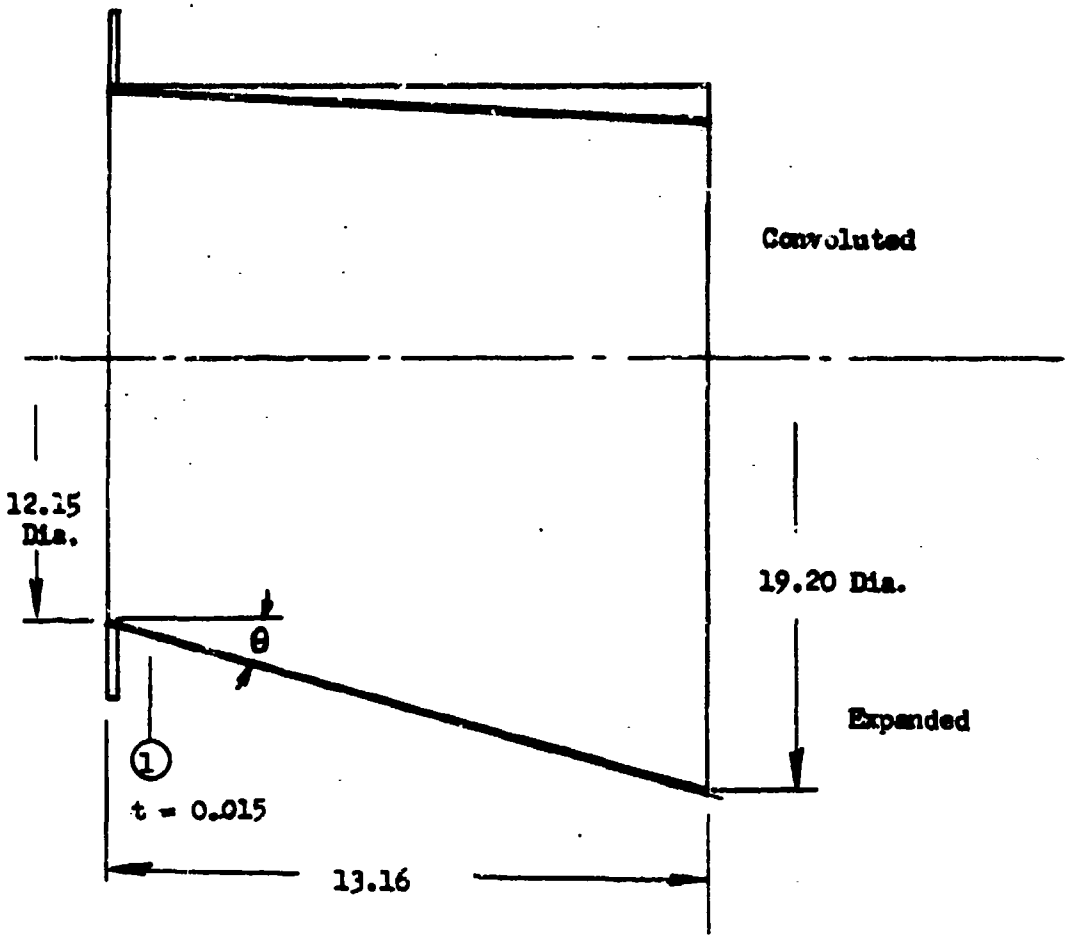

$$\tan \theta = \frac{19.20 - 12.15}{2 \times 13.16} = 0.26785$$

$$\theta = 15°$$

$$\cos \theta = 0.966$$

Section 1

$P = 2$ psi $(P_c = 500)$ $\quad R_2 = \frac{6.1}{0.966} = 6.31 \quad A = 115.9$

E, Structural Analysis (cont.)

Section 2

$P = 0.85$ psi ($P_c = 500$) $\quad R_2 = \frac{9.6}{0.966} = 9.94 \quad A = 289.5$

F.S. = 1.5

(2) Hoop Stresses

Section 1

$$\sigma_h = \frac{PR_2}{t} = \frac{2 \times 6.31 \times 1.5}{0.015} = 1262 \text{ psi}$$

Section 2

$$\sigma_h = \frac{PR_2}{t} = \frac{0.85 \times 9.6 \times 1.5}{0.015} = 816 \text{ psi}$$

(3) Allowable Stresses

90Ta - 10W at 3560°F = 6000 psi

F-85 columbium at 3800°F = 2000 psi

$$\text{M.S.} = \frac{2000}{1262} - 1 = \underline{0.58}$$

F-85

(4) Meridional Stress

Section 1

The compressive load on the exit cone at Section 1 is:

$$F_c = \left\{ P_1 A_1 \left[1 + \gamma M_1^2 \right] - P_2 A_2 \left[1 + \gamma M_2^2 \right] \right\} 1.5$$

$$= 487 \text{ lb}$$

$$\sigma_c = \frac{487}{\pi \times 12.15 \times 0.015} = 850 \text{ psi}$$

E, Structural Analysis (cont.)

The compressive allowable will be found by using Ref 12:

$\frac{R}{t} = 407$

$L/R = 2$

E for 90Ta - 10W at 3560°F = 7×10^6 psi

E for F-85 columbium at 3800°F = 4.5×10^6 psi

$\frac{\sigma_c}{E} \times 10^3 = 0.33$

$\sigma_c = 0.33 \times 4500 = 1500$

$$M.S. = \frac{1500}{850} - 1 = \underline{\underline{0.75}}$$

(5) Expansion of Exit Cone

(u) When the exit cone of the demonstration motor is convoluted, the aft end will appear as shown in the sketch at right. It becomes apparent that in this configuration the membrane forming the exit cone is statically unstable because high bending stresses would be required to resist T_1 and T_o. This bending stress would be

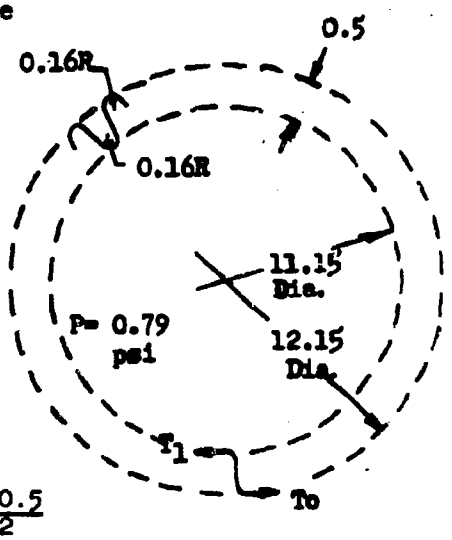

$$\sigma_b = \frac{6M}{t^2} = \frac{6\ T_1 \times 0.5}{0.015^2}$$

$T_1 = PR = 0.79 \times 5.575 = 4.4$ lb/in.

$\sigma_b = 57.5$ ksi

(u) Because this stress is much higher than the allowable, the convolutions will tend to straighten.

E, Structural Analysis (cont.)

(u) The maximum depth of the convolutions after expansion will be (the allowable moment is):

$$M = \frac{1.5 \times 2000 \times 225 \times 10^{-6}}{6}$$

$$= 0.1125 \text{ in.-lb}$$

$$T = 0.79 \times 9.6 = 7.58 \text{ lb/in.}$$

$$e = \frac{M}{T} = \frac{0.1125}{7.58} = 0.0148 \text{ in.}$$

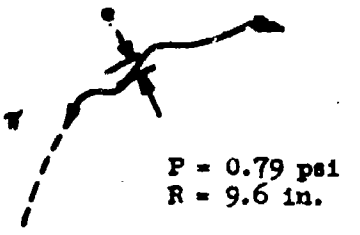

(6) Elongation

(u) The inner fibers will elongate as the exit cone expands. This elongation will be

$$e = \left(\frac{0.16}{0.1575} - 1\right) = 0.015 \text{ in./in.}$$

This indicates that the exit cone will not fail while opening.

F. NOMENCLATURE

Symbol	Definition
A	Area of cross-section, $in.^2$
b	Subscript (bending)
C	Distance from neutral axis to extreme fiber, in.
C	Subscript (compression)
D	Diameter, in.
D	Flexural rigidity $= \frac{Et^3}{12(1-\nu^2)}$, $lb\text{-}in.^2$
E	Modulus of elasticity, psi
e	Elongation or displacement, in.
F	Allowable stress, psi
f or σ	Applied stress, psi
h	Subscript (hoop) or (horizontal)
I	Moment of inertia (with proper axis subscripts), $in.^4$
L	Length, in.
M	Bending moment, in. - lb, or in. -lb/in.
m	Subscript (meridional)
N	Shell meridional membrane force, lb/in.
P	Applied load, lb or lb/in.
P_k	Pressure input for IBM 7094 Computer Program 663, psi
p	Pressure, psi
Q	Shear, lb or lb/in.
R	Radius, in.
R	Stress ratio
S	Subscript (Shear)

F, Nomenclature (cont.)

Symbol	Definition
T	Applied torsional moment or torque, in.-lb or in.-lb/in.
W	Weight, lb
w	Uniform weight distribution, lb/in.
X	Distance along x-axis, in.
y	Distance along y-axis, in.
α	Thermal coefficient of expansion, in./in.-°F
β	Damping function = $\frac{3(1-\nu^2)}{R^2t^2}^{1/4}$, $in.^{-1}$
ω	Radial deflection, in.
ν	Poisson's ratio
ε	Strain, in./in.
θ	Rotation or angle, radians or degrees
ρ	Density, $lb/in.^3$
ϕ	Angle, radians or degrees
c.g.	Center of gravity
°F	Degrees fahrenheit
in.	Inch
ksi	Kilo pounds per square inch
lb	Pounds
max	Maximum
min	Minimum
M.S.	Margin of safety = $\frac{\text{Allowable Stress}}{\text{Calculated Stress}} - 1$
psi	Pounds per square inch
BMF	Bending modulus factor

REFERENCES

1. Product Engineering Final Report Expandable Nozzles (u), Aerojet-General Report 652/SA4-2.2.-F-1, Volume 3, Contract AF 04(647)-652/SA4, 28 June 1963. (C)

2. Expandable Exit Cones for Rocket Engines (u), Aerojet-General Report 212/SA3-F, Volume 2, Contract AF 04(694)-212/SA19, Item 4, 5 April 1965. (C)

3. Technical Proposal to AFFTC/FTKR-5/F. L. Wong, Edwards AFB, California 93523, for Development, Design, Fabrication, and Demonstration of Packageable High-Expansion-Ratio Nozzles for Solid Propellant Rocket Motors, (u), Aerojet-General Technical Proposal SRR 64541, March 1964. (C)

4. Seban, R. A., Heat Transfer and Flow with Separated and Reattached Boundary Layers as Produced by Surface Irregularities, WADC Technical Report 56-217, 1956.

5. Final Report Development of Malfunction Detection System Sensors for Large Solid Propellant Rocket Motors (u), Aerojet-General Report 2904T, Contract NAS8-5357, August 1964. (C)

6. Culp, J. S., Demonstration Tests of Two Types of Packageable High-Expansion-Ratio Nozzles for Solid Propellant Rocket Motors (u), Report AEDC-TR-65-254, ARO, Inc., Bryan, Ohio, January 1966. (C)

7. Croy, E. L. and Schumacher, J. G., An Analysis of Thick Cylinders in the Plastic Range, Technical Memorandum 240, Solid Rocket Plant, Aerojet-General Corporation, December 1962.

8. Strength of Metal Aircraft Elements, Handbook MIL-HDBK-5, Armed Forces Supply Support Center, Washington 25, D.C., March 1959.

9. Roark, R. J. Formulas for Stress and Strain, Third Edition, McGraw-Hill Book Company, Inc., New York, New York, 1954.

10. SPS Bolts of the Aerospace Industry, Aircraft Missile Division SPS, Jenkintown, Pennsylvania, 1964-1965 Edition

11. Mangipane, J., Optimum Area of On-Center Bosses for Ellipsoids of Revolution, Solid Rocket Plant Structures Group, Aerojet-General Corporation, March 1959

12. Schumacher, J. C. and Lincoln, B., Report AZS-27-275, Convair Astronautics Division, General Dynamics Corporation, May 1959

13. Compressible Flow Tables, Solid Engine Design Handbook, Aerojet-General Corporation.

14. Data Sheets, Materials, and Fabrication, Aerojet-General Corporation

15. Materials in Design Engineering, Materials Selector Issue, Reinhold Publishing Corp., New York, N.Y., October 1963

Security Classification

DOCUMENT CONTROL DATA - R&D

(Security classification of title, body of abstract and indexing annotation must be entered when the overall report is classified)

1. ORIGINATING ACTIVITY (Corporate author) Aerojet-General Corporation Box 1947 Sacramento, California 95809	2a. REPORT SECURITY CLASSIFICATION CONFIDENTIAL 2b. GROUP 4

3. REPORT TITLE Development, Design, Fabrication, and Demonstration of Packageable High-Expansion-Ratio Nozzles for Solid Propellant Rocket Motors (u)

4. DESCRIPTIVE NOTES (Type of report and inclusive dates)
Final Report, June 1964 - April 1966

5. AUTHOR(S) (Last name, first name, initial)
Morris, R. E., Aerojet-General Corporation

6. REPORT DATE	7a. TOTAL NO. OF PAGES	7b. NO. OF REFS
April 1966	164	15

8a. CONTRACT OR GRANT NO.	9a. ORIGINATOR'S REPORT NUMBER(S)
AF 04(611) b. PROJECT NO.	AFFPL-TR-66-45
c.	9b. OTHER REPORT NO(S) (Any other numbers that may be assigned this report) None
d.	

10. AVAILABILITY/LIMITATION NOTICES
Foreign announcement and dissemination of this report by DDC is not authorized. Qualified requesters may obtain copies of this report from DDC.

11. SUPPLEMENTARY NOTES	12. SPONSORING MILITARY ACTIVITY
None	Air Force Rocket Propulsion Laboratory Air Force Systems Command Edwards Air Force Base, California

13. ABSTRACT

See attached sheets.

DD FORM 1 JAN 64 1473

Unclassified
Security Classification

Unclassified
Security Classification

14. KEY WORDS	LINK A		LINK B		LINK C	
	ROLE	WT	ROLE	WT	ROLE	WT
1. Expandable Exit Cone 2. Packageable Exit Cone 3. Elastomeric Exit Cone 4. Radiation Cooling 5. Erosion 6. Deployment						

INSTRUCTIONS

1. ORIGINATING ACTIVITY: Enter the name and address of the contractor, subcontractor, grantee, Department of Defense activity or other organization (*corporate author*) issuing the report.

2a. REPORT SECURITY CLASSIFICATION: Enter the overall security classification of the report. Indicate whether "Restricted Data" is included. Marking is to be in accordance with appropriate security regulations.

2b. GROUP: Automatic downgrading is specified in DoD Directive 5200.10 and Armed Forces Industrial Manual. Enter the group number. Also, when applicable, show that optional markings have been used for Group 3 and Group 4 as authorized.

3. REPORT TITLE: Enter the complete report title in all capital letters. Titles in all cases should be unclassified. If a meaningful title cannot be selected without classification, show title classification in all capitals in parenthesis immediately following the title.

4. DESCRIPTIVE NOTES: If appropriate, enter the type of report, e.g., interim, progress, summary, annual, or final. Give the inclusive dates when a specific reporting period is covered.

5. AUTHOR(S): Enter the name(s) of author(s) as shown on or in the report. Enter last name, first name, middle initial. If military, show rank and branch of service. The name of the principal author is an absolute minimum requirement.

6. REPORT DATE: Enter the date of the report as day, month, year; or month, year. If more than one date appears on the report, use date of publication.

7a. TOTAL NUMBER OF PAGES: The total page count should follow normal pagination procedures, i.e., enter the number of pages containing information.

7b. NUMBER OF REFERENCES: Enter the total number of references cited in the report.

8a. CONTRACT OR GRANT NUMBER: If appropriate, enter the applicable number of the contract or grant under which the report was written.

8b, 8c, & 8d. PROJECT NUMBER: Enter the appropriate military department identification, such as project number, subproject number, system numbers, task number, etc.

9a. ORIGINATOR'S REPORT NUMBER(S): Enter the official report number by which the document will be identified and controlled by the originating activity. This number must be unique to this report.

9b. OTHER REPORT NUMBER(S): If the report has been assigned any other report numbers (*either by the originator or by the sponsor*), also enter this number(s).

10. AVAILABILITY/LIMITATION NOTICES: Enter any limitations on further dissemination of the report, other than those imposed by security classification, using standard statements such as:

(1) "Qualified requesters may obtain copies of this report from DDC."

(2) "Foreign announcement and dissemination of this report by DDC is not authorized."

(3) "U. S. Government agencies may obtain copies of this report directly from DDC. Other qualified DDC users shall request through _____."

(4) "U. S. military agencies may obtain copies of this report directly from DDC. Other qualified users shall request through _____."

(5) "All distribution of this report is controlled. Qualified DDC users shall request through _____."

If the report has been furnished to the Office of Technical Services, Department of Commerce, for sale to the public, indicate this fact and enter the price, if known.

11. SUPPLEMENTARY NOTES: Use for additional explanatory notes.

12. SPONSORING MILITARY ACTIVITY: Enter the name of the departmental project office or laboratory sponsoring (*paying for*) the research and development. Include address.

13. ABSTRACT: Enter an abstract giving a brief and factual summary of the document indicative of the report, even though it may also appear elsewhere in the body of the technical report. If additional space is required, a continuation sheet shall be attached.

It is highly desirable that the abstract of classified reports be unclassified. Each paragraph of the abstract shall end with an indication of the military security classification of the information in the paragraph, represented as (TS), (S), (C), or (U).

There is no limitation on the length of the abstract. However, the suggested length is from 150 to 225 words.

14. KEY WORDS: Key words are technically meaningful terms or short phrases that characterize a report and may be used as index entries for cataloging the report. Key words must be selected so that no security classification is required. Identifiers, such as equipment model designation, trade name, military project code name, geographic location, may be used as key words but will be followed by an indication of technical context. The assignment of links, roles, and weights is optional.

Unclassified
Security Classification

Report AFRPL-TR-66-45

Attachment
to
DD Form 1473
DOCUMENT CONTROL DATA - R&D

UNCLASSIFIED ABSTRACT

(u) The objectives of this program were the development, design, fabrication, and demonstration of packageable high-expansion-ratio nozzles for solid propellant rocket motors. A subscale testing program conducted at Aerojet-General's Von Karman Center altitude facility was successful in providing information for evaluating three elastomeric materials (nitrile butadiene (V-44®), styrene butadiene, and butyl) and two refractory metals (90Ta-10W and columbium) for use in exit cones. Erosion data was also gathered on these elastomeric materials. A demonstration test program was conducted at Arnold Engineering Development Center, using three 30KS-5000 solid propellant motors, two with an elastomeric V-44® exit cone and one with a columbium expandable exit cone. Objectives were to test deployment, determine the materials' integrity under operating conditions, obtain data pertaining to specific impulse at altitude conditions, and obtain postfire heat-soak data for 30 sec. Successful motor ignition, operation, and postfire heat-soak for all three tests were conducted at simulated altitudes in excess of 100,000 feet. Attempts to deploy the elastomeric V-44® exit cone from a folded position at altitude conditions were only partially successful. However, the principle of deployment was demonstrated during sea-level tests. All three exit cones were stable during motor operation and were in excellent postfire condition. The columbium exit cone did not expand fully (area ratio of 38.0, instead of 50). High-quality optical data were obtained of the nozzle deployment, nozzle performance during motor operation, and postfire condition.